APPLICATION OF QUANTUM MECHANICAL COMPUTATIONAL TECHNIQUES: THE UNSATURED BINUCLEAR CHROMIUM CARBONYLS AND SINGLET EXCITED ELECTRONIC STATES OF ALUMINUM HYDROXIDE

by

SE LI

(Under the Direction of H. F. Schaefer)

ABSTRACT

Advanced quantum mechanical computational techniques have been applied to probe two disparate systems. First, density functional theory (DFT) is used to obtain the first structural characterizations of the unsaturated dichromium carbonyl complexes $Cr_2(CO)_x$ (x=10, 9, 8), which may contain metal-metal multiple bonds. Chromium is unique among the first row transition metal elements in its ability to form compounds with multiple bonds in the formal metal oxidation state chromium(0). The global minimum energy structure of $Cr_2(CO)_{10}$ for the lowest singlet state of C_{2h} symmetry is consistent with a model of two interacting $Cr(CO)_5$ fragments, with chromium-chromium distances of 2.93 Å (B3LYP) or 2.83 Å (BP86). The minimum energy $Cr_2(CO)_9$ structure of C_s symmetry is predicted to have a remarkably short metal-metal bond length of 2.31 Å (B3LYP) or 2.28 Å (BP86). This chromium-chromium distance is essentially identical to that reported experimentally for the established Cr≡Cr triple bond in $(\eta^5\text{-}Me_5C_5)_2Cr_2(CO)_4$. $Cr_2(CO)_8$ is predicted to have a short metal-metal bond length of 2.30 Å (B3LYP) or 2.28 Å (BP86) for the minimum energy structure of C_s symmetry.

Second, extensive *ab initio* quantum mechanical methods have been employed to five lowest-lying electronic singlet states of astrophysically interesting AlOH, particularly for the two excited singlet states. To avoid the difficulty involved in applying multi-reference methods, we use the equation-of-motion coupled cluster method. The first singlet excited state ($\tilde{A}\ ^1A'$) is predicted to have a bond angle of 110° and to lie 114 kcal/mol (39 900 cm^{-1}, 4.94 eV) above the ground state, whereas the second singlet excited state ($B\ ^1A''$) is predicted to have a bond angle of 116° and to be located 119 kcal/mol (41 700 cm^{-1}, 5.17 eV) above the ground state. These theoretical energy separations are in excellent agreement with the experimental values T_0 ($\tilde{A}\ ^1A'$) = 114.57 kcal/mol (40 073 cm^{-1}, 4.968 eV) and T_0 (B^1A'') = 119.36 kcal/mol (41 747 cm^{-1}, 5.176 eV).

INDEX WORDS: Density Functional Theory, Transition Metal Carbonyls, Unsatured Dichromium Carbonyl, Metal-Metal Mutiple Bonds, Chromium-Chromium Distances, Ab initio Methods, Coupled Cluster Theory, Singlet Excited States, Multi-reference Methods, Equation-of-Motion Coupled Cluster Method, AlOH.

APPLICATION OF QUANTUM MECHANICAL COMPUTATIONAL TECHNIQUES: THE UNSATURED BINUCLEAR CHROMIUM CARBONYLS AND SINGLET EXCITED ELECTRONIC STATES OF ALUMINUM HYDROXIDE

by

SE LI

B.S., Jilin University, China, 1997

M.S., Beijing Institute of Technology, China, 2000

A Dissertation Submitted to the Graduate Faculty

of The University of Georgia in Partial Fulfillment

of the

Requirements for the Degree

DOCTOR OF PHILOSOPHY

ATHENS, GEORGIA

2004

APPLICATION OF QUANTUM MECHANICAL COMPUTATIONAL TECHNIQUES: THE UNSATURED BINUCLEAR CHROMIUM CARBONYLS AND SINGLET EXCITED ELECTRONIC STATES OF ALUMINUM HYDROXIDE

by

SE LI

Major Professor: H. F. Schaefer

Committee: R. Bruce King
Nigel Adams
Lucia Babcock
Henning Meyer

Electronic Version Approved:

Maureen Grasso
Dean of the Graduate School
The University of Georgia
May 2004

To my parents and my beloved husband

ACKNOWLEDGEMENTS

There are many people that deserve my deepest thanks and respect for their continued support. Without them, I could never have completed my dissertation.

First and foremost, I would like to thank my parents, Qianshu Li and Peiqin Ma, who brought me to the world, who gave me a happy childhood, provided my education, and taught me the values I treasure. They are my greatest source of inspiration at all times. Also I would like to thank my sisters for their love and understanding. Especially, my younger sister, Nan, who has taken care of our parents since I left home and I miss her very much. Another person that deserves my greatest thanks is my husband, Jin Zhou. He supports me in all aspects and is definitely the other half of my life. He serves as my bodyguard for when I work late at the Center for Computational Chemistry (CCC) almost every night.

Secondly, I must deeply thank my advisor Professor Henry Schaefer for providing an excellent opportunity to become part of the CCC. He is enjoyable to work with and over the past four years has patiently kept me on the right track. Professor Schaefer is a nice and humorous boss. He knows how to provide us with the ideal atmosphere in which we can study and work efficiently. Also he has impacted my knowledge of science, belief, life, language, self, education, culture, and identity in a completely new and deep way. His influence extends well beyond my research projects.

Next, I would like to thank the members of my dissertation committee. Professor Bruce King has been an invaluable teacher who provided me with key advice at the outset of my

chromium project. Professor Nigel Adams, Professor Lucia Babcock, and Professor Henning Meyer are very nice and respectable. I received their considerable encouragement and important suggestions during my stay at the CCC. I also want to thank some professors outside my committee, Professor Norman Allinger and Professor Paul Schleyer, for their encouragement.

I would like to particularly thank Dr. Yukio Yamaguchi for all the hours of consultation, meetings, comments, suggestions, references, insights, lectures, enthusiasm, professionalism, faith in me, and friendship. Dr. Yamaguchi has been a source of strength and support throughout my graduate studies. He has made my study at CCC an unparalleled experience. Also I want to thank Dr. Yaoming Xie for much support and encouragement during the earlier stages of studying and Dr. Wesley Allen for teaching, comments and encouragement.

In addition I would like to thank many former group members. I especially thank Nancy Richardson for her fervent and unselfish support, patience, and guidance. I was extremely fortunate to meet her during my first days in the U.S.A. I also want to thank Levent Sari for sharing his knowledge of Psi II, Shawn Brown for exchanging ideas, and Joe Kenny for helpful discussion.

Next, I am grateful to current group members that help me during my research. My officemate, Justin, is one of the best officemates on the planet. He is always smiling and ready to help others. Has anyone ever seen him mad? I also sincerely thank Michael, Kurt, Eric, Joseph, Nathan, Holly, Veronika, David, Martin, and all other group members.

I want to thank our CCC mother, Linda Rowe, for taking care of every detail of our lives in the CCC, and I also thank Karen, Amy and Richard.

Finally, I would like to thank to all my close friends in or out of chemistry, U.S.A or China or wherever they may be. I will send my thanks to all you, Michael Chen, Yang, Min, Ting, and blus blus.

TABLE OF CONTENTS

Page

LIST OF FIGURES

Page

LIST OF TABLES

Page

CHAPTER 1

INTRODUCTION AND BACKGROUND MATERIAL

1.1 DENSITY FUNCTIONAL THEORY

Density functional theory (DFT) is a powerful and successful quantum mechanical technique for ground state properties of large systems, owing to its capability of obtaining very accurate results at low cost. The basic idea of DFT is to describe *n*-electron interacting system only via its density instead of the wave function depending on the *3n* spatial and an *n* spin coordinates. "*The density-functional (DF) molecular wave function is not a Slater determinant of spin-orbitals. In fact, there is no DF molecular wave function."* In the Kohn-Sham DFT, the theory is a one-electron theory and very similar to the Hartree-Fock theory. The electronic Hamitonian is the sum of electronic kinetic-energy terms, electron-nuclear attractions, and electron-electron repulsions.

$$\hat{H}_e = -\sum_i^N \frac{1}{2}\nabla_i^2 - \sum_A^M \sum_i^N \frac{Z_A}{|R_A - r_i|} + \sum_{i>j}^N \frac{1}{r_{ij}}$$

In the DFT electronic energy expression, each sum is a functional of ρ:

$$E_{DFT}[\rho] = T_S[\rho] + V_{ne}[\rho] + J[\rho] + E_{xc}[\rho]$$

where the subscript *s* denotes the fictitious reference system of *n* noninteraction electrons.

E_{xc} is defined as the *exchange-correlation* energy functional by

$$E_{XC}[\rho] = (T[\rho] - T_S[\rho]) + (V_{ee}[\rho] - J[\rho]) = (T[\rho] - T_S[\rho]) + K[\rho]$$

$T[\rho] - T_S[\rho]$ is the difference in the average ground-state electronic kinetic energy between the molecule and the reference system of noninteracting electrons with electron density equal to that in the molecule. The kinetic energy of the reference system turns out to be close to the real molecule, but the $T[\rho] - T_S[\rho]$ term is not negligible. No one knows the exact form $E_{xc}(\rho)$ is, so approximations must be used. The key to improve the accuracy of KS DFT calculation of molecular properties is to get a good approximation to $E_{xc}(\rho)$. There are various approximations of $E_{xc}(\rho)$ are used in molecular DF calculations.

The first functional is the local density approximation (LDA), for which the exchange-correlation functional consists of the Dirac-Slater exchange and the Vosko, Wilks and Nadir (VWN) correlation terms. Some commonly used functionals, BLYP, BP86, B3LYP are all 'gradient corrected' (sometimes called non-local) functionals. BLYP is obtained by adding gradient corrections to the LDA method - specifically the exchange correction of Becke and the correlation function of Lee, Yang and Parr. BP86 was developed by Becke and Perdew in 1986. This functional has the same exchange correction as BLYP, but uses the older Perdew86 correlation functional - and BP91, which again has the Becke exchange terms, but uses a more recent correlation functional (Perdew91). B3LYP is a modification of BLYP in which a three-parameter functional developed by Axel Becke is used. The B3LYP functional has been widely used in theoretical chemistry.

To study the accuracies of the various approximations used for $E_{xc}(\rho)$, we need to compare

the calculated molecular properties with the experimental ones. Unfortunately, unlike the conventional *ab initio* theory, DFT results cannot be improved in a systematical way. Also, DFT is basically a ground-state theory and the extension from the ground states to excited states is not obvious.

1.2 EQUATION-OF-MOTION COUPLED-CLUSTER

Over the past two decades, the coupled-cluster (CC) theory has been established as one of the most accurate and efficient methods for describing the ground electronic states of small and medium size molecules. However, few excited electronic states of polyatomic systems have been accurately characterized owing to the difficulties in obtaining the appropriate wave functions. As the size of the system increases, the application of multi-configuration self-consistent field (MCSCF) and multi-reference configuration interaction (MR-CI) become increasingly difficult. In contrast, the equation-of-motion coupled-cluster (EOM-CC) method has the merit of accurately treating excited states of relatively large-scale systems. For instance, EOM-CCSD calculations involve only a sixth-power dependence on the basis set size, the same as that associated with evaluation of the ground state CCSD energy. In general, EOM-CCSD energy calculations require about twice the computer time needed for the CCSD ground state treatment.

In EOM-CC models, the excited state energies and corresponding wave functions are obtained by diagonalizing a similarity transformed Hamiltonian operator in a specially defined

quasiparticle excitation basis. Notably, the excitations in the basis are based on CC reference wave functions rather than the determinants in the more familiar configuration interaction (CI), usually using the coupled-cluster singles and doubles (CCSD) wave function as the ground states. Excited states dominated by single electron transitions are accurately treated by the EOM-CCSD model. Since most low-lying electronic levels of chemical interest are of this type, EOM-CCSD method provides a powerful tool to study energies of excited states, excited state potential surfaces, and photochemical reactions.

1.3 LITERATURE REFERENCES

1. Kohn, W.; Sham, L. J. *Phys. Rev.*, **1964**, *136*, B864.
2. Vosko, S. H.; Wild, L.; Nusair, M. Can. *J. Phys*., **1980**, *58*, 1200.
3. Slater, J. C. *Phys. Rev*., **1951**, 81, 385
4. Hohenberg, P.; Kohn, W. *Phys. Rev.,* **1964**, *136*, B864.
5. Slater, J. C. *Quantum Theory of Molecules and Solids: The Self-Consistent Field for Molecules and Solids, Vol. IV.* McGraw-Hill, New York, **1974**.
6. Becke, A. D. *Phys. Rev. A*., **1988**, *38*, 3098.
7. Perdew, J. P. *Phys. Rev B*, **1986**, *33*, 8822.
8. Lee, C.; Yang, W.; Parr, R. G. *Phys. Rev. B.,* **1988**, *37*, 785.
9. Becke, A. D. *J. Chem. Phys*., **1993**, *98*, 5648.
10. Becke, A. D. *J. Chem. Phys*., **1993**, *98*, 1372.

11. Frisch, M. J.; etc. Gaussian 94, (revision c.3). (Pittsburgh, PA: Gaussian, Inc.), **1995**.

12. Kong, J.; White, C. A.; etc. *J. Comput.Chem.*, **2001**, *21*, 1532.

13. Huzinaga, S. *J. Chem. Phys*., **1965**, *42*, 1293.

14. Dunning, T. H. *J. Chem. Phys*., **1970**, *53*, 2823.

15. Thomas, J. R.; Deleeuw, B. J.; Vacek, G.; Crawford, T. D.; Yamaguchi, Y.; Schaefer, H. F. *J. Chem. Phys.*, **1993**, *99*, 403.

16. Dunning, T. H. *J. Chem. Phys*., **1971**, *55*, 716.

17. Wachters, A. J. H. *J. Chem. Phys.,* **1970**, *52*, 1033.

18. Stanton, J. F. *J. Chem. Phys.,* **1993**, *99*, 8804

19. Stanton, J. F.; Bartlett, R. J. *J. Chem. Phys.,* **1993**, *98*, 7029.

20. Purvis, G. D.; Bartlett, R. J. *J. Chem. Phys.,* **1982**, *76*, 1910.

CHAPTER 2

THE RULE BREAKING $Cr_2(CO)_{10}$. A 17 ELECTRON Cr SYSTEM OR A Cr=Cr DOUBLE BOND?[1]

[1] Se Li, Nancy A. Richardson, Yaoming Xie, R. Bruce King, Henry F. Schaefer III. 2003. Faraday Discuss., 124: 315–329. Reprinted by permission of the Royal Society of Chemistry.

2.1 ABSTRACT

Density functional theory (DFT) has been used to investigate the conformations and thermochemistry on the singlet and triplet potential energy surfaces (PES) of $Cr_2(CO)_{10}$. The global minimum energy structure for the lowest singlet state of C_{2h} symmetry is consistent with a model of two interacting $Cr(CO)_5$ fragments in which one carbonyl in each fragment acts as an asymmetric four-electron donor bridging carbonyl, with chromium-chromium distances of 2.93 Å (B3LYP) or 2.83 Å (BP86). Avoiding a Cr···Cr bond by incorporating four-electron donor CO groups in this way allows each chromium atom in singlet $Cr_2(CO)_{10}$ to attain the favored 18-electron configuration by using, in a simple picture of the bonding, only the six octahedral sp^3d^2 hybrids. The dissociation energy to two $Cr(CO)_5$ fragments or to $Cr(CO)_6$ + $Cr(CO)_4$ fragments is predicted to be 10 kcal/mol. The lowest triplet state of $Cr_2(CO)_{10}$ is predicted to lie ~10 kcal/mol above the singlet global minimum. In the case of triplet $Cr_2(CO)_{10}$ the lowest energy minima were found to be of C_2 and C_{2h} symmetry, with similar energies. The chromium-chromium distances in triplet $Cr_2(CO)_{10}$ were found to be shorter than those in the corresponding singlet structures, namely 2.81 (B3LYP) or 2.68 Å (BP86) suggesting a $\sigma + 2(^1/_2)$ π Cr=Cr double bond similar to the O=O bond in O_2 or the Fe=Fe bond in the experimentally observed triplet state $(Me_5C_5)_2Fe_2(\mu\text{-}CO)_3$.

2.2 INTRODUCTION

Recently our group has studied saturated homoleptic binuclear carbonyls of first row transition metals such as nickel, iron, and cobalt using carefully calibrated methods from density functional theory (DFT). The results are in reasonable agreement with available experimental values for geometries and thermodynamic quantities. These theoretical methods have been extended to unsaturated binuclear metal carbonyls. Optimized structures were found exhibiting the following features: (a) Metal-metal multiple bonds with the favored 18-electron rare gas metal electronic configuration such as formal M=M double bonds in $Ni_2(CO)_6$ and $Fe_2(CO)_8$, and formal M≡M triple bonds in $Ni_2(CO)_5$, $Co_2(CO)_6$, and $Fe_2(CO)_7$; (b) Four-electron bridging carbonyl groups with the favored 18-electron metal electronic configuration such as in C_{2h} symmetry $Fe_2(CO)_6$; (c) Metal electron configurations with fewer than 18 electrons, such as the 16-electron configurations for d^8 metal atoms found in unbridged $Co_2(CO)_7$, analogous to the known $CoRh(CO)_7$.

These results lead to further exploration of structures for as yet undetected unsaturated homoleptic binuclear carbonyls of the first row transition metals by DFT methods. This paper reports our $Cr_2(CO)_{10}$ research. Simple electron counting indicates that if all ten CO groups are the usual donors of two electrons each, then a Cr=Cr double bond is required to give each chromium atom the favored 18-electron configuration in $Cr_2(CO)_{10}$.

Our previous results for the saturated homoleptic binuclear chromium carbonyl $Cr_2(CO)_{11}$ showed this compound to have a flat potential energy surface and to be

thermodynamically unstable with respect to dissociation to $Cr(CO)_5$ and $Cr(CO)_6$. This accounts for the experimental lack of $Cr_2(CO)_{11}$ isolation. Substitution of the bridging CO in $Cr_2(CO)_{11}$ with a hydride produces the stable and well-known $HCr_2(CO)_{10}^-$, for which we also predicted the gas phase structure and compared it to two X-ray structures. Deprotonation of $HCr_2(CO)_{10}^-$ results in the known $Cr_2(CO)_{10}^{2-}$, which has also been structurally characterized. Electrochemical experiments have examined the one-electron oxidation of $Cr_2(CO)_{10}^{2-}$ to form $Cr_2(CO)_{10}^-$ and the process of Cr-Cr bond cleavage. Two-electron oxidation of $Cr_2(CO)_{10}^{2-}$ results in neutral $Cr_2(CO)_{10}$. Transient (lifetime ~ 10^{-3} seconds) $Cr_2(CO)_{10}$ has been observed in photochemical studies in which $Cr(CO)_4$ reacts with $Cr(CO)_6$. These experimental results indicate that $Cr_2(CO)_{10}$ may have greater stability than $Cr_2(CO)_{11}$, and thus theoretical investigation of $Cr_2(CO)_{10}$ has been undertaken to determine the nature of this molecule and reasons for its stability.

Since in some unsaturated binuclear metal compounds, the triplet state may lie lower in energy than the singlet, both electronic states have been investigated for $Cr_2(CO)_{10}$. The computed optimized structures for both the singlet and triplet states of the neutral $Cr_2(CO)_{10}$ molecule are presented in Figure 1 (singlet) and Figure 2 (triplet). Analysis of the relationships between the geometries, harmonic vibrational frequencies, and thermodynamic stabilities of the structures in each electronic state illustrate how the loss of two electrons perturbs the highly symmetric D_{4h} dianion $Cr_2(CO)_{10}^{2-}$. These analyses also provide some insight into the nature of

this unsaturated Cr-Cr bond as well as the difference in predictions between the B3LYP and BP86 functionals.

2.3 THEORETICAL METHODS

Our basis set for C and O begins with Dunning's standard double-ζ contraction of Huzinaga's primitive sets and is designated (9s5p/4s2p). The double-ζ plus polarization (DZP) basis set used here adds one set of pure spherical harmonic *d* functions with orbital exponents α_d(C) = 0.75 and α_d(O) = 0.85 to the DZ basis set. For Cr, our loosely contracted DZP basis set, the Wachters' primitive set, is used, but augmented by two sets of *p* functions and one set of *d* functions, contracted following Hood, Pitzer and Schaefer and designated (14s11p6d/10s8p3d). For $Cr_2(CO)_{10}$, there are 398 contracted Gaussian functions in the present flexible DZP basis set.

Electron correlation effects were included employing DFT methods, which are acknowledged to be a practical and effective computational tool, especially for organometallic compounds. Among density functional procedures, the most reliable approximation is often thought to be the hybrid Hartree-Fock (HF)/DFT method, B3LYP, which uses the combination of the three-parameter Becke exchange functional with the Lee-Yang-Parr correlation functional.[9] However, another DFT method, which combines Becke's 1988 exchange functional with Perdew's 1986 nonlocal correlation functional method (BP86)[10], has proven effective and is also used in this research.

We fully optimized the geometries of all structures with the DZP B3LYP and DZP BP86 methods. At the same levels we also computed the vibrational frequencies by analytically evaluating the second derivatives of the energy with respect to the nuclear coordinates. The

corresponding infrared intensities are evaluated analytically as well. All of the computations were carried out with the Gaussian 94 program, exercising the fine grid (75 302) option for evaluating integrals numerically, and the tight (10^{-8} hartree) designation is the default for the self-consistent field (SCF) convergence. Cases for which finer integration grids were used are addressed below.

In the search for minima using all currently implemented DFT methods, low- magnitude imaginary vibrational frequencies are suspect because of significant limitations in the numerical integration procedures used. Thus, for an imaginary vibrational frequency with a magnitude less than $100\,cm^{-1}$, there is an energy minimum identical to or very close to the structure of the stationary point in question. Therefore, we generally do not follow such low imaginary vibrational frequencies. However, we reevaluated the D_{4h} structure of $Cr_2(CO)_{10}$ with finer integration grids, but the small imaginary vibrational frequencies persisted. For low harmonic vibrational frequencies, the DFT methodology requires further development to yield rock solid predictions. However, continued efforts to discover and document patterns within systems which display these discrepancies will provide both direction in the development of DFT and insight into "unusual" bonding situations.

2.4 RESULTS

2.4.1 THE RELIABILITY OF DFT FOR CHROMIUM CARBONYLS

Our previous work has shown that geometries and vibrational frequencies predicted using B3LYP and BP86 DFT functionals were in reasonable agreement (~0.02 Å for bond distances)

with experimental and higher level theoretical results for $Cr(CO)_6$, $Cr(CO)_5$, $[Cr(CO)_5H]^-$, and $[Cr(CO)_4H]^-$. In that work similar agreement was also found for $[(\mu\text{-}H)Cr_2(CO)_{10}]^-$, for which an experimental geometry is known. The prediction for the bridged species is similar to that for the solid crystal owing to the Cr-H interaction and the stabilizing nature of the bridging species. This is in contrast to the $[Cr_2(CO)_{10}]^{2-}$ dianion which is predicted to have a somewhat longer Cr—Cr distance, (3.30 Å, both functionals) than the experimental distances (2.98-3.00 Å) for Cr—Cr in $[Cr_2(CO)_{10}]^{2-}$ crystals. The difference between the isolated gas phase species, in which some bond lengthening is possible, and the constrained environment of the solid crystal may account for this difference in the dianion geometry. With only the dianion differing significantly from experimentally determined geometry (explainable by the effects of excess charge), these results indicate at least a qualitative reliability of DFT for these molecules.

2.4.2 SINGLET $Cr_2(CO)_{10}$

The fully optimized structures for the singlet electronic state of $Cr_2(CO)_{10}$ (sketched in Figure 1) are displayed in Figures 3, 4, and 5. The relative energies of the structures and corresponding imaginary harmonic vibrational frequencies are listed in Table 1.

Figure 3 shows the dibridged C_{2h} structure having all real harmonic vibrational frequencies; the electronic state is ^1A_g. This structure is a genuine minimum with both the B3LYP and BP86 functionals and has the lowest energy among all nine neutral $Cr_2(CO)_{10}$ structures examined here. In addition, the energy of the C_{2h} conformer is lower than that of two $Cr(CO)_5$ fragments by 8.6 (B3LYP) or 16.6 kcal/mol (BP86), respectively. For fragmentation to

$Cr(CO)_6$ and $Cr(CO)_4$ the energy differences are 7.9 kcal/mol (B3LYP) and 15.1 kcal/mol (BP86).

The relatively long Cr–Cr distance (B3LYP, 2.928 Å; BP86, 2.832 Å) in the $Cr_2(CO)_{10}$ structure of C_{2h} symmetry suggests that the Cr···Cr interaction takes place primarily through the π bonds of the bridging CO groups rather than through multiple bonding between the two chromium atoms. The Cr–C distances of the four symmetry equivalent perpendicular terminal carbonyls are 1.925 Å (B3LYP) or 1.909 Å (BP86). The four unique Cr–C distances in the C–Cr–Cr–C plane are found to be 1.923 Å for the shorter bridging Cr–C and 1.931 Å for the terminal Cr–C opposite to the shorter bridging Cr–C. Similarly, the distances are 2.589 Å for the longer bridging Cr-C and 1.865 Å for the terminal Cr-C opposite to the longer bridging Cr–C with the B3LYP method. With the BP86 functional the respective distances are 1.920 Å, 1.905 Å, 2.463 Å and 1.848 Å. The first two Cr–C distances in $Cr_2(CO)_{10}$ are very close to the analogous computed Cr–C distances in $Cr(CO)_5$ (1.923 Å B3LYP and 1.905 Å BP86), specifically the ^1A_g state of C_{4v} symmetry.[7] However, the Cr–C distances for the remaining bridging carbonyls are much longer. The increased distance reflects the significantly weaker interaction in the bridging Cr–C compared to the terminal Cr–C distance computed for the $Cr(CO)_5$ fragment. The corresponding C–O distances are as follows: 1.155 Å, 1.159 Å, 1.162 Å and 1.152 Å with B3LYP and 1.169 Å, 1.173 Å, 1.178 Å and 1.167 Å with BP86, which are again nearly the same as the computed C–O distances in $Cr(CO)_5$ (1.162 Å with B3LYP and 1.171 with BP86). These distances also compare favorably with the experimentally known values in $Cr(CO)_6$ of 1.916±0.002 Å ($r_{Cr\text{-}C}$) and 1.140±0.003 Å ($r_{C\text{-}O}$).

Finally, consideration of the Cr–C–O angles for the shorter bridging carbonyl shows significant deviation from linearity at 165.7º (B3LYP) and 164.8º (BP86). This deviation is in accord with the proposed π-bonding from the C–O bond of this carbonyl to a chromium atom. The other four Cr–C–O angles remain close to 180°. The C–Cr–C angles are also computed to be close to 90º, as shown in Figure 3. Thus it is logical to conclude that the lowest energy structure for $Cr_2(CO)_{10}$ is an 18-electron species, in which the longer bridging carbonyls contribute two π electrons to complete the 18 electron configuration for each chromium atom.

Imposing C_{2v} symmetry forces the bridging carbonyls to produce the C_{2v} structure with an $^1A_1$ electronic wavefunction. The two structures thus produced are shown in Figures 4a (B3LYP) and 4b (BP86). With the B3LYP method this structure has no imaginary harmonic vibrational frequencies and is only 1.6 kcal/mol higher than the C_{2h} structure. However, with the BP86 method this structure has one significantly large imaginary harmonic vibrational frequency of b_2 symmetry at 348i cm^{-1} and two small imaginary vibrational frequencies at 50i (a_2) and 40i cm^{-1} (b_1). The larger BP86 imaginary vibrational frequency corresponds to a return to the lower energy C_{2h} structure that lies 7.9 kcal/mol lower. As discussed above, we only consider imaginary vibrational frequencies with magnitudes over 100 cm^{-1} to be indisputable. This is another example showing that the B3LYP and BP86 are sometimes inconsistent in predicting the number of the imaginary frequencies for these metal dimers. In either case, we conclude that the C_{2v} structure is not a genuine minimum but rather a higher order stationary point on the energy surface for BP86.

The geometric differences between the B3LYP and BP86 C_{2v} structures for singlet $Cr_2(CO)_{10}$ (Figure 4) are also striking. Unexpectedly, the chromium–chromium distance is a very long 4.311 Å with the B3LYP functional. It appears that a loosely associated complex of

$Cr(CO)_4$ and $Cr(CO)_6$ forms with a bridging Cr ···O distance of 2.545 Å (B3LYP), implying that the two fragments have a very weak connection. However, with BP86 the Cr–Cr bond distance is 2.834 Å, which is essentially the same as the Cr–Cr bond distance in C_{2h} symmetry (2.832 Å, BP86). This C_{2v} structure behaves similarly to other binary homoleptic transition metal carbonyls where the B3LYP and BP86 methods sometimes lead to widely different structural predictions[3,5] and so a direct comparison cannot be made. However, in previous work the BP86 functional performed better for the prediction of the $[(\mu\text{-H})Cr_2(CO)_{10}]^-$ structure, and similar confidence may be warranted here since the HF component without electron correlation can lead to the errors in B3LYP.

Imposition of further symmetry constraints produces the dibridged D_{2h} structure, the last of the singlet structures considered (Figure 5). Both the B3LYP and BP86 functionals yield several imaginary vibrational frequencies above 100 cm^{-1} for this structure, including the b_{2g} frequency at 404i cm^{-1} (B3LYP) or 438i cm^{-1} (BP86) and the b_{3u} frequency at 153i cm^{-1} (B3LYP). These normal modes correspond to motions that reduce the symmetry to the lower energy C_{2v} and C_{2h} structures. Also, the D_{2h} structure is higher by 9.2 kcal/mol (B3LYP) or 8.4 kcal/mol (BP86) than the C_{2h} global minimum. Clearly, this symmetric dibridged $Cr_2(CO)_{10}$ structure is a not a minimum. However, the predicted chromium-chromium distance for this structure is the shortest among the three singlet structures, namely 2.724 Å (B3LYP) or 2.678 Å (BP86) but obviously still in the range of a single bond. The dibridging Cr–C distance is 2.170 Å (B3LYP) or 2.135 Å (BP86) which is longer than the Cr–C distance in the $Cr(CO)_5$ fragment (1.923 Å B3LYP and 1.905 Å BP86) and also longer than the experimental $Cr(CO)_5$ distance of 1.916 Å.

2.4.3 TRIPLET $Cr_2(CO)_{10}$

For singlet $Cr_2(CO)_{10}$, stationary points were found for three symmetries, all lying close in energy. However, for triplet $Cr_2(CO)_{10}$, structures were found of six different symmetries, all lying about 10 kcal/mol above the singlet structures in energy. Thus the singlet C_{2h} structure is the global energy minimum among all of the $Cr_2(CO)_{10}$ structures studied. The relative energies of the triplet $Cr_2(CO)_{10}$ structures and their imaginary harmonic vibrational frequencies are listed in Table 2. For triplet $Cr_2(CO)_{10}$ (Figure 2) the fully optimized structures are shown in Figures 6–11.

Figure 6 shows the unbridged staggered C_2 structure of the lowest energy B3LYP triplet electronic state, ^3B, which is a genuine minimum with both the B3LYP and BP86 methods. However, using the BP86 functional the doubly bridged C_{2h} structure shown in Figure 7 lies lower than the C_2 structure by 0.1 kcal/mol. Remarkably, the C_2 and the C_{2h} structures differ considerably in geometry. Furthermore, the C_2 triplet $Cr_2(CO)_{10}$ is higher in energy than its two constituent singlet fragments of $Cr(CO)_5$ by 4.1 kcal/mol with B3LYP and lower by 3.4 kcal/mol with BP86. In order to explore the accommodation of electrons around Cr in terms of the 18-electron rule, the Cr-Cr distance, the Cr-C distances, and the Cr-Cr-C angles in this triplet $Cr_2(CO)_{10}$ isomer are compared with those in $Cr_2(CO)_{10}^{2-}$, which is a saturated compound where the Cr-Cr single bond gives each chromium atom the favored 18-electron noble gas configuration. The Cr–Cr distance in $Cr_2(CO)_{10}$ is computed to be 2.805 Å (B3LYP) and 2.726

Å (BP86), which is significantly shorter than the theoretical Cr–Cr distance of 3.30 Å in the $Cr_2(CO)_{10}^{2-}$ dianion. This might suggest the existence of a weak Cr=Cr double bond, similar to the oxygen-oxygen double bond in O_2 in which a single σ bond is complemented by "half-bonds" involving a single bonding electron in each of the two perpendicular π orbitals. An organometallic example of a similar triplet metal-metal double bond is the Fe=Fe double bond in $(\eta^5\text{-}Me_5C_5)_2Fe_2(\mu\text{-}CO)_3$ (**I**), which has been characterized

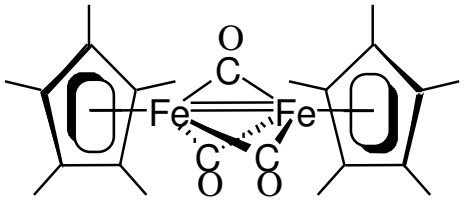

I

structurally (Fe=Fe of 2.27 Å) and which has an experimental magnetic moment of 2.5 ± 0.1 μ_B, corresponding to a triplet ground state.

The Cr–C bond lengths of the five nonequivalent carbonyls in the triplet C_2 symmetry $Cr_2(CO)_{10}$ are in the range: 1.903 Å–1.946 Å (B3LYP) or 1.873 Å–1.925 Å (BP86). The two methods both show that the axial Cr–C bond lengths are shorter than those of the Cr–C (1.923 Å B3LYP and 1.905 Å BP86) in the constituent $Cr(CO)_5$ fragments or in $Cr(CO)_6$ with the experimentally known 1.916±0.002 Å ($r_{Cr\text{-}C}$). This suggests an increased interaction between the chromium and the carbon atoms (along the C_{4v} axis in the $Cr(CO)_5$ fragment) leading to formation of the Cr=Cr bond. The corresponding C–O distances remain nearly the same

compared to the C–O bond length in the $Cr(CO)_5$ fragment. In similar fashion to the singlet, the terminal Cr–C–O bond angle closes up from 180º to 172.5º with B3LYP and to 166.5º with BP86. However, these two corresponding carbonyls are no longer in the same plane and have very long distances (2.892 Å B3LYP and 2.628 Å BP86) to the opposite chromium atom. These distances are even greater than the Cr–C long-bridging distance (2.589 Å B3LYP and 2.463 Å BP86) in the singlet C_{2h} minimum. Also, the Cr–Cr–C angles (with the axial carbonyls) are 159.4º (B3LYP) and 150.8º (BP86). This implies a much weaker interaction between the bridging Cr–C in the triplet C_2 structure, providing further indication of greater bond strength than in the three previously discussed singlet structures. Finally, both the Cr–C–O and the C–Cr–C angles remain nearly unchanged compared to the corresponding angles in the $Cr(CO)_5$ fragments.

Lying close in energy to the C_2 structure but with two bridging carbonyls is the ^3B_g electronic state of C_{2h} symmetry shown in Figure 7. With the BP86 functional it lies the lowest energetically (by about 0.1 kcal/mol) among the six triplet structures and has all real harmonic vibrational frequencies. However, with the B3LYP functional it has one very small imaginary vibrational frequency of a_{1u} symmetry at 18i cm^{-1} and an energy 2 kcal/mol higher than the C_2 minimum, indicating that this structure is either a minimum or very close to one. The C_{2h} structures of the singlet and the triplet electronic states differ in three parameters: the Cr–Cr distance, the difference in bridging lengths, and the different Cr–C–O angle. Firstly, the Cr–Cr distance is shortened from 2.928 Å to 2.818 Å (B3LYP) and from 2.832 Å to 2.677 Å (BP86). Secondly, for the longer bridging carbonyl, the B3LYP functional predicts lengthening from 2.589 Å to 2.652 Å whereas BP86 suggests shortening from 2.463 Å to 2.258 Å. Lastly, B3LYP

computes the Cr–C–O angle to be 165º, which is nearly the same as in the singlet C_{2h} structure, while BP86 computes the value of 152º, which is much more bent than in the singlet C_{2h} structure, 164º. This not only provides evidence that a double bond for the triplet structure may exist with B3LYP, like the triplet C_2 structure, but also that bridging π interactions may occur similar to those in the singlet C_{2h} structure for BP86.

The further geometric constraint of forcing the bridging carbonyls to be symmetric leads to the C_{2v} dibridged structure (the $^3A_2$ electronic state lies lower with B3LYP, and the $^3B_2$ electronic state lies lower with BP86) shown in Figure 8. This structure is higher lying energetically by 2.5 kcal/mol and 5.7 kcal/mol above the triplet minima, namely the C_2 structure, with B3LYP and the C_{2h} structure, with BP86, respectively. The C_{2v} structure has only one imaginary vibrational frequency at 74i cm^{-1} b_2 symmetry, B3LYP and at 119i cm^{-1} b_1 symmetry, BP86. However, it should be noted that the imaginary mode is not along the same coordinate for each functional at 74i cm^{-1} (b_2 symmetry, B3LYP) and at 119i cm^{-1} (b_1 symmetry, BP86). This imaginary vibrational frequency shows that the structure is not a minimum, since it leads back to the staggered C_2 minimum. Similarly, for BP86, the frequencies lead back to the eclipsed C_{2h} minimum.

Imposing further symmetry constraints on the triplet structure leads to the dibridged D_{2h} structure ($^3B_{3g}$ electronic state) which is shown in Figure 9. Similar to the singlet D_{2h} structure (Figure 5), the dibridged $Cr_2(CO)_{10}$ has the shortest Cr–Cr distance (2.679 Å B3LYP and 2.648 Å BP86) among the nine structures considered here. The bridging Cr–C distances (2.110 Å B3LYP and 2.098 Å BP86) for this structure are longer than the Cr–C bond distance in $Cr(CO)_5$ (1.923 Å B3LYP and 1.905 Å BP86). Thus we assign to this structure a four-center six π

electron bond. For the B3LYP method the dibridged D_{2h} $Cr_2(CO)_{10}$ has two imaginary vibrational frequencies: one at 105i cm^{-1} (b_{2g} symmetry) that corresponds to the C_{2h} structure and one at 80i cm^{-1} (b_{3u} symmetry) that corresponds to the C_{2v} structure. The one imaginary frequency of the BP86 functional, namely a b_{2g} mode, is predicted at 95i cm^{-1}. The energy is 2.9 kcal/mol above the triplet minimum C_2 with B3LYP and 0.2 kcal/mol above the triplet minimum C_{2h} with BP86. Therefore we conclude that the D_{2h} structure is not a genuine minimum, but energetically very close to the C_{2h} minimum.

Our highest symmetry structures that might formally possess a Cr=Cr double bond are the unbridged D_{4d} ($^3A_1$ electronic state) and D_{4h} ($^3A_{2g}$ electronic state) structures of $Cr_2(CO)_{10}$ shown in Figures 10 and 11. Unexpectedly, both the D_{4d} and D_{4h} structures have quite long chromium-chromium distances, for the former 2.731 Å (B3LYP) and 2.704 Å (BP86), and 2.827 Å (B3LYP) or 2.795 Å (BP86) for the latter. The staggered D_{4d} structure (Figure 10) is qualitatively similar to the eclipsed D_{4h} structure (Figure 11). However, the latter has a chromium-chromium distance that is longer by 0.096 Å (B3LYP) and 0.091 Å (BP86), consistent with simple steric repulsion arguments. For the D_{4d} structure the two equatorial and one axial Cr–C bond distances are predicted to be 1.937 Å and 1.941 Å (B3LYP), respectively or 1.921 Å and 1.910 Å (BP86), which are quite similar to the corresponding bond lengths of $Cr(CO)_5$ and to the experimental $Cr(CO)_6$ distance of 1.916 Å. The axial C–O distances are interesting in that these are identical to the B3LYP and BP86 results for $Cr(CO)_5$ and the experimental result for $Cr(CO)_6$. However, the Cr–C distances are slightly longer. This lengthening suggests a very weak interaction between the two equivalent $Cr(CO)_5$ fragments.

From vibrational frequency analyses neither the D_{4d} nor D_{4h} structure is a true minimum on the potential energy surface. For the D_{4d} structure, both methods yield a degenerate harmonic vibrational frequency, e_3, at 509i cm^{-1} (B3LYP) and 235i cm^{-1} (BP86). For the D_{4h} structure B3LYP yields one harmonic imaginary vibrational frequency of 22i cm^{-1} (a_{1u}), while BP86 yields three harmonic imaginary vibrational frequencies of 363i cm^{-1} (e_g) mode and 20i cm^{-1} (a_{1u} mode). The a_{1u} mode (for both B3LYP and BP86) corresponds to an internal rotation changing the symmetry to D_{4d}. Similarly, the BP86 e_g symmetry normal modes lead to the lower symmetry C_{2h} structure.

With B3LYP, we have pursued the possibility that the small imaginary vibrational frequency (22i cm^{-1}, a_{1u}) is fictitious for the D_{4h} structure. As discussed in the Theoretical Methods section, these results are obtained with the (75 302) grid. For the D_{4h} structure of Figure 11, we reoptimized the B3LYP geometry with the (99 590) numerical integration grid. The B3LYP structure is essentially unchanged, with the Cr–Cr distance decreasing insignificantly from 2.827 Å to 2.826 Å. With the tighter grid the a_{1u} vibrational frequency increases slightly to 24i cm^{-1}. Therefore, we conclude that this imaginary a_{1u} vibrational frequency is genuine and that this structure is extremely close to a structure of slightly lower symmetry.

2.5 DISCUSSION

The optimized structures for $Cr_2(CO)_{10}$ may be related to resonance between (a) structure **IIa** with no direct Cr ···Cr bond and two special bridging carbonyls donating four electrons each; and (b) structure **IIb** with a Cr=Cr double bond and only terminal CO

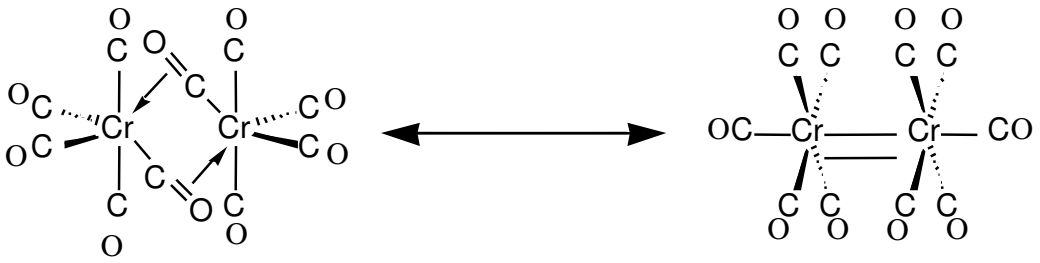

IIa **IIb**

groups donating two electrons each. In structure **IIa**, which is favored for singlet $Cr_2(CO)_{10}$ (Figure 3), each of the bridging CO groups thus donates a lone pair to one chromium atom through a Cr–C two-electron two-center bond. The latter is similar to the usual bonds between metal atoms and terminal CO groups in most metal carbonyls including $Cr(CO)_6$. In addition, these bridging CO groups donate a second electron pair to the other chromium atom through a longer π-bond from the multiple carbon-oxygen bond. These two bridging carbonyl groups in structure **IIa** are thus similar to the unique bridging carbonyl group in the binuclear manganese carbonyl complex $(Ph_2PCH_2PPh_2)_2$–$Mn_2(CO)_4$(μ-CO) (**III**), which has been isolated and its structure

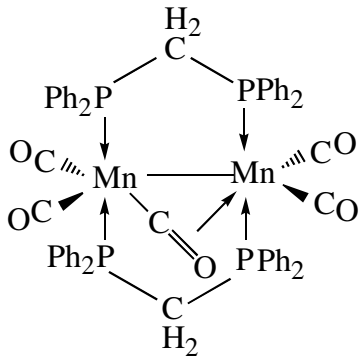

III

determined by X-ray diffraction. Each chromium atom in structure **IIa** for $Cr_2(CO)_{10}$ uses octahedral sp^3d^2 hybridization to form six bonds to carbonyl groups, sufficient to give each chromium atom the favored 18-electron rare gas configuration, since the two bridging CO groups each form bonds with such a hybrid from each chromium atom. The pervasive tendency of zerovalent chromium to form such octahedral hybrid orbitals is reflected first in the high stability of octahedral $Cr(CO)_6$. However, this tendency is also seen in the preference of $H_2Cr(CO)_5$, which has been characterized spectroscopically at low temperatures, for the structure of a dihydrogen complex $(H_2)Cr(CO)_5$ (**IVa**). The latter uses six octahedral hybrid orbitals rather than the dihydride $(H)_2Cr(CO)_5$ (**IVb)**, which requires a less favorable set of seven hybrid orbitals, presumably some type of sp^3d^3 hybrid.

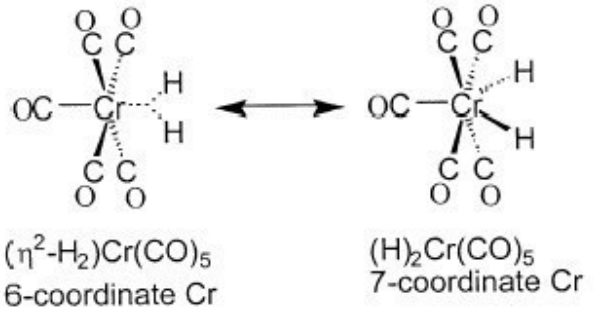

IVa **IVb**

The lowest energy structure for triplet $Cr_2(CO)_{10}$ (Figure 6) is a Cr=Cr doubly bonded structure (**IIb**) having only terminal CO groups. In this structure the Cr=Cr double bond consists of two perpendicular one-electron π "half-bonds" (designated $^2/_2$ π here and in our abstract) similar to the O=O bond in O_2 or the Fe=Fe bond in $(\eta^5\text{-}Me_5C_5)_2Fe_2(\mu\text{-}CO)_3$ (**I**). Assuming that the metal-metal bond axis is the *z*-axis, these perpendicular one-electron π-half-bonds use the metal d_{xz} and d_{yz} orbitals, which are not involved in the $sp^3d^2(z^2, x^2–y^2)$ octahedral hybridization of each chromium atom required for the six σ bonds (i. e., the bonds to the five terminal CO groups and the Cr–Cr σ-bond). In the symmetry point group for the lowest energy triplet $Cr_2(CO)_{10}$ structure (C_2), the metal d_{xz} and d_{yz} orbitals are not strictly degenerate since the C_2 point group has only non-degenerate irreducible representations. This differs from both the $D_{\infty h}$ point group of O_2 and the D_{3h} local symmetry of the Fe=Fe bond in $(\eta^5\text{-}Me_5C_5)_2Fe_2(\mu\text{-}$

$CO)_3$ (**I**) in which the metal d_{xz} and d_{yz} orbitals belong to the two-fold degenerate irreducible representations e″ and π_g, respectively. However, the analysis of the imaginary vibrational frequencies for D_{4h} triplet $Cr_2(CO)_{10}$ discussed above suggests that the lowest energy C_2 structure for triplet $Cr_2(CO)_{10}$ (Figure 6) may be very close to the D_{4h} structure (Figure 11), differing only by tilting the $Cr(CO)_5$ "halves" of local C_{4v} symmetry. If this is the case, then the energy difference between the metal d_{xz} and d_{yz} orbitals in the C_2 structure of triplet $Cr_2(CO)_{10}$ may be smaller than the pairing energy of the two electrons so that a triplet rather than a singlet structure is preferred. Note that in the D_{4h} point group the metal d_{xz} and d_{yz} orbitals belong to the two-fold degenerate irreducible representation E_g.

2.6 ACKNOWLEDGMENTS

We are grateful for the support of this work by NSF Grant CHE-0136186. We also thank Joseph Kenny for helpful discussions and technical assistance with the computations.

2.7 LITERATURE REFERENCES

1 Ignatyev, I. S.; Schaefer, H. F.; King, R. B.; Brown, S. T. *J. Amer. Chem.* Soc., **2000**, *122*, 1989.

2 Xie, Y.; Schaefer, H. F.; King, R. B. *J. Amer. Chem. Soc.*, **2000**, *122*, 8746.

3 Kenny, J. P.; King, R. B.; Schaefer, H. F. *Inorg. Chem.*, **2001**, *40*, 900.

4 Kohn, W.; Sham, L. J.; *Phys. Rev. A,* **1965,** *140*, 1133.

5 Horvath, I. T.; Bor, G.; Garland, M.; Pino, P., *Organometallics*, **1986**, *5*, 1441.

6 Green, M. L. *J. Organomet. Chem*. **1995**, *500*, 127.

7 Richardson, N. A.; Xie, Y.; King, R. B.; Schaefer, H. F. *J. Phys. Chem.A,* **2001**, *105*, 11134.

8 Barnes, L. A.; Liu, B. W.; Lindh, R. *J. Chem. Phys.* **1993**, *98*, 3978.

9 Rees, B.; Mitschler, A. *J. Am. Chem. Soc.* **1976**, *98*, 7918.

10 Hey-Hawkins, E.; von Schnering, H. G. *Chem. Ber*. **1991**, *124,* 1167.

11 Lee, I.; Geib, S. J.; Copper, N. H. *Acta Crystallogr., Sect. C* **1996,** *C52*, 292.

12 Borrmann, H.; Pirani, A. M.; Schrobilgen, G. J. *Acta Crystallogr., Sect. C* **1997**, *C53*, 19.

13 Phillips, J. R.; Trogler, W. C. *J. Phys. Chem.*, **1992**, *198*, 633.

14 Fletcher, T. R.; Rosenfeld, R. N. *J. Am. Chem. Soc.*, **1985**, *107*, 2203.

15 Dunning, T. *J. Chem. Phys.*, **1970**, *53*, 2823.

16 Huzinaga, S. *J. Chem. Phys.* **1965**, *42*, 1293.

17 Wachters, A. J. H. *J. Chem. Phys.* **1970**, *52*, 1033.

18 Hood, D. M.; Pitzer, R. M.; Schaefer, H. F. *J. Chem. Phys*. **1979**, *71*, 705.

19 Ziegler, T. *Can. J. Chem*. **1995**, *73*, 743.

20 Becke, A. D. *J. Chem. Phys.*, **1993**, *98*, 5648.

21 Lee, C., Yang, W., Parr, R. G. *Phys. Rev. B*, **1988**, *37*, 785.

22 Becke, A. D. *Phys. Rev. A*, **1988**, *38*, 3098.

23 Perdew, J. P. *Phys. Rev. B*, **1986**, *33*, 8822; *34*, 7046.

24 Jonas, V.; Thiel, W. *Organometal.* **1998**, *17*, 353.

25 Gaussian 94 (Revision B. 3), Frisch, M. J.; Trucks, G. W.; Schlegel, H. B.; Gill, P. M. W.; Johnson, B. G.; Robb, M. A.; Cheeseman, J. R.; Keith, T.; Petersson, G. A.; Montgomery, J. A.; Raghavachari, K.; Al-Laham, M. A.; Zakrzewski, V. G.; Ortiz, J. V.; Foresman, J. B.; Cioslowski, J.; Stefanov, B. B.; Nanayakkara, A.; Challacombe, M.; Peng, C. Y.; Ayala, P. Y.; Chen, W.; Wong, M. W.; Andres, J. L.; Replogle, E. S.; Gomperts, R.; Martin, R. L.; Fox, D. J.; Binkley, J. S.; Defrees, D. J.; Baker, J.; Stewart, J. P.; Head-Gordon, M.; Gonzalez, C.; Pople, J. A., Gaussian, Inc., Pittsburgh PA, **1995**.

26 Hey-Hawkins, E.; von Schnering, H. G. *Chem. Ber.* **1991**, *124*, 1167.

27 Lee, I.; Cooper, N. H., *Acta Crystallogr., Sect. C*, **1996***, 52*, 292.

28 Jost, A.; Rees, B.; Yelon, W. B. *Acta Crystallogr., Sect. B: Struct. Chrstallorgr. Chryst. Chem.* **1975**, *31*, 2649.

29 Blaha, J. P.; Bursten, B. E.; Dewan, J. C.; Frankel, R. B.; Randolph, C. L.; Wilson, B. A.; Wrighton, M. S., *J. Am. Chem. Soc.*, **1985***, 107*, 4561.

30 Colton, R.; Commons, C. J., *Aust. J. Chem.*, **1975**, *28*, 1673.

31 Commons, C. J.; Hoskins, B. F., *Aust. J. Chem.*, **1975**, *28*. 1663.

32 Upmacis, R. K.; Poliakoff, M.; Turner, J. J., *J. Am. Chem. Soc.*, **1986**, *108*, 3645.

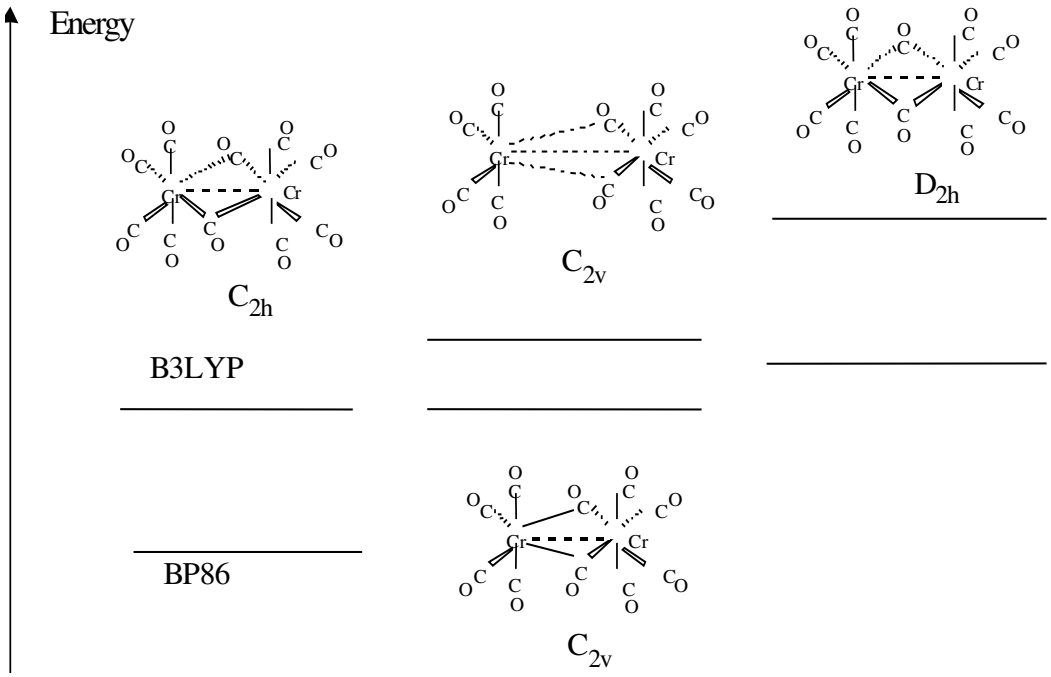

Figure 2.1 Three singlet $Cr_2(CO)_{10}$ structures predicted with the B3LYP and BP86 functionals. The energetic relationship of the structures is $E(C_{2h}) < E(C_{2v}) < E(D_{2h})$. Significant geometric differences exist between the B3LYP and BP86 methods for the C_{2v} structure.

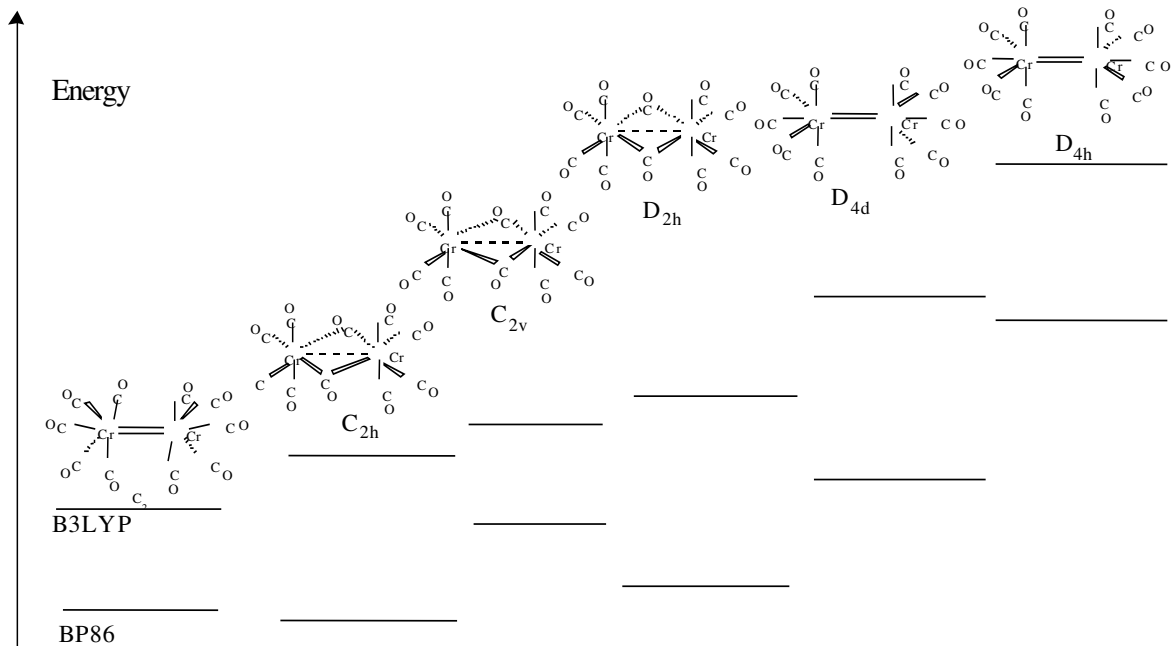

Figure 2.2 Six triplet $Cr_2(CO)_{10}$ structures predicted with the B3LYP and BP86 functionals. The energetic relationship of the structures is $E(C_2) < E(C_{2h}) < E(C_{2v}) < E(D_{2h}) < E(D_{4d}) < E(D_{4h})$ for the B3LYP functional, while it is $E(C_{2h}) < E(C_2) < E(D_{2h}) < E(C_{2v}) < E(D_{4d}) < E(D_{4h})$ for BP86.

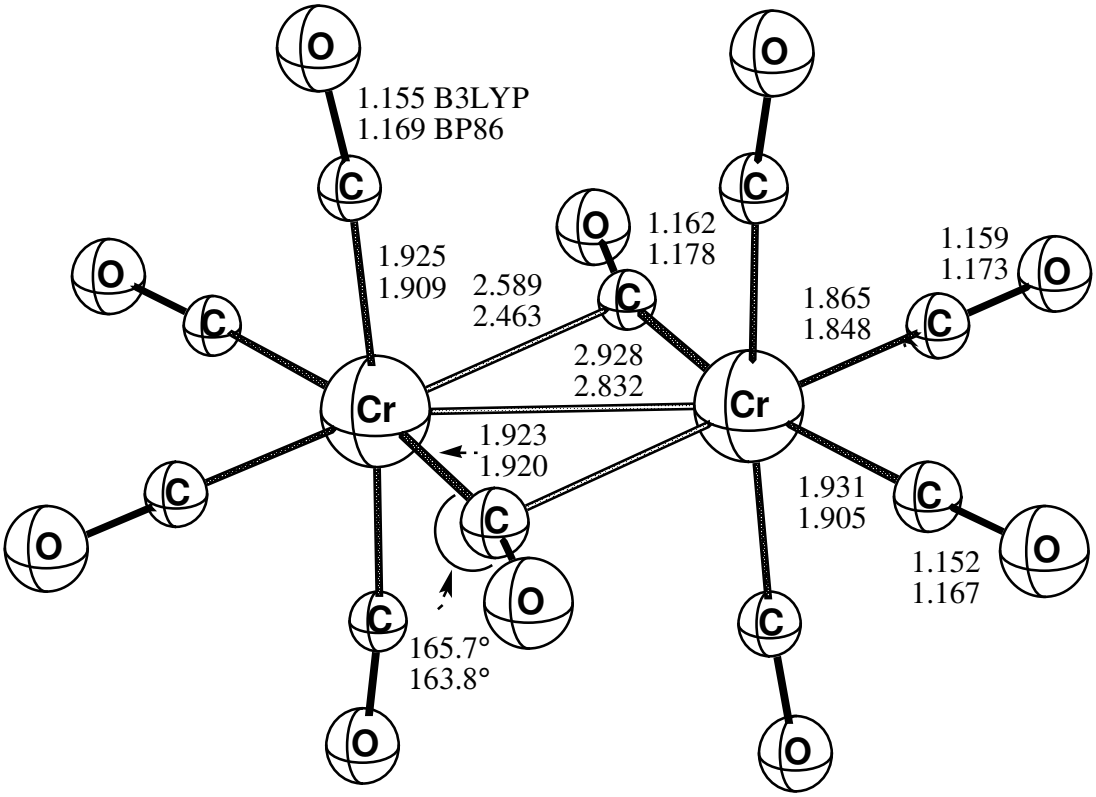

C_{2h}

Figure 2.3 The asymmetrically bridging C_{2h} global minimum energy structure for singlet $Cr_2(CO)_{10}$ (all real harmonic vibrational frequencies) from the B3LYP and BP86 methods. Distances are reported in Å.

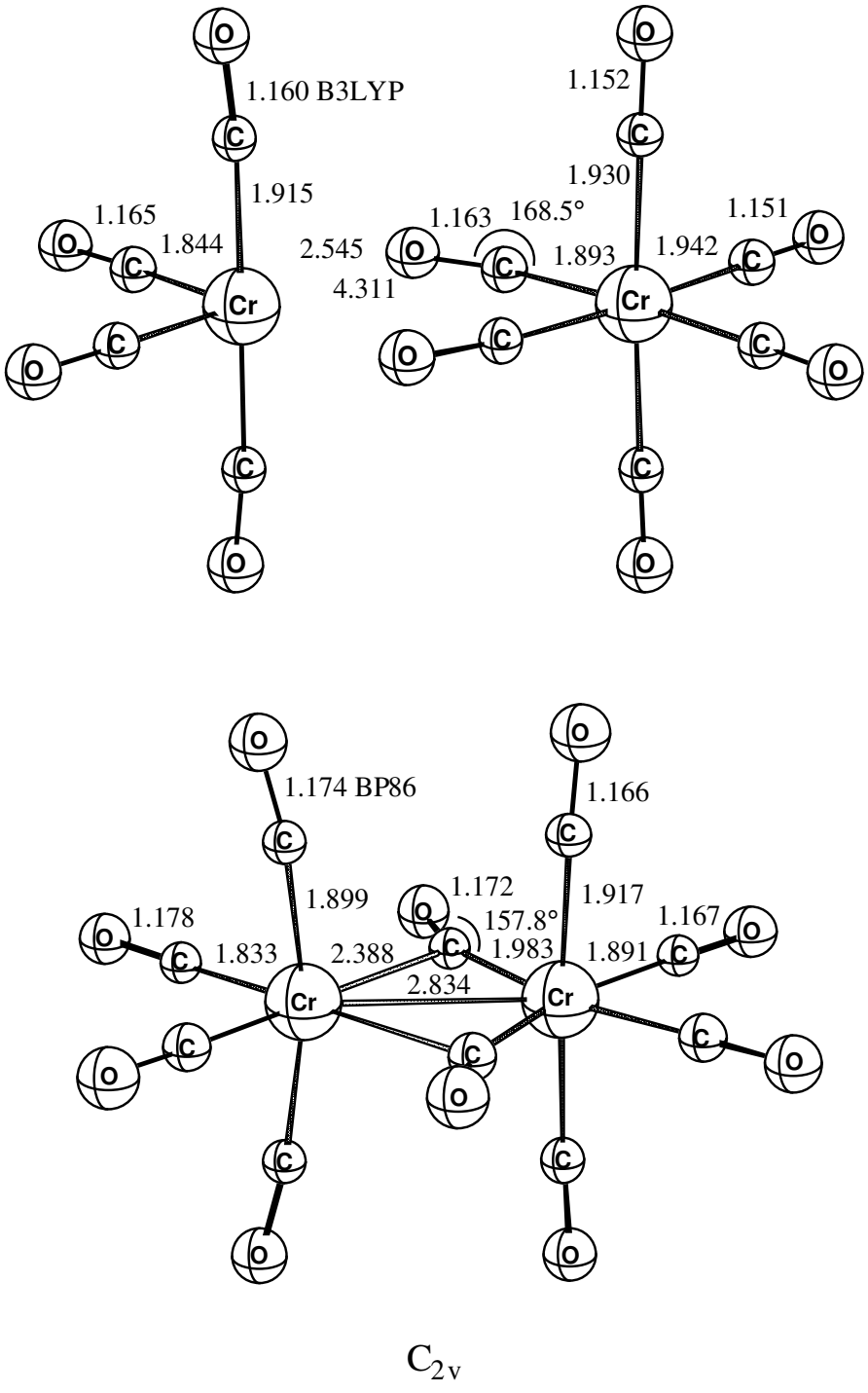

Figure 2.4 The second lowest energy singlet structure for $Cr_2(CO)_{10}$, with C_{2v} symmetry, all real harmonic vibrational frequencies (B3LYP) and one large imaginary harmonic vibrational frequency (BP86). Distances are reported in Å.

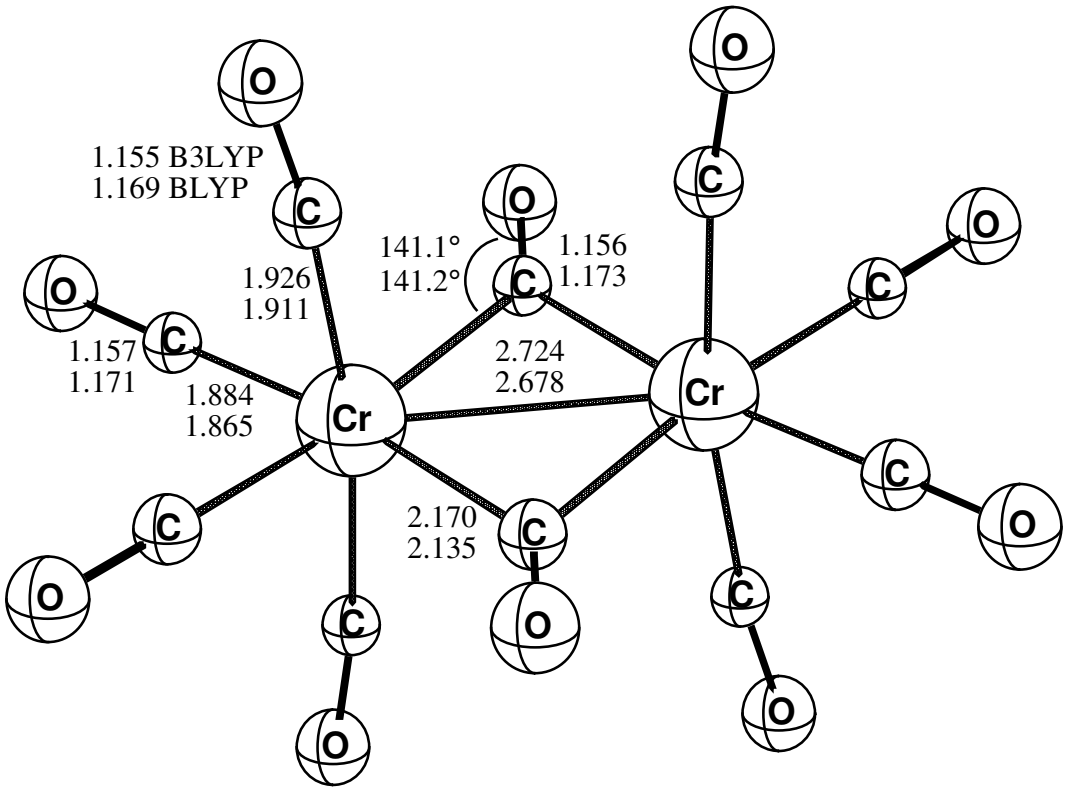

D_{2h}

Figure 2.5 The symmetrically dibridged singlet $Cr_2(CO)_{10}$ structure with D_{2h} symmetry and one large imaginary harmonic vibrational frequency for both B3LYP and BP86. Distances are reported in Å.

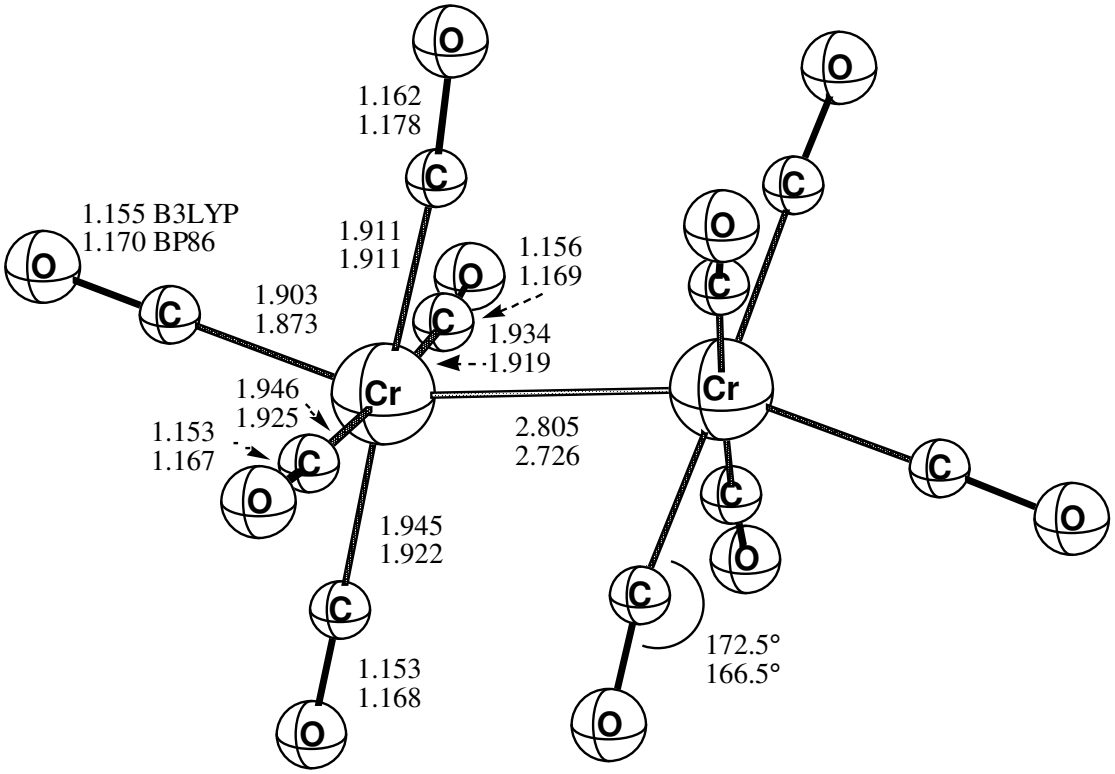

C_2

Figure 2.6 The unbridged C_2 symmetry B3LYP minimum energy structure for triplet $Cr_2(CO)_{10}$ redicted from B3LYP and BP86 methods. Distances are reported in Å .

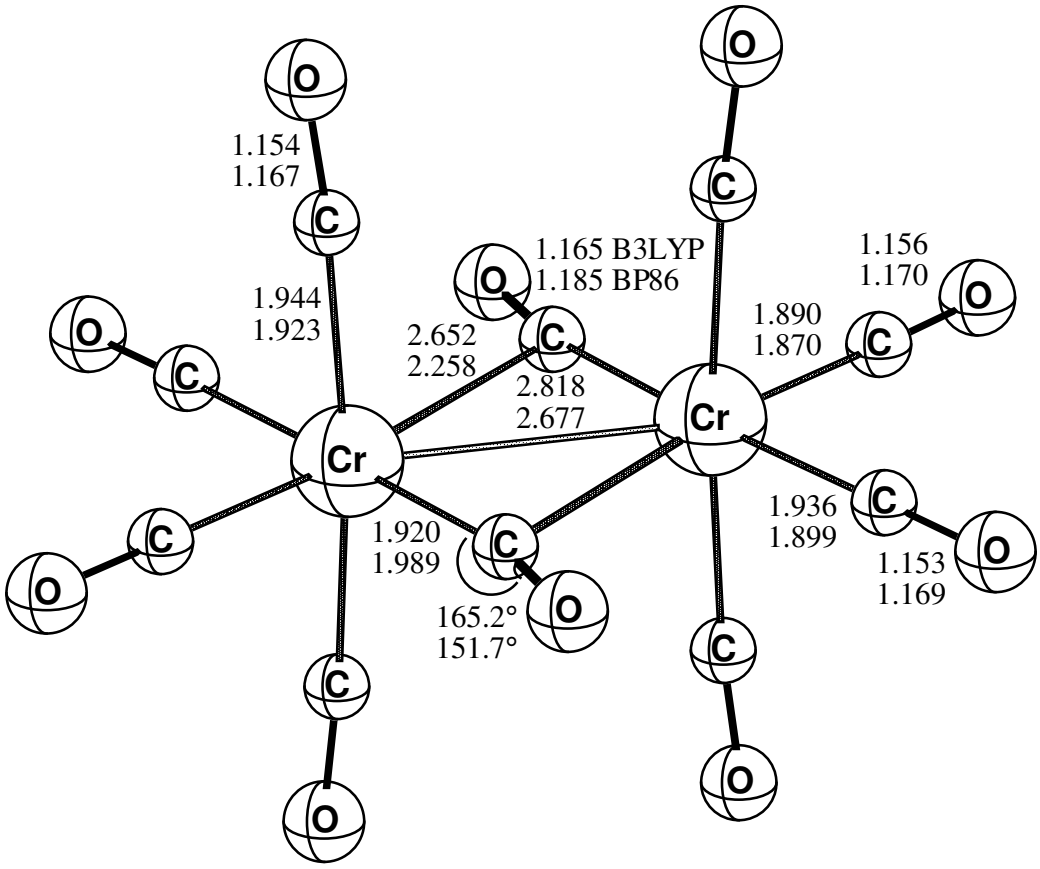

C_{2h}

Figure 2.7 The dibridged BP86 minimum energy structure for triplet $Cr_2(CO)_{10}$ with C_{2h} symmetry. This structure has one small imaginary harmonic vibrational frequency for B3LYP and is a genuine minimum with the BP86 method. Distances are reported in Å.

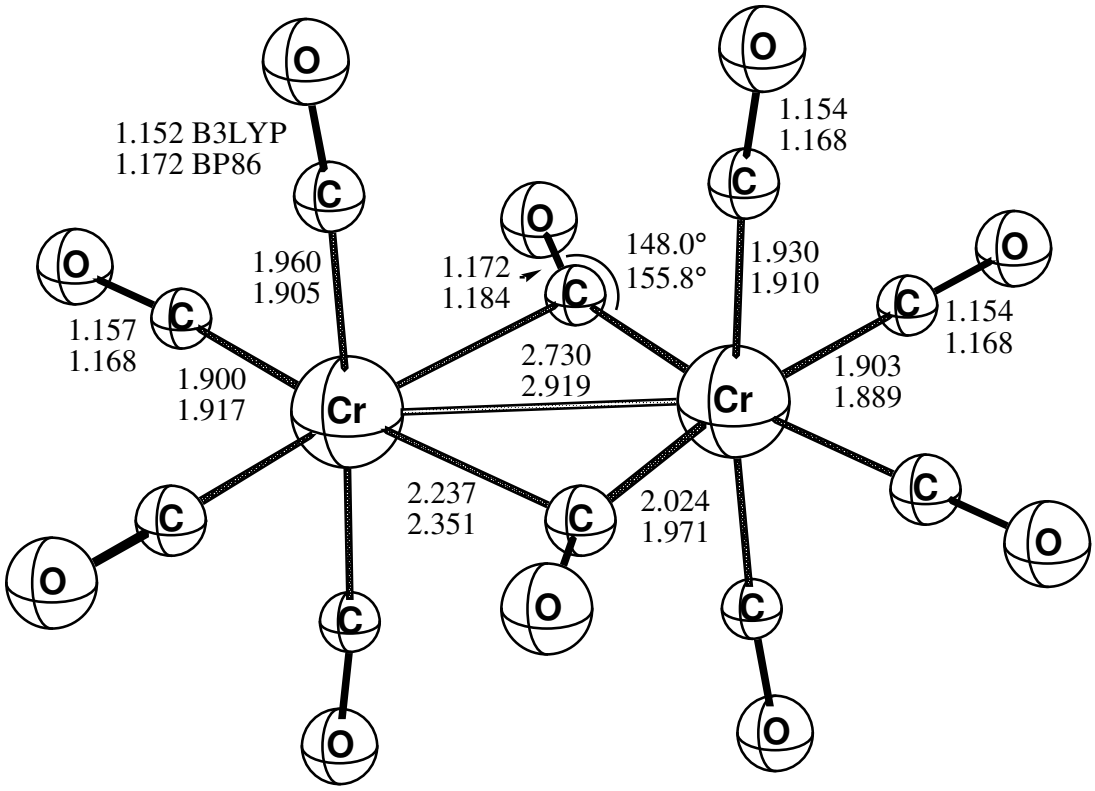

Figure 2.8 The dibridged structure for triplet $Cr_2(CO)_{10}$ with C_{2v} symmetry and one imaginary vibrational frequency with both the B3LYP and BP86 methods. Distances are reported in Å.

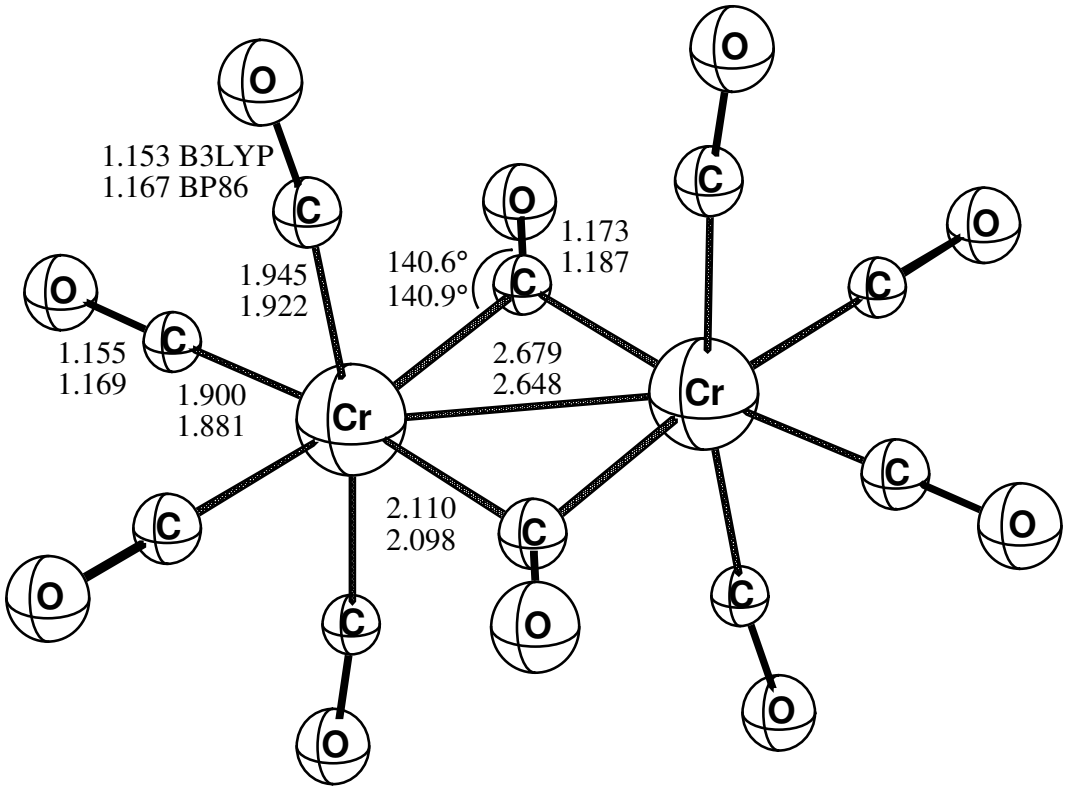

D_{2h}

Figure 2.9 The dibridged structure for triplet $Cr_2(CO)_{10}$ with D_{2h} symmetry. This structure has two imaginary harmonic vibrational frequencies for B3LYP and one imaginary harmonic vibrational frequency with the BP86 method. Distances are reported in Å.

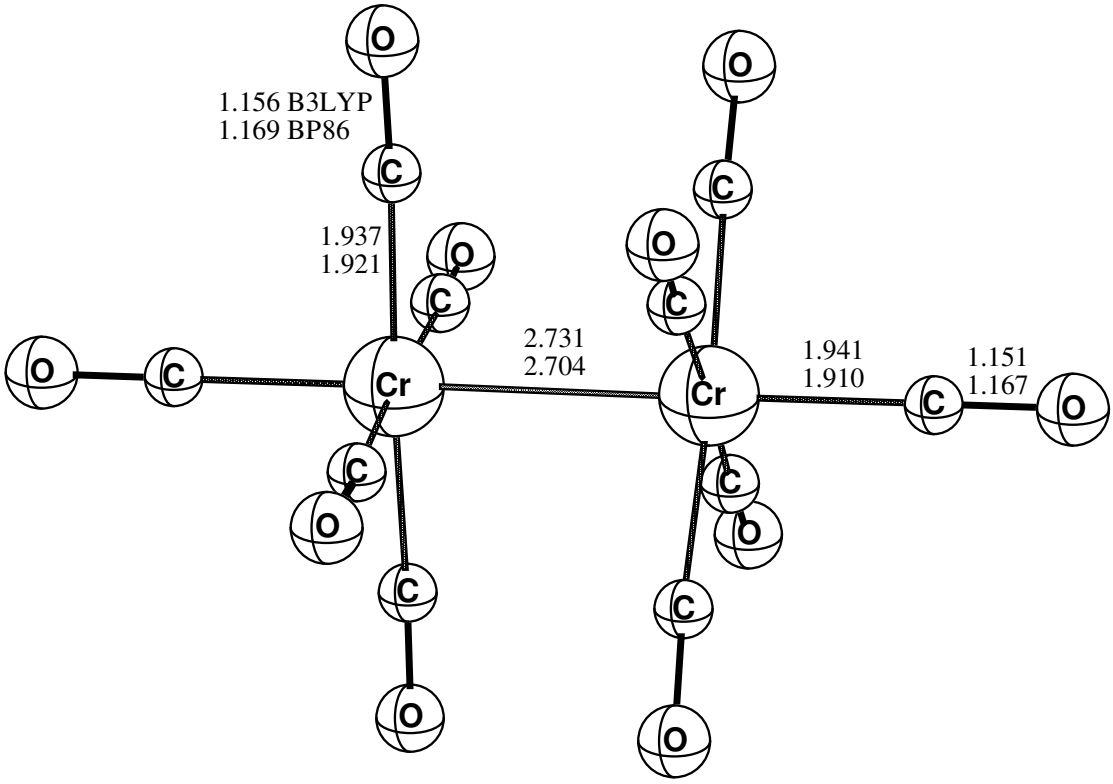

D_{4d}

Figure 2.10 The staggered nonbridging structure for triplet $Cr_2(CO)_{10}$ with D_{4d} symmetry. This conformer has one small imaginary harmonic vibrational frequency with B3LYP and two large imaginary harmonic vibrational frequencies with BP86 method. Distances are reported in Å.

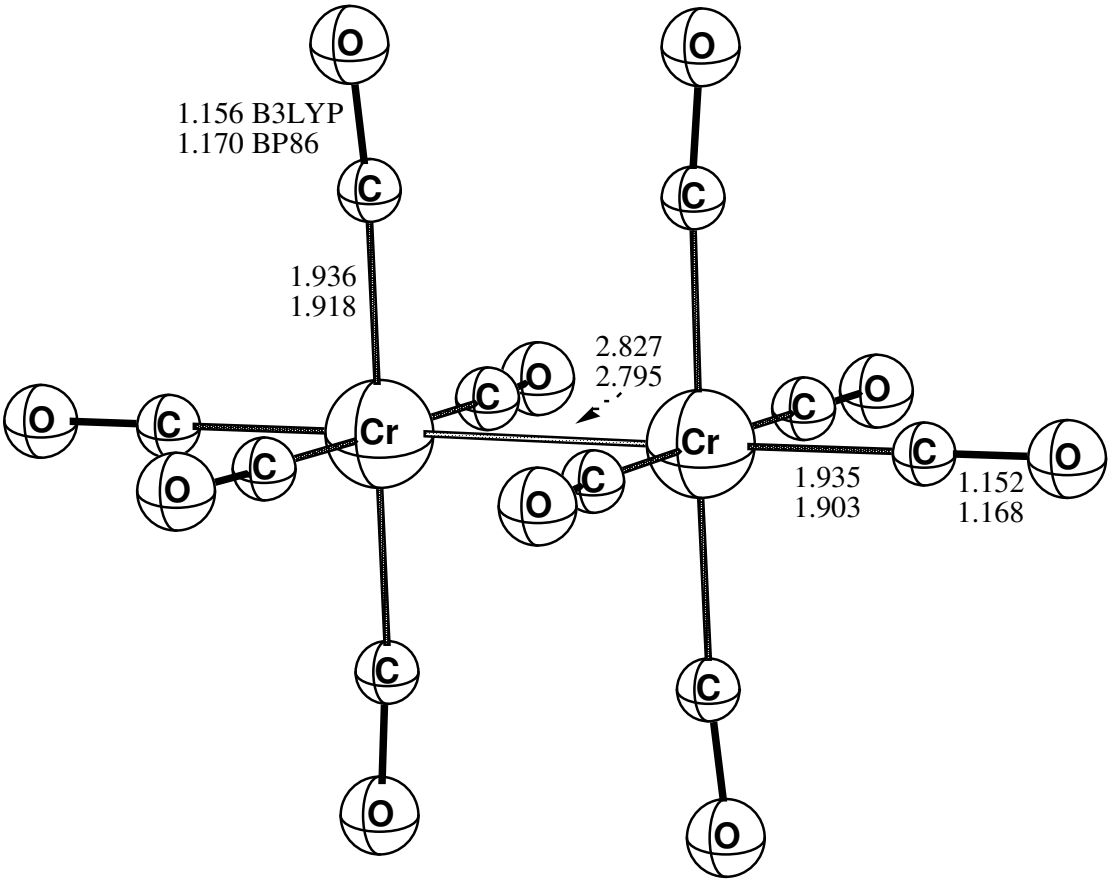

D_{4h}

Figure 2.11 The eclipsed nonbridging structure for triplet $Cr_2(CO)_{10}$ with D_{4h} symmetry and one large imaginary harmonic vibrational frequency with both the B3LYP and BP86 methods. Distances are reported in Å.

Table 2.1 Relative energies of singlet $Cr_2(CO)_{10}$ and related structures

SPECIES	SYM	STATE	FIGURE	IMAGINARY HARMONIC VIBRATIONAL FREQUENCIES		TOTAL ENERGY/E_H		RELATIVE ENERGY/KCAL MOL^{-1}	
				B3LYP	BP86	B3LYP	BP86	B3LYP	BP86
$Cr_2(CO)_{10}$	C_{2h}	^1A_g	3	(none)	(none)	–3222.64440	–3223.06806	0.0	0.0
	C_{2v}	$^1A_1$	4a, 4b	(none)	348i(b_2), 50i(a_2), 40i(b_1)	–3222.64178	–3223.05547	1.6	7.9
	D_{2h}	^1A_g	5	404i(b_{2g}), 153i(b_{3u}), 41i(b_{2u})	438i(b_{2g}), 78i(b_{3u}), 73i(b_{3g}), 70i(b_{2u})	–3222.62970	–3223.05462	9.2	8.4
$2Cr(CO)_5$	C_4	$^1A_1$		(none)	(none)	–3222.63069	–3223.04167	8.6	16.6
$Cr(CO)_4$ + $Cr(CO)_6$	C_{2v}, O_h	$^1A_1$, ^1A_g		(none)	(none)	–3222.63176	–3223.04393	7.9	15.1

Table 2.2 Energies and stationary point characteristics of triplet $Cr_2(CO)_{10}$. Relative energies refer to the C_{2h} symmetry ^1A_g ground state of $Cr_2(CO)_{10}$

SYM.	STATE	FIGURE	IMAGINARY HARMONIC VIBRATIONAL FREQUENCIES		TOTAL ENERGY E_H		RELATIVE ENERGY/KCAL MOL^{-1}	
			B3LYP	BP86	B3LYP	BP86	B3LYP	BP86
C_2	^3B	6	(none)	(none)	– 3222.62407	– 3223.04695	12.7	13.2
C_{2h}	^3B_g	7	18i(a_{1u})	(none)	– 3222.62117	– 3223.04714	14.6	13.1
C_{2v}	$^3A_2$, $^3B_2$	8	74i(b_2)	119i(b_1)	– 3222.62011	– 3223.03799	15.2	18.9
D_{2h}	$^3B_{3g}$	9	105i(b_{2g}), 80i(b_{3u})	95i(b_{2g})	– 3222.61951	– 3223.04692	15.6	13.3
D_{4d}	$^3A_1$	10	509i(e_3)	235i(e_3)	– 3222.61362	– 3223.03652	19.3	19.8
D_{4h}	$^3A_{2g}$	11	22i(a_{1u})	363i(e_g), 20i(a_{1u})	– 3222.60488	– 3223.02812	24.8	25.1

CHAPTER 3

CHROMIUM-CHROMIUM MULTIPLE BONDING IN $Cr_2(CO)_9$[1]

[1] Se Li, Nancy A. Richardson, R. Bruce King, Henry F. Schaefer III. 2003. Journal of Physical Chemistry A. 107: 10118-10125. Reprinted by permission of the American Chemical Society.

3.1 ABSTRACT

Density functional theory (DFT) is used to obtain the first structural characterization of the unsaturated dichromium carbonyl $Cr_2(CO)_9$, which is predicted to have a remarkably short metal-metal bond length of 2.31 Å (B3LYP) or 2.28 Å (BP86). This chromium-chromium distance is essentially identical to that reported experimentally for the established Cr≡Cr triple bond in $(\eta^5\text{-}Me_5C_5)_2Cr_2(CO)_4$. The dissociation energy to the fragments $Cr(CO)_4$ and $Cr(CO)_5$ is determined to be 32 kcal/mol (B3LYP) or 43 kcal/mol (BP86). For comparison, the $Cr_2(CO)_{10}$ molecule and the saturated $Cr_2(CO)_{11}$ system have negligible dissociation energies. The minimum energy $Cr_2(CO)_9$ structure is of C_s symmetry with the two chromium atoms asymmetrically bonded to the bridging carbonyls. However, within 0.1 kcal/mol lies a C_2 symmetry structure with one symmetric and two asymmetric bridging carbonyls. Furthermore, the high symmetry D_{3h} structure analogous to $Fe_2(CO)_9$ lies only ~1 kcal/mol higher in energy. The $Cr_2(CO)_9$ molecule is thus highly fluxional. The extremely flat potential energy surface in the region adjacent to these minima suggests that $Cr_2(CO)_9$ will be labile. The relationship between the $Cr_2(CO)_9$ molecule and the experimentally known binuclear manganese $(\eta^5\text{-}Me_5C_5)_2Mn_2(\mu\text{-}CO)_3$ compound is explored.

3.2 INTRODUCTION

The nature of the metal-metal bond in the absence of the bridging carbonyls (μ_2-CO) in polynuclear metal carbonyls continues to be the subject of considerable discussion. The presence of bridging carbonyls (μ_2-CO) adds to the complexity of the problem owing to

alternative possibilities for metal-metal interactions. Although bridging unsaturated metal carbonyls have not been isolated in gram quantities under normal laboratory conditions, the synthesis of related organometallic species continues.[1,2,3] Some very recent work includes the successful synthesis[4] of (μ-S_2)-$Mn_2(CO)_7$ and the high yield synthesis of the phosphinidene bridged dimolybdenum complex [$Cp_2Mo_2(\mu$-PR)$(CO)_4$ (R = 2,4,6-$C_6H_2{}^tBu_3$)].[5] Other and perhaps more important syntheses include the metathesis reactions that involve the M≡M triple bond in bridging $M_2(OH)_6$ and $M_2(SH)_6$ (M= Mo and W) and alkylidene environments which have become crucial in metal mediated preparative procedures.[6] Such experimental work shows the importance of species containing M-M multiple bonds with bridging groups. In addition, new theoretical understandings of these types of multiple bonds may aid in further syntheses and in their use as catalysts.

Metal-metal interactions through metal-carbon bonds to carbonyl groups upon transformation from terminal to semibridging and then to symmetrical bridging carbonyl groups have been studied in the laboratory via the electron density distribution[7] in $[FeCo(CO)_8]^-$. The results showed some evidence for covalent bonds in unsupported metal-metal bonds. However, no bond path was found to directly link the two metals in the bridging carbonyl complex. This result indicated that bridging carbonyls require more metal orbital participation than the terminal carbonyls and thus compete with direct metal-metal interaction.

However, this observation appears to be valid only for iron and cobalt compounds. Thus among the known stable first row transition metal carbonyls, only neutral $Mn_2(CO)_{10}$ (D_{4h} symmetry) lacks bridging carbonyls where only a weak single d-d σ bond exists between the pair of manganese atoms.[8] Iron has one more electron than manganese so an iron dimer provides two more bonding electrons than the corresponding manganese dimer. In this scheme the additional

electrons interact with the bridging carbonyl and thus no direct metal-metal multiple bond occurs. This accounts for why the singly bonded iron carbonyl $Fe_2(CO)_9$ has been long known while unsaturated bridging homoleptic iron carbonyls with a multiple Fe=Fe or Fe≡Fe bond have not been isolated.[9,10]

In considering the changes from manganese back to chromium in homoleptic binuclear metal carbonyls, we note that the pair of metal atoms provides two less electrons for bonding, so that additional ligands are required for each metal atom to achieve the favored 18-electron noble gas configuration. However, the additional ligands are likely to lead to additional repulsion between the coordination spheres of the two metal atoms, thereby hampering the formation of the normal single or double metal-metal bond. This may explain our previous computational results indicating thermodynamic instability for $Cr_2(CO)_{11}$[11] and a long metal-metal distance in singlet $Cr_2(CO)_{10}$.[12] With fewer ligands and *d* electrons, the possibility of unsaturated compound formation with a multiple metal-metal bond is enhanced greatly.

To this end, we have used theoretical methods to explore the stability of the novel unsaturated species $Cr_2(CO)_9$ with three bridging carbonyls (i.e., $Cr_2(CO)_6(\mu\text{-}CO)_3$). Of particular interest is the existence and nature of the metal-metal multiple bond, together with its most characteristic structural manifestation, namely the metal-metal bond length. Along with optimization of the geometry, we compute the molecular coefficients and the energy levels for all the MOs, and analyze which *d*-orbitals give the largest contributions.[13] The symmetry-adapted linear combinations of the *d* atomic orbitals will provide the bonding and antibonding interactions between the metal atoms. The greater the accumulation of electron density, the lower the MO energy, which reflects the metal-metal overlap population values. This

elementary concept provides a qualitative description of the *d-d* binding. Quantitatively this is shown in the electron density plots of the orbitals.

3.3 THEORETICAL METHODS

Our basis set for C and O begins with Dunning's standard double-ζ contraction[14] of Huzinaga's primitive sets[15] and is designated (9s5p/4s2p). The double-ζ plus polarization (DZP) basis set used here adds one set of pure spherical harmonic *d* functions with orbital exponents α_d(C) = 0.75 and α_d(O) = 0.85 to the DZ basis set. For Cr, our loosely contracted DZP basis set, the Wachters' primitive set,[16] is used, but augmented by two sets of *p* functions and one set of *d* functions, contracted following Hood, Pitzer and Schaefer [17] and designated (14s11p6d/10s8p3d). For $Cr_2(CO)_9$, there are 368 contracted Gaussian functions in the present DZP basis set.

Electron correlation effects were included employing DFT methods, which are acknowledged to be a practical and effective computational tool, especially for organometallic compounds.[18] Among density functional procedures, the most reliable approximation is often thought to be the hybrid Hartree-Fock (HF)/DFT method, B3LYP, which uses the combination of the three-parameter Becke exchange functional with the Lee-Yang-Parr correlation functional.[19,20] However, another DFT method, which combines Becke's 1988 exchange functional with Perdew's 1986 nonlocal correlation functional method (BP86), has proven perhaps even more effective[21] and is also used in this research.[22,23]

We fully optimized the geometries of all structures with the DZP B3LYP and DZP BP86 methods. At the same levels we also computed the vibrational frequencies by analytically evaluating the second derivatives of the energy with respect to the nuclear coordinates. The

corresponding infrared intensities are evaluated analytically as well. All of the computations were carried out with the Gaussian 94 program,[24] in which the fine grid (75 302) is the default for evaluating integrals numerically, and the tight (10^{-8} hartree) designation is the default for the self-consistent field (SCF) convergence.

In the search for minima using all currently implemented DFT methods, low magnitude imaginary vibrational frequencies are suspect because of significant limitations in the numerical integration procedures used in the DFT computations.[9,11,12] Thus, for an imaginary vibrational frequency with a magnitude less than 100 cm^{-1}, there is an energy minimum identical to or very close the structure that of the stationary point in question. Therefore, we generally do not follow such low imaginary vibrational frequencies. In the present case the B3LYP and BP86 methods agree with each other fairly well for predicting the structural characteristics of $Cr_2(CO)_9$. The slight discrepancy in the appearance of artifactual imaginary harmonic vibrational frequency remains, however. Population and density analysis procedures use the Gaussian package.

3.4 RESULTS

3.4.1 GEOMETRIC CONFORMATIONS

Since $Fe_2(CO)_9$ was found by X-ray crystallography to exhibit a staggered tri-bridged structure with D_{3h} symmetry,[16] this symmetry was chosen initially for optimization of $Cr_2(CO)_9$ as shown in Figure 1. Viewed from the Cr-Cr axis, each chromium center has a local symmetry of O_h. The computational results show this structure to be a stationary point with a significant degenerate imaginary frequency of 174i (e″) with B3LYP or 138i (e″) with BP86. The three symmetrical bridging CO groups draw the chromium atoms close to each other leading to a short

Cr-Cr distance of 2.262 Å with B3LYP or 2.249 Å with BP86. The terminal carbonyl bond angles are roughly 180° and the bridging carbonyls are bent to about 147.6°. The Cr-Cr-C angle is 57.5° (B3LYP) or 57.6° (BP86); or alternately, the "bridging angle," the Cr-C-Cr angle is 64.8° (B3LYP) or 64.9° (BP86). Two lower symmetry structures C_2 (Figure 2) and C_s (Figure 3) were obtained by following the degenerate modes of the imaginary frequency.

Notably, the Cr-Cr distances in the $Cr_2(CO)_9$ structures with C_2 and C_s symmetries increase slightly (2.310 Å or 2.315 Å B3LYP, respectively, and 2.285 Å BP86 for both). Nevertheless, these Cr-Cr distances are much smaller than those in $Cr_2(CO)_{10}$[21] (2.81 Å B3LYP, 2.68 Å BP86) and $Cr_2(CO)_{11}$[20] (no B3LYP value is available, 3.15 Å BP86). Two (C_s) or three (C_2) bridging CO groups deviate from the central symmetry plane that perpendicularly crosses halfway between the two metal atoms. The structure of C_s symmetry has an asymmetric Cr-Cr bonding mode: one chromium atom is closer to the two bridging carbonyls that reside symmetrically on the opposite sides of the C_s plane. Except for this structural difference for the bridging carbonyls, the predictions are almost exactly same as for the M-M distance and terminal carbonyls. The bridging angles (Cr-C-Cr) are similar to the above D_{3h} values for C_s 63.6°, 65.3° (B3LYP) or 63.7°, 65.3° (BP86) and for C_2, 66.4°, 64.0° (B3LYP) or 66.1°, 64.2° (BP86). The similarity of these angles indicates energetic similarity among the structures and supports the idea that the ligands are interacting with the chromium atoms individually rather than through some three center interaction which would be indicated in the presence of a more obtuse angle. Since the D_{3h} symmetry lies only 2 kcal/mol (B3LYP) or 1 kcal/mol (BP86) higher than C_s and C_2 symmetries which differ only by 0.1 kcal/mol energetically, there are essentially no definite energy preferences for any of the three conformations (energies shown in Table 1). The potential

surface in the region adjacent to the three D_{3h}, C_s and C_2 symmetries is extremely flat, which leads to the effective indistinguishability of the $Cr_2(CO)_9$ structures.

3.4.2 VIBRATIONAL FREQUENCIES

Since the two conformations deviate slightly from D_{3h} symmetry, either of these structures could be considered as minima on the PES, with the imaginary harmonic vibrational frequency being an artifact of the DFT method. As in previous work,[9,11,12] an interesting contradiction again exists between the B3LYP and BP86 functionals. Only the B3LYP method predicts one imaginary vibrational frequency 55i (b) for the C_2 symmetry structure while in contrast, only the BP86 method predicts one imaginary frequency 22i (a) for the C_s symmetry structure.

The B3LYP and BP86 vibrational frequencies for the $Cr_2(CO)_9$ global minimum of C_s symmetry are reported in Table 3. As expected, the CO stretching frequencies have the highest infrared intensities and are expected to dominate the vibrational spectrum. Note also that for systems such as $Mn_2(CO)_{10}$, $Fe_2(CO)_9$, and $Co_2(CO)_8$, the BP86 method predicts vibrational frequencies more reliably than B3LYP. For $Mn_2(CO)_{10}$, for example, agreement between BP86 and experimental CO stretching frequencies is typically to within 10 cm^{-1}.

For the predicted C_s symmetry global minimum (Figure 3), the CO stretches for the semi-bridging carbonyls are predicted (BP86) at 1919 (a′), 1927 (a″), and 1932 (a′) cm^{-1}. As expected, these three vibrational frequencies lie below the terminal carbonyl stretches, which range from 1970 (a″) to 2060 (a′) cm^{-1}. The most intense infrared fundamental is the terminal a′ CO stretch at 2008 cm^{-1}, with intensity 2213 km/mole.

As noted above, the high symmetry D_{3h} structure of $Cr_2(CO)_9$ is predicted to lie only ~1 kcal/mole above the C_s structure. Candidly, it is not possible exclude the possibility that the D_{3h}

structure is the true global minimum, as DFT methods sometimes incorrectly favor lower symmetry structures. Thus the D_{3h} vibrational frequencies are of interest (Table 4). The bridging CO stretches for the D_{3h} structure are predicted (BP86) at 1911 (a_1') and 1923 (e′) cm^{-1}. The terminal CO stretches are similarly predicted at 1978 cm^{-1} (e″), 1982 cm^{-1} (e′), 2004 cm^{-1} (a_2'') and 2059 cm^{-1} (a_1'). The most intense IR fundamental is predicted at 2004 cm^{-1} (intensity 2462 km/mol). The analogy with the C_s frequencies is strong, as expected, since the D_{3h} and C_s structures are closely related.

3.4.3 THERMOCHEMISTRY

Thermodynamically, the dissociation energy of $Cr_2(CO)_9$ to $Cr(CO)_4$ and $Cr(CO)_5$ fragments is predicted to be 32 kcal/mol with the B3LYP functional or 43 kcal/mol with the BP86 functional while dissociation to $Cr(CO)_3$ and $Cr(CO)_6$ fragments is predicted to be 41 kcal/mol (B3LYP) or 30 kcal/mol (BP86). This demonstrates the remarkably stronger [than predicted for $Cr_2(CO)_{11}$ and $Cr_2(CO)_{10}$] interaction between the two chromium fragments. In previous work, the unstable saturated $Cr_2(CO)_{11}$ was predicted[20] to lie above the stable dissociated fragments[25,26] $Cr(CO)_5$ and $Cr(CO)_6$ in energy and only slightly metastable with respect to the transition state leading to this dissociation. The barely stable $Cr_2(CO)_{10}$ was found[21] to lie 56 kcal/mol (B3LYP) above the well known[27] $Cr_2(CO)_{10}^{2-}$; the dissociation energy to two $Cr(CO)_5$ or to $Cr(CO)_6$ plus $Cr(CO)_4$ was determined to be about 10 kcal/mol.

To what might we compare our predicted $Cr_2(CO)_9$ dissociation energies? Perhaps the best comparison is with $Mn_2(CO)_{10} \rightarrow 2Mn(CO)_5$. In the latter case the B3LYP dissociation energy is 24.2 kcal/mol, while that for BP86 is 31.1 kcal/mol. As with $Cr_2(CO)_9$, the BP86

dissociation energy is larger. The experimental dissociation energy for $Mn_2(CO)_{10}$ is problematic, with the most reliable result probably the solution result of Pugh and Meyer[28], namely 37.7 ± 4.1 kcal/mol. Weitz[29] has argued that the gas phase dissociation energy of such system should be greater than the solution value. In any case, our comparisons seem to show unambiguously that the dissociation energy of $Cr_2(CO)_9$ is greater than that for the known molecule $Mn_2(CO)_{10}$. This supports our contention that it should be possible to make $Cr_2(CO)_9$.

In the next section, we explore the strong interaction of the fragments in $Cr_2(CO)_9$ which is so different from that in $Cr_2(CO)_{10}$ and $Cr_2(CO)_{11}$. The answer lies in analysis of the metal-metal bonding.

3.4.4 METAL-METAL BONDING

In terms of formal electron counting in $Cr_2(CO)_9$, each bridging CO ligand provides one electron to each metal atom. Without assuming any Cr-Cr bonding, each chromium atom with three bridging carbonyls and three terminally bonded carbonyls has 15 electrons. The 18-electron[30] rule then suggests that a direct Cr≡Cr triple bond is present. In terms of hybrid orbitals, each chromium center may be considered to be sp^3d^2 hybridized consistent with its octahedral environment. Six hybrid orbitals are used for bonding to the CO ligands, leaving the metal d_{xy}, d_{xz} and d_{yz} orbitals for metal-metal bond formation. However the orientations of the carbonyl ligands mean that these three orbitals available for Cr-Cr bond[31] formation do not point directly towards each other. Compared to the classic $[Re_2Cl_8]^{2-}$ molecule, the result should be a “bent” Cr-Cr bond.

Owing to the ineffective nature of *d*-orbital overlap as compared to *s*- or *p*-orbital overlaps, the electrons in *d*-orbitals are more localized than those in *s*- or *p*-orbitals. The metal-

metal bonding using *d* orbitals was analyzed by searching for the participation percentage of the *d* orbitals in each of the relevant molecular orbitals (MOs).

The MOs to which the *d*-orbitals give the largest contributions for $Cr_2(CO)_9$ in C_s symmetry are listed in Table 2. Seven orbitals are listed from the sixth lowest occupied orbital (HOMO-5) to the first lowest unoccupied orbital (LUMO). The molecular orbital coefficient analysis shows that the main covalent contribution is directly provided by the mixing of the different percentages of *d* orbitals on the two chromium atoms. For instance, the HOMO-5 consists of the mixture of about 56% or 58% of the d_{x2-y2} orbitals and about 27% or 37% of the d_{z2} orbitals depending upon the computational method used. The HOMO-4 is also composed of a d_{x2-y2}, d_{xy} and d_{z2} combination (owing to the C_s symmetry the *d*-orbitals are inseparable).

The symmetry-adapted linear combinations of the *d*-orbitals are graphically displayed in Figure 4 according to the chosen Cartesian coordinates, the phase of the atomic orbital, and the relative ratio of the participation percentage of the *d*-orbital. (Note that the metal-metal bond here lies on the *y* axis). Figures 5 and 6 show density plots of the orbitals. The results suggest that HOMO-5, HOMO-4 and HOMO-3 are the bonding orbitals among the six highest occupied orbitals. The metal orbitals with π bonding character are $d_{xy,}$ or d_{yz}. The δ bonding orbital is d_{xz} and the distorted σ bonding orbitals are d_{x2-y2} and d_{z2} (owing to the distortion of the pair of CrC_6 octahedra). The corresponding antibonding orbitals are HOMO-2 to HOMO. Notably, there is a substantial energy gap (–6.41 eV to –7.08 eV) between the lowest antibonding orbital HOMO-2 and the highest bonding orbital HOMO-3, which confirms the existence of the overlaps between the d_{yz} orbitals and the d_{xz} orbitals in HOMO-3. The main contribution to the metal-metal bond comes from the d_{yz} orbitals in a π bond after considering the smaller overlap of the d_{xz} orbitals to form a δ bond. The HOMO-4 and HOMO-5 are stabilized by the bonding of the $d_{xy,}$, d_{x2-y2} and

d_{z^2} orbitals. In the HOMO-4, the stabilization of this energy level arises from the bonding of the d_{xy} and d_{z^2} orbitals if the small contribution from the $d_{x^2-y^2}$ is neglected. The presence of the bonding of the d_{xy} and d_{z^2} orbitals make HOMO-4 lower than HOMO-3 by 7.21 – 7.08 = 0.13 eV. The HOMO-5 is lowered mainly by the $d_{x^2-y^2}$ bonding orbitals from 7.43 to 7.21 eV. Thus we obtain the three *d-d* bonding MOs for the metal-metal bond.

Interestingly, the two antibonding orbitals (HOMO-1 and HOMO-2) are almost degenerate in energy, which may be consistent with the two symmetrical bridging carbonyls with respect to the C_s plane. The HOMO itself is slightly higher in energy than the degenerate occupied antibonding MOs. HOMO-1 and HOMO-3 are a pair of bonding and antibonding orbitals with δ character. The relatively larger energy gap between the three bonding orbitals suggests that more electron density accumulates in the bonding orbitals between the two metals. In other words, the d_{xy}, d_{yz} and d_{xz} orbitals contribute to the stabilization of this compound. Thus the metal-metal bond is mainly composed of two degenerate π bonds and one δ bond.

Also significant is the large gap between the HOMO and LUMO which measures the chromium-chromium bond stability in $Cr_2(CO)_9$. The large energy difference indicates the singlet configuration is the favored state rather than the triplet. At the same time it shows the singlet configuration is the dominant configuration among all the correlated configurations.

In practice, molecular orbitals involve combinations of all available atomic orbitals. In addition to the *d*-orbitals of the metal atoms, *s*- and *p*-orbitals from the carbonyl groups also make contributions to the MOs. Thus Cr-CO σ- and π- bonding have a major effect on the shapes and energies of the MOs as well as the chromium-chromium bonding discussed above. Nevertheless, the MO plots provide useful insight into the nature of the chromium-chromium

multiple bond in $Cr_2(CO)_9$ and suggests that it is a potentially stable molecule in contrast to $Cr_2(CO)_{10}$ and $Cr_2(CO)_{11}$.

3.5 DISCUSSION

We emphasize that these interactions occur in the framework of the complex; without the ligands such bonding could not be reasonably described by DFT. Distinction must be made between genuine transition metal *complexes*, cases in which ligands are attached to chromium, and the bare chromium-chromium dimer, where virtually all methods fail. Massive multi-configurational character occurs in the latter, where the only interaction occurring is that of a chromium atom with another chromium. Studies at various levels of theory, including CCSD,[32] CCSD(T),[33] various DFT,[34,35,36] CASPT2,[37,38] CASPT2 with relativistic corrections[39], MRACPF plus relativistic corrections,[40] and CASSCF plus an Epstein-Nesbet second-order perturbation treatment,[41] found a wide range of bond lengths and frequencies. The chromium dimer remains a difficult case for the most sophisticated methods. Even the recent study by Dachsel, Harrison, and Dixon[42] employing a very large MRCI/MRACPF was not in entirely adequate agreement with experiment. The CASPT2 method appears to be the most successful to date, and an excellent review has recently been given by Roos [43]. These theoretical challenges result from the inability of most methods to describe the bonding situation: formally, the chromium-chromium dimer has a bond order of six but with a low dissociation energy (< 2eV). This phenomena, however, is an uncommon circumstance, as noted by Siegbahn and Blomberg in their recent review of DFT applied to transition metal systems:[44] "The (extreme) multiple bonding is almost unique with its severe near-degeneracy problems, so this situation does not need to be accurately

described by a method used to study more normal chemical systems." They note that this recognition that metal behavior is different in complexes has paved the way for diverse applications of DFT to transition metal complexes: "Another significant insight gained from the modeling of transition-metal complexes is that some of the problems encountered early, which were thought to be necessary to solve, are in fact very atypical for transition-metal complexes. The examples of the nickel atom and the chromium dimer … are illustrative of this point."

Regarding this point, Morokuma[45] also noted, "The established problem of the $s^0 d^n$ vs. $s^1 d^{n-1}$ description by DFT methods dominates the picture for coordinatively unsaturated molecules, but should not play any role for systems [with more ligands]." Several such studies with DFT confirm this finding.[46,47,48]

We could ask the question, at what point will the homoleptic carbonyl dimetallic system fail to be described by DFT. To this end, we compare $Cr_2(CO)_9$ to less unsaturated structures. The optimized structure for $Cr_2(CO)_9$ (**I**), like those of singlet $Cr_2(CO)_{10}$ (**II**) and $Cr_2(CO)_{11}$ (**III**) retains an approximately octahedral environment of the six carbonyl groups around each chromium atom similar to that in the very stable $Cr(CO)_6$. Thus the structures of $Cr_2(CO)_{11}$ (**III**), $Cr_2(CO)_{10}$ (**II**), and $Cr_2(CO)_9$ (**I**) may be regarded as consisting of two $Cr(CO)_6$ octahedra with a vertex, edge, and face in common, respectively. However, the structure of $Cr_2(CO)_9$ (**I**) is unique among the three structures **I**, **II**, and **III** in having the two chromium atoms close enough together for strong metal-metal bonding. Furthermore, the metal-metal distance of 2.31 Å (B3LYP) or 2.28 Å (BP86) is consistent with the Cr≡Cr triple bond required to give each chromium atom the favored 18-electron rare gas electronic configuration as indicated by the experimentally determined Cr≡Cr distance of 2.28 Å in $(\eta^5\text{-}Me_5C_5)_2Cr_2(CO)_4$ (**IV**),[49] also required to be a triple bond in order to give each chromium atom the favored 18-electron rare gas

electronic configuration. The metal-metal bond analysis in $Cr_2(CO)_9$ (**I**) indicates the main covalent contribution is provided by the *d*-orbitals of the chromium atoms, not by the *p*-orbitals of the bridging carbonyls. The metal-metal triple bond thus was found to consist of two π bonds, together with a weak δ bond. This Cr≡Cr triple bond thus differs significantly from the familiar carbon-carbon triple bond in acetylene, which consists of two bonds and a σ bond.

One should note that our affinity for some sort of bond order — bond distance relationship is not universally held. A minority, but still substantial view, is that bond order — bond distance correlations are meaningless, and that bond order can only be determined via electron density analysis. Without criticizing this approach, we are more comfortable with relating bond orders to quantities more familiar to experimentalists, e.g., bond distances, rotational barriers, and force constants.

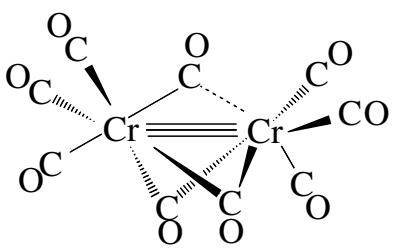

I

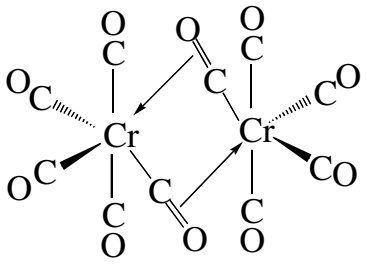

II

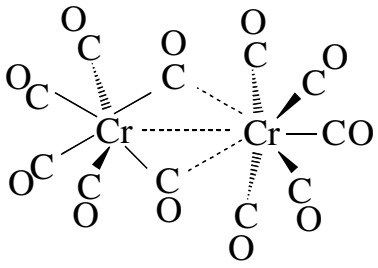

III

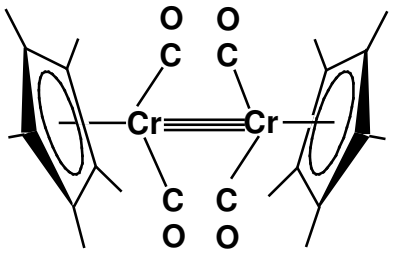

IV

Overall $Cr_2(CO)_9$ (**I**) is a thermodynamically stable compound and should be isolable experimentally. However, a feasible synthetic route would need to avoid $Cr_2(CO)_{11}$ or $Cr_2(CO)_{10}$ intermediates, since these have been shown in our previous papers[11,12] to be thermodynamically unstable with respect to mononuclear species. A possible method to synthesize $Cr_2(CO)_9$ (**I**) might be to combine $Cr(CO)_5$ and $Cr(CO)_4$ fragments generated by decomposition of labile octahedral $L_2Cr(CO)_4$ and $LCr(CO)_5$ derivatives. In this connection, the binuclear manganese derivative $(\eta^5\text{-}Me_5C_5)_2Mn_2(\mu\text{-}CO)_3$ (**V**) has been isolated by the spontaneous decomposition of $(\eta^5\text{-}Me_5C_5)Mn(CO)_2THF$.[50] This manganese compound (**V**) is closely related to the optimized structure for $Cr_2(CO)_9$ (**I**) by substitution of each $Cr(CO)_3$ unit linked by the three bridging carbonyls with an isoelectronic and isolobal $(\eta^5\text{-}Me_5C_5)Mn$ unit. Thus $(\eta^5\text{-}Me_5C_5)_2Mn_2(\mu\text{-}CO)_3$ (**V**) would be expected to have an Mn≡Mn triple bond similar to the Cr≡Cr triple bond found for $Cr_2(CO)_9$ (**I**). In this connection determination of the structure of $(\eta^5\text{-}Me_5C_5)_2Mn_2(\mu\text{-}CO)_3$ (**V**) by X-ray diffraction indicates an Mn≡Mn distance of 2.17 Å.[51] This short distance is consistent

with a metal-metal triple bond similar to that suggested for $Cr_2(CO)_9$ (**I**) after making allowance for differences in the electronic properties of carbonyl and pentamethylcyclopentadienyl ligands.

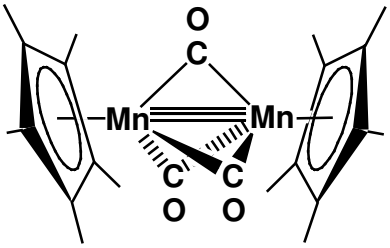

V

3.6 CONCLUSION AND OUTLOOK

In this research a stable $Cr_2(CO)_9$ molecule is predicted with a chromium-chromium bond having a relatively short metal-metal distance of about 2.3 Å. Based on the comparison to other well-known metal carbonyl compounds, our calculated distances appear reasonable. The Cr-Cr distance is similar to that of the triply bonded (pentamethyl $Cp)_2Cr_2(CO)_4$ compound[44] but significantly longer than 1.96 Å in a quadruply bonded dichromium tetracarboxylate[52] with its $\sigma^2\pi^4\delta^2$ configuration.[53] Thus the theoretical distance is reasonable as the sigma component (which is expected to be the major contributor to the length of the Cr-Cr bond) is missing in $Cr_2(CO)_9$. Such theoretical insights give this work the potential to serve as inspiration for synthetic chemists to go to the bench and try to prepare $Cr_2(CO)_9$, predicted to be a makeable molecule.

Though DFT predicts $Cr_2(CO)_9$ to be a stable compound with a rather labile structure and a unique sort of metal-metal bond, we anticipate a point at which DFT will not be useful for

some $Cr_2(CO)_x$, ($x < 8$). Certainly, the bare metal dimer is not describable with DFT. We would hope the work of this paper would be a step along the pathway to discovering the point at which there are no longer enough ligands for a $Cr_2(CO)_x$ species to behave as a "normal" molecule. Such work would give further insight into both DFT methods in general and the infamous bare chromium dimer problem in particular as well as provide novel insights into even more highly saturated homoleptic dimetallic chromium compounds.

3.7 ACKNOWLEDGMENTS

We are grateful for the support of this work by NSF Grant CHE-0136186. We thank Dr. Yukio Yamaguchi for helpful discussions about the metal-metal bonding, Dr. Wang Zhi Xiang for guidance in the analysis of the electron density and Dr. Steven S. Wesolowski for help in producing the orbital plots as well as several helpful discussions. We also thank the referees for their helpful suggestions and insights.

3.8 LITERATURE REFERENCES

1. Shyu, S.-G.; Calligaris, M.; Nardin, G.; Wojcicki, A. *J. Am. Chem. Soc.* **1987**, *109*, 3617.
2. Wong, W.-T.; Wong, W.-K. *Acta Crystallogr.* **1994**, *C50*, 1404.
3. Maitra, K.; Catalano, V. J.; Nelson, J. H. *J. Organomet. Chem.* **1997**, *529*, 409.
4. Adams, R. D.; Kwon, O.; Smith, M. D. *J. Organomet. Chem.* **2002**, *41*, 6281.
5. Garcia, M. E.; Riera, V.; Ruiz, M. A.; Saez, D.; Vaissermann, J.; Jeffery, J. C. *J. Am. Chem. Soc.* **2002**, *124*, 14304.
6. Chisholm, M. H.; Davidson, E. R.; Quinlan, K. B. *J. Am. Chem. Soc.* **2002**, *124*, 15351.

7. Macchi, P.; Garlaschelli, L.; Sironi, A. *J. Am. Chem. Soc*. **2002**, *124*, 14173.

8. Hall, M. B. In *Electron Distribution and the Chemical Bond*; Coppens, P., Hall, M. B., Eds.; Plenum Press: New York, 1982; p 205.

9. Xie, Y.; Schaefer, H. F.; King, R. B. *J. Am. Chem. Soc.* **2000**, *122*, 8746.

10. Winter, M. J. *Adv. Organometal. Chem.* **1989**, *29*, 101.

11. Richardson, N. A.; Xie, Y.; King, R. B.; Schaefer, H. F. *J. Phys. Chem. A.* **2001**; 105, 11134.

12. Li, S.; Richardson, N. A.; Xie, Y.; King, R. B.; Schaefer, H. F. *Faraday Discussions*, **2003**, *124*, 315.

13. Jezowska-Trzebiatowska, B.; Nissen-Sobocinska, B. *J. Organomet. Chem*. **1987**, *322*, 331.

14. Dunning, T. H. *J. Chem. Phys.* **1970**, *53*, 2823.

15. Huzinaga, S. *J. Chem. Phys.* **1965**, *42*, 1293.

16. Wachters, A. J. H. *J. Chem. Phys.* **1970**, *52*, 1033.

17. Hood, D. M.; Pitzer, R. M.; Schaefer, H. F. *J. Chem. Phys*. **1979**, *71*, 705.

18. Ziegler, T. *Can. J. Chem*. **1995**, *73*, 743.

19. Becke, A. D. *J. Chem. Phys.* **1993**, *98*, 5648.

20. Lee, C., Yang, W.; Parr, R. G. *Phys. Rev. B* **1988**, *37*, 785.

21. Jonas, V.; Thiel, W. *Organometal.* **1998**, *17*, 353.

22. Becke, A. D. *Phys. Rev. A* **1988**, *38*, 3098.

23. Perdew, J. P. *Phys. Rev. B* **1986**, *33*, 8822; *34*, 7046.

24. Gaussian 94 (Revision B. 3), Frisch, M. J.; Trucks, G. W.; Schlegel, H. B.; Gill, P. M. W.; Johnson, B. G.; Robb, M. A.; Cheeseman, J. R.; Keith, T. A.; Petersson, G. A.;

Montgomery, J. A.; Raghavachari, K.; Al-Laham, M. A.; Zakrzewski, V. G.; Ortiz, J. V.; Foresman, J. B.; Cioslowski, J.; Stefanov, B. B.; Nanayakkara, A.; Challacombe, M.; Peng, C. Y.; Ayala, P. Y.; Chen, W.; Wong, M. W.; Andres, J. L.; Replogle, E. S.; Gomperts, R.; Martin, R. L.; Fox, D. J.; Binkley, J. S.; Defrees, J. D.; Baker, J.; Stewart, J. P.; Head-Gordon, M.; Gonzalez, C.; Pople, J. A. Gaussian, Inc., Pittsburgh PA, **1995.**

25. Barnes, L. A.; Liu, B.; Lindh, R. *J. Chem. Phys.* **1993**, *98*, 3978.
26. Rees, B.; Mitschler, A. *J. Am. Chem. Soc.* **1976**, *98*, 7918.
27. Borrmann, H.; Pirani, A. M.; Schrobilgen, G. J. *Acta Crystallogr., Sect. C* **1997**, *53*, 19.
28. Pugh, J. R. and Meyer, T. J. *J. Am. Chem. Soc.* **1992**, *114*, 3784.
29. Weitz, E. J. *J. Phys. Chem.* **1994**, *98*, 11256.
30. Green, M. L. H. *J. Organomet. Chem.* **1995**, *500*, 127.
31. Cotton, F. A.; Wilkinson, G.; Murillo, C. A.; Bochmann, M. *Advanced Inorganic Chemistry*, Wiley and Sons, 6th edition: New York, **1999**.; Cotton, F. A.; Walton, R. A. *Multiple Bonds Between Metal Atoms* Clarendon Press: Oxford **1993**.
32. Scuseria, G. E. *J. Chem. Phys.* **1991**, *94*, 442.
33. Scuseria, G. E.; Schaefer, H. F. *Chem. Phys. Lett.* **1990**, *174*, 501.
34. Bauschlicher, C. W.; Partridge, H. *Chem. Phys. Lett.* **1994**, *231*, 277.
35. Barden, C. A.; Rienstra-Kiracofe, J. C.; Schaefer, H. F. *J. Chem. Phys*. **2000**, *113*, 690.
36. Yanagisawa, S.; Tsuneda, T.; Hirao, K. *J. Chem. Phys.* **2000**, *112*, 545.
37. Andersson, K. *J. Chem. Phys.* **1995**, *237*, 212.
38. Mitrushenkov, A.O.; Palmieri, P. *Chem. Phys. Lett.* **1997**, *278*, 285.
39. Andersson, K.; Roos, B. O. Malmqvist, P. A. *Chem. Phys. Lett.* **1999**, *103*, 152.
40. Stoll, H.; Werner, H. J. *Mol. Phys.* **1996**, *88*, 793.

41. Roos, B. O.; Andersson, K. *Chem. Phys. Lett.* **1995**, *245*, 215.

42. Dachel, H.; Harrison, R. J.; Dixon, D. A. *J. Phys. Chem. A* **1999**, *103*, 152.

43. Roos, B. O. *Collect. Czech Chem. Comm.* **2003**, *68*, 265.

44. Siegbahn, P. E. M.; Blomberg, M. R. A. *Chem. Rev.* **2000**, *100*, 421.

45. Khoroshun, D. V.; Djamaladdin, G. M., Vreven, T.; Morokuma, K. *Organometal.* **2001**, *20*, 2007.

46. Koch, W.; Holthausen, M. C. *A Chemist's Guide to Density Functional Theory* Wiley-VCH: Weinheim, FRG, **2000**.; pp. 251-259.

47. Holthausen, M. C.; Fiedler, A.; Schwarz, H.; Koch, W. *J. Phys. Chem.* **1996**, *100*, 6236.

48. Holthausen, M. C.; Koch, W. *J. Am. Chem. Soc.* **1996**, *118*, 9932.

49. Potenza, J.; Giordano, P.; Mastropaolo, D.; Efraty, A. *Inorg. Chem.* **1974**, *13*, 2540.

50. Herrmann, W. A.; Serrano, R.; Weichmann, J. *J. Organometal. Chem.* **1983**, *246*, C57.

51. Bernal, I.; Korp, J. D.; Hermann, W. A.; Serrano, R. *Chem. Ber.* **1984**, *117*, 434.

52. Cotton, F. A.; Hillard, E. A.; Murillo, C. A.; Zhou, H. *J. Am. Chem. Soc.* **2000**, *122*, 416. For a more general discussion of Cr-Cr quadruple bonds, see S. N. Ketkar and M. Fink, *J. Am. Chem. Soc.* **1985**, *107*, 338.

53. Note that in going from $Cr_2(CO)_9$ to $Cr_2(CO)_8$, the number of formal metal-metal bonding electrons increases from six to eight. This is because removal of a bridging CO from $Cr_2(CO)_9$ returns one electron, in a simple picture, to each chromium atom.

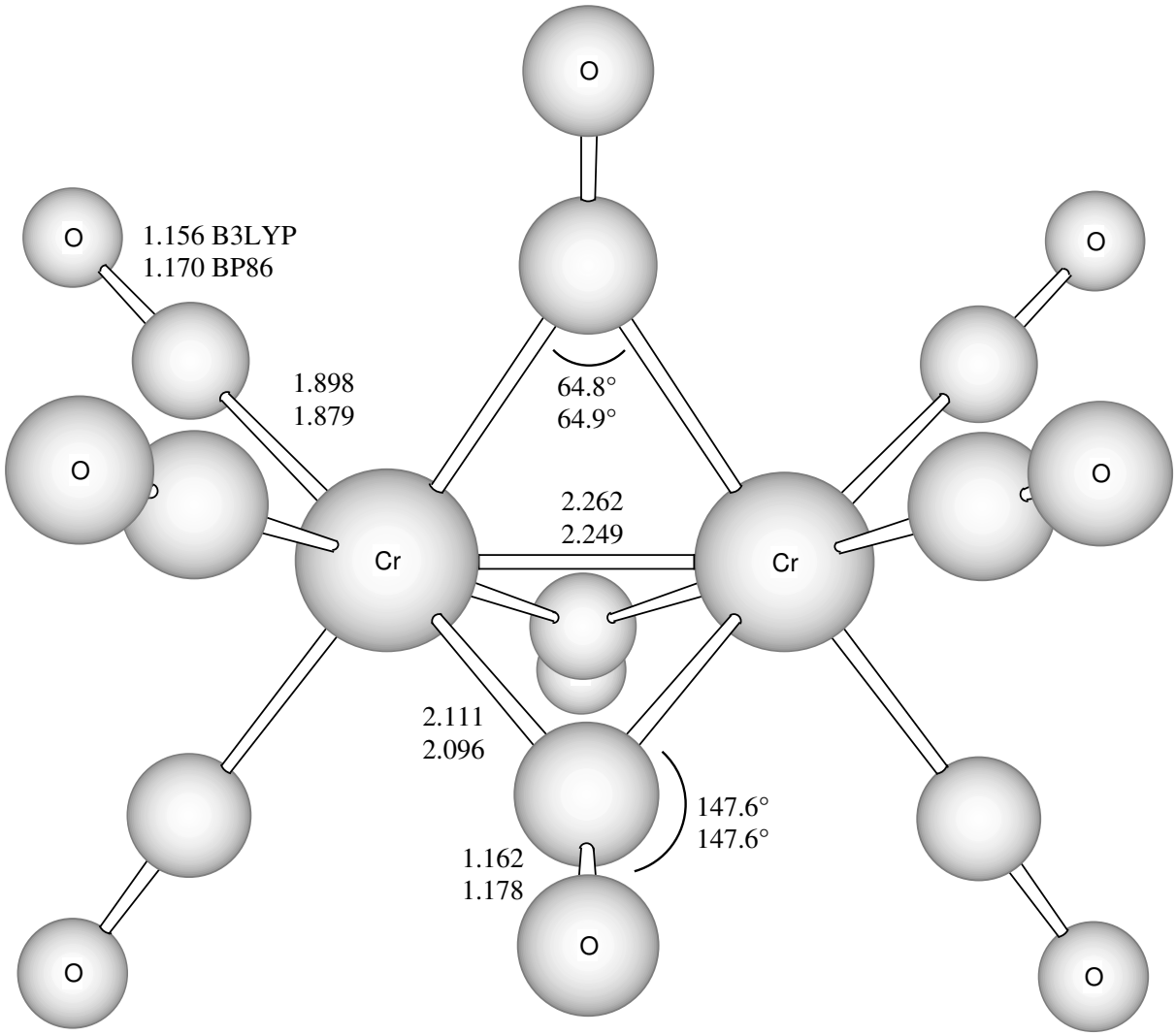

Figure 3.1 Symmetrically tribridged D_{3h} transition state structure for singlet $Cr_2(CO)_9$. This structure possesses a significant degenerate imaginary harmonic vibrational frequency for both B3LYP and BP86 functionals. Distances are reported in angstroms.

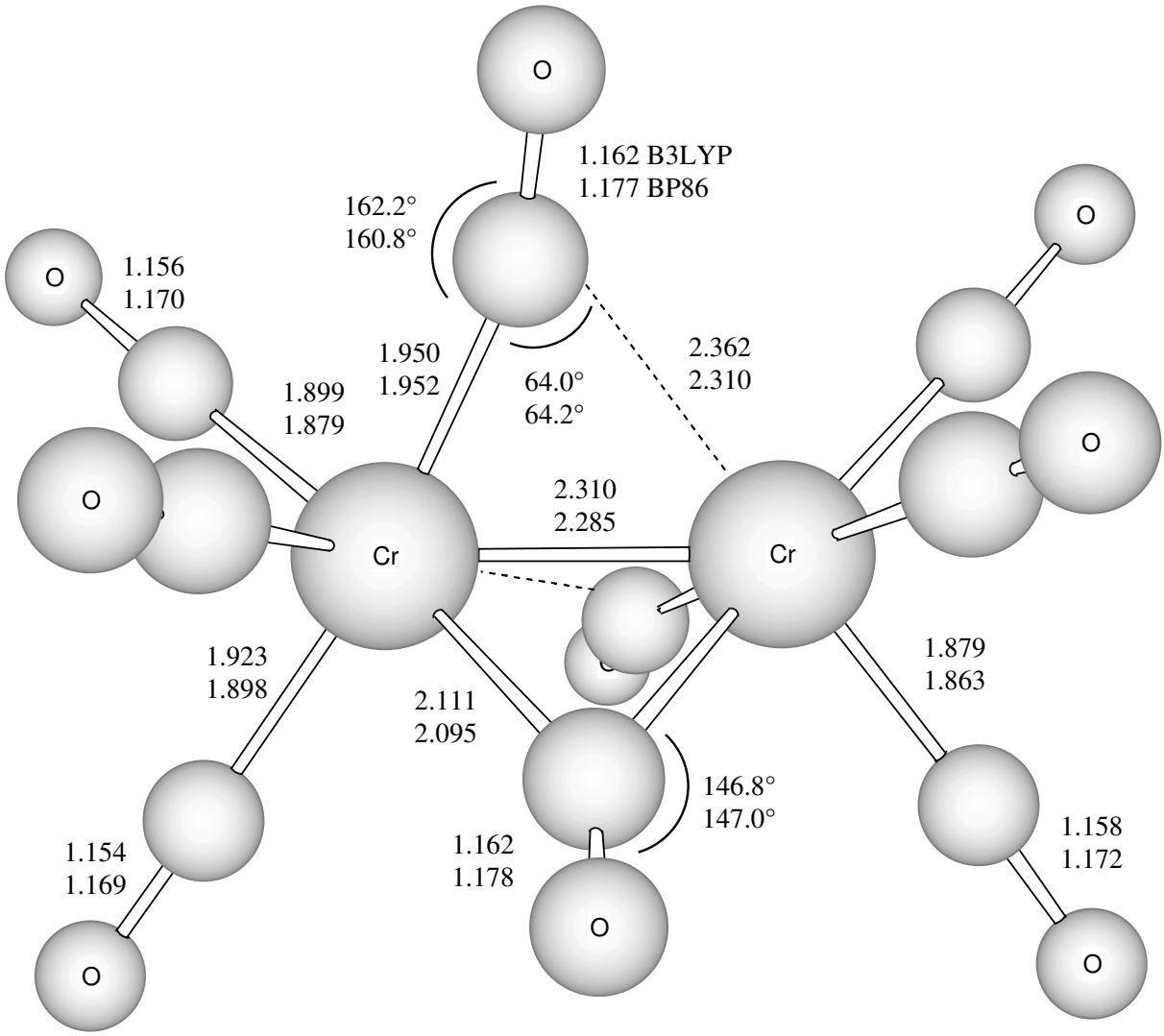

Figure 3.2 Asymmetrically tribridged BP86 minimum energy structure for singlet $Cr_2(CO)_9$ with C_2 symmetry. This structure has one small imaginary harmonic vibrational frequency for B3LYP and none with the BP86 method. Distances are reported in angstroms.

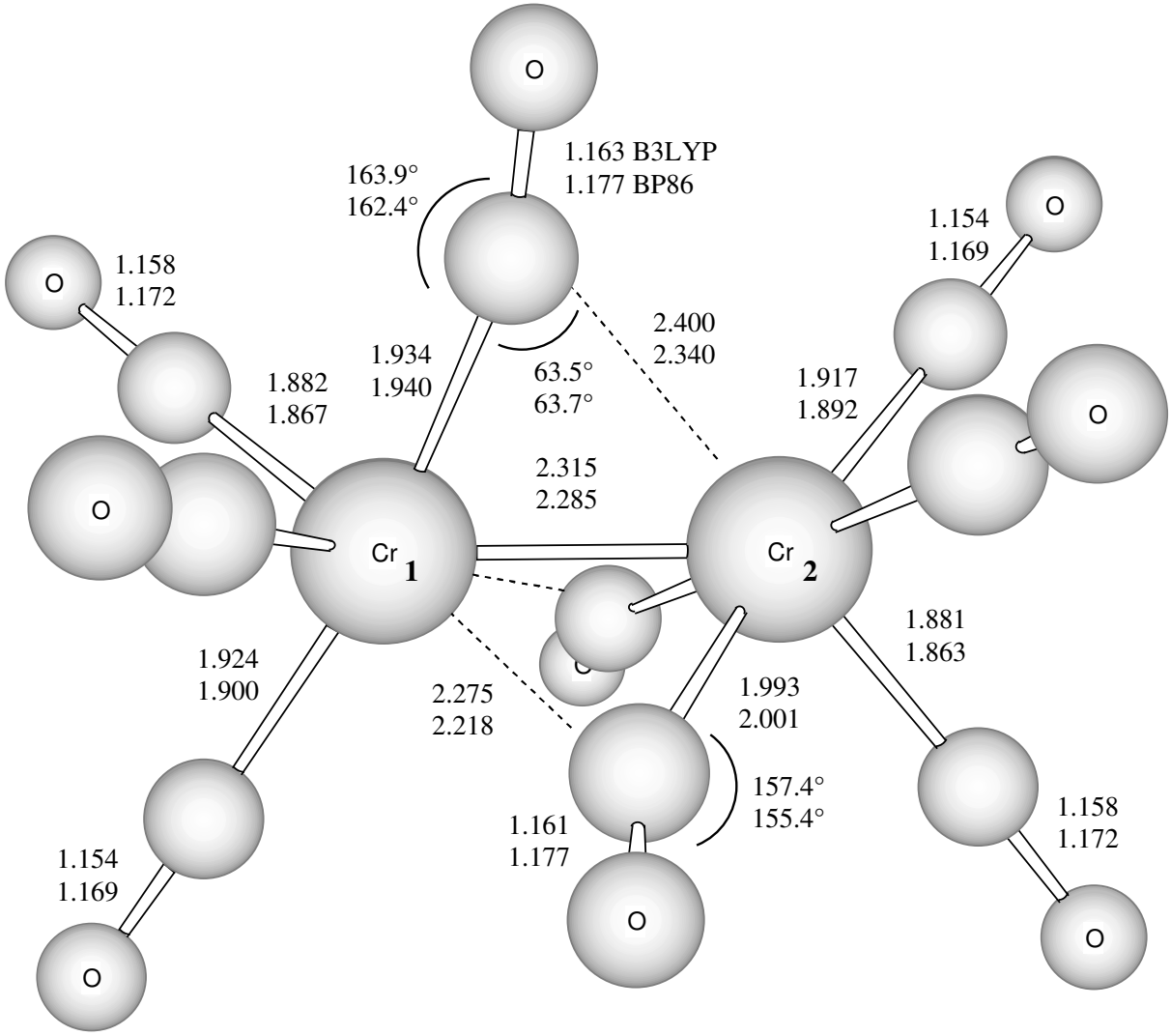

Figure 3.3 Asymmetrically tribridged B3LYP minimum energy structure for singlet $Cr_2(CO)_9$ with C_s symmetry. This structure has one small imaginary harmonic vibrational frequency for BP86 and none with the B3LYP method. Distances are reported in angstroms.

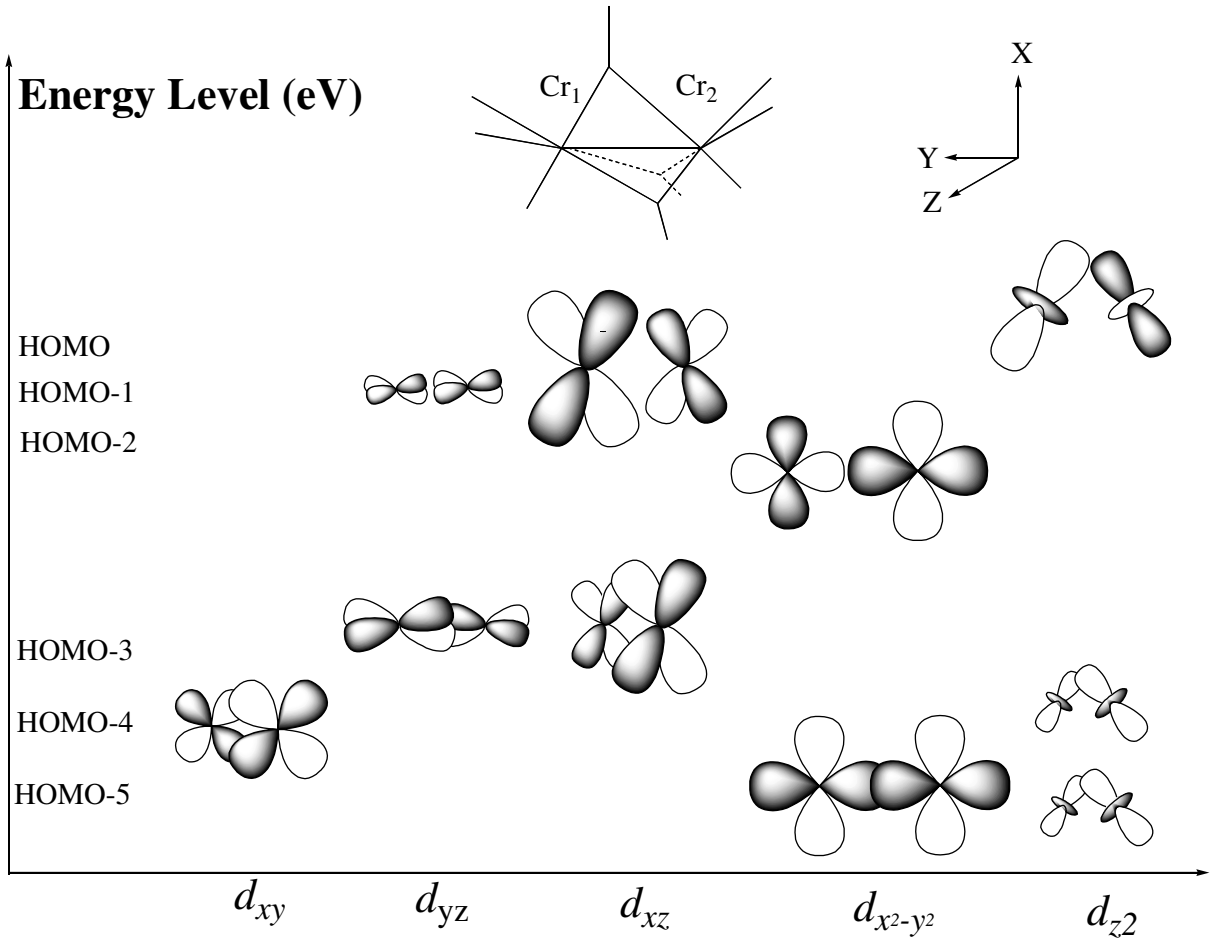

Figure 3.4 Symmetry-adapted linear combinations of the d atomic orbitals of the metal atoms (Cr_1 and Cr_2 assigned in Figure 3) for the molecular energy levels of the singlet $Cr_2(CO)_9$ with *Cs* symmetry.

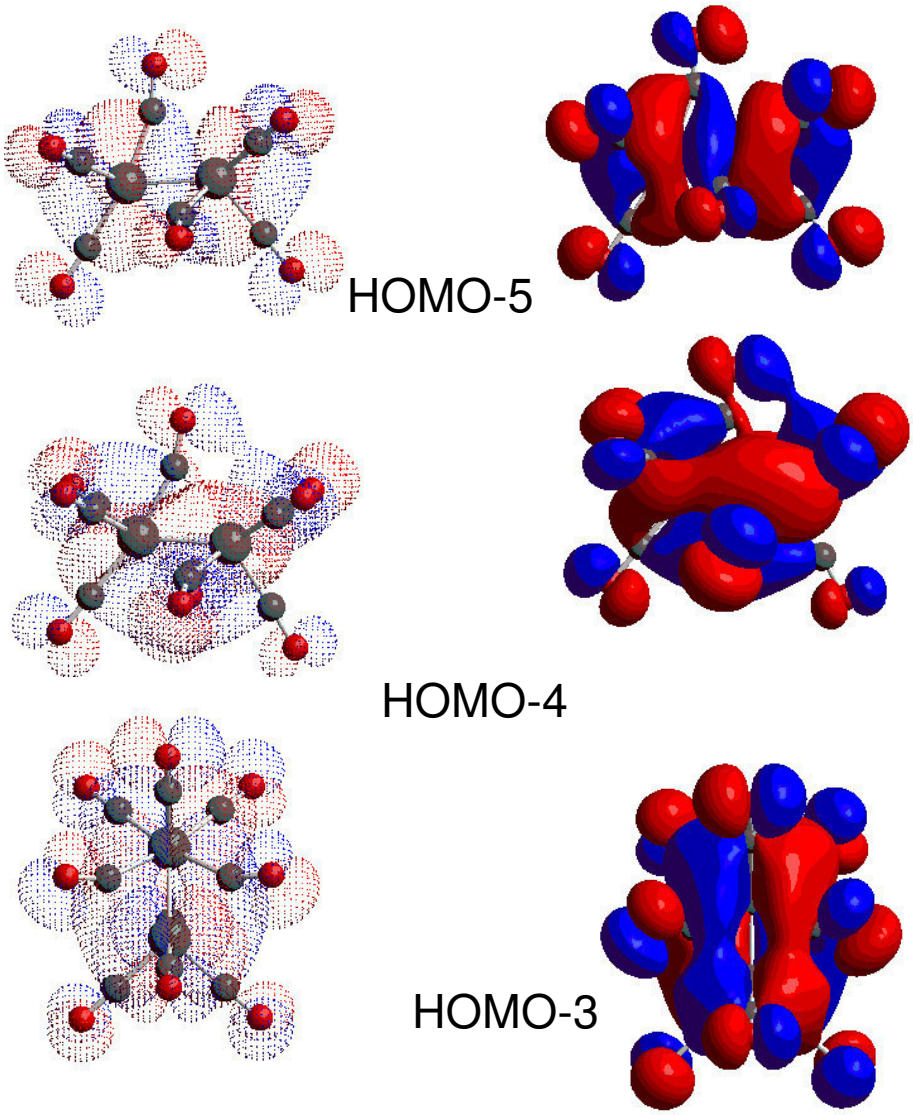

Figure 3.5 Molecular orbital plots of bonding orbitals of singlet $Cr_2(CO)_9$ in C_s symmetry, showing from the sixth valence molecular orbital HOMO-5 from the HOMO up to HOMO-3. For HOMO-5, the C_s plane is in the plane of the paper (*xy* plane) and viewed along the *z*axis. For HOMO-4, shown similarly to the HOMO-5. For HOMO-3, the C_s plane is perpendicular to the plane of the paper (*xz* plane)and viewed along the *x* axis.

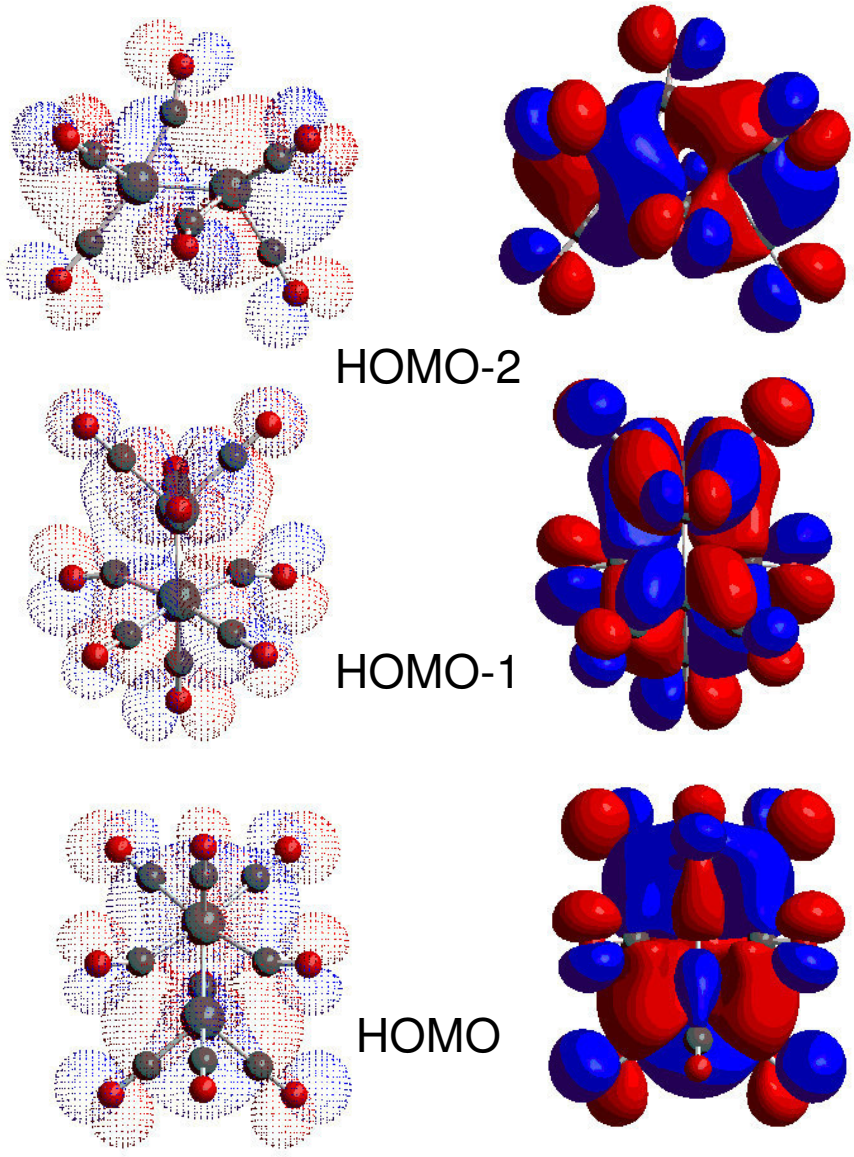

Figure 3.6 Molecular orbital plots of antibonding orbitals of singlet$Cr_2(CO)_9$ in C_s symmetry, showing from the third valence molecular orbital HOMO-2 from the HOMO up to the HOMO. For HOMO-2,the C_s plane is in the plane of the paper (xy plane) and viewed along the z axis. For HOMO-1, the C_s plane is perpendicular to the paper plane (xz plane) and viewed from the x axis. For HOMO, shown similarly to the HOMO-1.

Table 3.1 Relative Energies of Singlet $Cr_2(CO)_9$ and Its Dissociation Limits $Cr(CO)_4$ + $Cr(CO)_5$ and $Cr(CO)_3$ + $Cr(CO)_6$

			imaginary harmonic vibrational frequencies			relative energy (kcal/mol)	
species	sym	state	B3LYP	BP86	HF	B3LYP	BP86
$Cr_2(CO)_9$	D_{3h}	^1A_g	174i (e' ')	138i (e' ')	203i (e' ')	1.7	0.9
	C_2	^1A	55i (b)	none	162i (b)	0.1	0.0
	C_s	$^1A'$	none	22i (a' ')	none	0.0	0.0
$Cr(CO)_4$ + $Cr(CO)_5$	C_{2v} and C_{4v}	$^1A_1$ and $^1A_1$	none	none	none	31.8	42.9
$Cr(CO)_3$ + $Cr(CO)_6$	C_{3v} and O_h	$^1A_1$ and $^1A_1$	none	none	none	29.8	40.7

Table 3.2 Molecular Orbital Energy Levels and Percentage Contributions of d Atomic Orbitals to the MOs of $Cr_2(CO)_9$ with C_s symmetry

MO	energy (eV)	LARGEST CONTRIBUTIONS OF THE VALENCE ATOMIC ORBITALS (%)									
LUMO+1	-4.52	d_{xy} π*	53,[a] 53[b]								
LUMO	-4.55			d_{yz} π*	54,[a] 53[b]						
HOMO	-6.35	d_{xy} π*	-31, -16					d_{x2-y2} σ*	-13, 25	d_{z2} σ*	58, -47
HOMO-1	-6.40			d_{yz} π*	-23, -26	d_{xz} δ*	64, -47				
HOMO-2	-6.41	d_{xy} π*	-7, -15					d_{x2-y2} σ*	-47, 58	d_{z2} σ*	-37, 7
HOMO-3	-7.08			d_{yz} π	-42, 33	d_{xz} δ	36, 55				
HOMO-4	-7.21	d_{xy} π	-33, 45					d_{x2-y2} σ	-33,-5	d_{z2} σ	27, 47
HOMO-5	-7.43							d_{x2-y2} σ	56, 58	d_{z2} σ	27, 37

Table 3.3 Harmonic Vibrational Frequencies (cm^{-1}) and Their Infrared Intensities (km/mol, in parentheses) for the $Cr_2(CO)_9$ global Minimum Structure, of C_s Symmetry

B3LYP		BP86	
a' '			
32 (0)	424 (2)	44 (0)	431 (5)
47 (0)	433 (6)	52 (0)	435 (3)
56 (0)	474 (16)	58 (0)	471 (1)
68 (0)	485 (0)	83 (0)	480 (6)
84 (0)	525 (0)	86 (0)	510 (0)
88 (0)	554 (1)	-22 (0)	537 (1)
111 (1)	611 (70)	107 (1)	611 (72)
129 (2)	641 (45)	124 (0)	634 (26)
282 (1)	2016 (673)	274 (0)	1927 (696)
365 (0)	2046 (1306)	374 (0)	1970 (819)
377 (0)	2077 (743)	378 (0)	1987 (721)
414 (12)		422 (0)	
a'			
45 (2)	450 (5)	48 (2)	464 (10)
77 (0)	464 (39)	73 (0)	474 (7)
81 (0)	482 (38)	80 (0)	477 (17)
86 (1)	518 (4)	85 (1)	508 (1)
93 (1)	551 (16)	90 (0)	539 (12)
99 (1)	610 (96)	97 (1)	606 (99)
111 (0)	618 (99)	108 (0)	619 (84)
153 (4)	634 (186)	156 (1)	631 (176)
158 (11)	674 (7)	166 (13)	674 (2)
228 (8)	2002 (130)	237 (6)	1919 (6)
345 (72)	2019 (868)	336 (38)	1932 (784)
358 (2)	2057 (596)	359 (38)	1975 (430)
377 (12)	2062 (1449)	384 (15)	1981 (1130)
400 (13)	2090 (2282)	409 (24)	2008 (2213)
427 (59)	2149 (15)	440 (1)	2060 (5)
432 (1)		448 (56)	

Table 3.4: BP86 Harmonic Vibrational Frequencies (cm^{-1}) and Their Infrared Intensities (km/mol, in Parentheses) for the $Cr_2(CO)_9$ Structure, of D_{3h} Symmetry

a_1''	
41 (0)	425 (0)
a_1'	
82 (0)	667 (0)
280 (0)	1911 (0)
370 (0)	2059 (0)
472 (0)	
a_2''	
96 (1)	464 (4)
169 (18)	610 (264)
380 (341)	2004 (2462)
a_2'	
49 (0)	459 (0)
376 (0)	
e''	
87 (0)	508 (0)
87 (0)	508 (0)
113 (0)	623 (0)
113 (0)	623 (0)
270 (0)	-138 (0)
270 (0)	-138 (0)
441 (0)	1978 (0)
441 (0)	1978 (0)
e'	
56 (0)	470 (7)
56 (0)	470 (7)
86 (0)	531 (1)
86 (0)	531 (1)
92 (1)	608 (96)
92 (1)	608 (96)
365 (0)	1923 (783)
365 (0)	1923 (783)
439 (6)	1982 (1431)
439 (6)	1982 (1431)

CHAPTER 4

THE HIGHLY UNSATURATED BINUCLEAR CHROMIUM CARBONYL $Cr_2(CO)_8$[1]

[1] Se Li, R. Bruce King, Henry F. Schaefer III. Submitted to The Journal of Chemical Physics, 2/5/2004.

4.1 ABSTRACT

The first structural characterization of the highly unsaturated dichromium carbonyl $Cr_2(CO)_8$ is reported using density functional theory (DFT). $Cr_2(CO)_8$ is predicted to have a short metal-metal bond length of 2.30 Å (B3LYP) or 2.28 Å (BP86). The minimum energy structure exhibits distorted C_s symmetry, with non-equivalent chromium atoms and two equivalent asymmetrically bridging carbonyls. A high symmetry (D_{2d}) structure with a nominal chromium-chromium quadruple bond lies ~ 22 kcal/mol higher in energy. Three other higher energy structures are also found, including two geometries with two bridging carbonyls best interpreted as four-electron donors. The dissociation energy of $Cr_2(CO)_8$ to the fragments $2Cr(CO)_4$ or $Cr(CO)_3$ plus $Cr(CO)_5$ is predicted to be about 34 kcal/mol (B3LYP) or 44 kcal/mol (BP86) indicating that $Cr_2(CO)_8$, like $Cr_2(CO)_9$ but unlike $Cr_2(CO)_{10}$ and $Cr_2(CO)_{11}$, is stable with respect to dissociation into its fragments.

4.2 INTRODUCTION

In recent years there have been several studies of highly unsaturated homoleptic binuclear carbonyls of the first-row transition metals. This work has included the carbonyls $Co_2(CO)_5$,[1] $Fe_2(CO)_6$,[2] and $Mn_2(CO)_7$,[3] all of which are required by the simple 18-electron rule[4] to have formal metal-metal quadruple bonds[5], assuming that all of their carbonyl groups are simple two-electron donors. Indeed, in all three cases structures were found with short metal-metal distances (2.171 Å for $Co_2(CO)_5$, 2.00 Å for $Fe_2(CO)_6$, and 2.21–2.26 Å for $Mn_2(CO)_7$), consistent with such metal-metal quadruple bonding. However, for $Fe_2(CO)_6$ and $Mn_2(CO)_7$ other structures were also found having longer metal-metal bond distances and two bridging CO groups oriented

to suggest four-electron rather than the usual two-electron donors. In these cases the 18-electron rule would require formal metal-metal double bonding rather than formal metal-metal quadruple bonding, in accord with the lengthened metal-metal bond distances found computationally.

The system of homoleptic binuclear carbonyls of chromium is different from those of manganese, iron, and cobalt in a number of significant ways. Most obvious to the experimentalist is the fact that among the species predicted by the 18-electron rule to have formal metal-metal single bonds, the molecule $Cr_2(CO)_{11}$ [6] is not isolable in contrast to $Mn_2(CO)_{10}$, $Fe_2(CO)_9$, and $Co_2(CO)_8$, which are all stable metal carbonyls and even commercially available. Consistent with this experimental observation are our studies of $Cr_2(CO)_{11}$ indicating a relatively long chromium-chromium distance (no B3LYP value is available, 3.15 Å by BP86) and thermodynamic instability with respect to $Cr(CO)_6$ and $Cr(CO)_5$. A similar thermodynamic instability was predicted for $Cr_2(CO)_{10}$.[7] Only in the case of the more highly unsaturated $Cr_2(CO)_9$[8] was a thermodynamically stable binuclear derivative found with a short chromium-chromium distance (2.315 Å B3LYP or 2.285 Å BP86) consistent with the Cr≡Cr triple bond required by the 18-electron rule.

The objective of the present study was to extend this computational work on homoleptic binuclear chromium carbonyls to the next most highly unsaturated member, namely $Cr_2(CO)_8$, required by the 18-electron rule to contain a chromium-chromium quadruple bond. Such chromium-chromium quadruple bonds have been postulated for chromium(II) compounds with short chromium-chromium distances including chromium(II) acetate, $Cr_2(O_2CCH_3)_4 \cdot 2H_2O$ (2.362 Å),[9] which has been known since the nineteenth century, as well as more recently discovered strictly organometallic derivatives exhibiting much shorter chromium-chromium distances such as $Li_4[Cr_2(CH_3)_8] \cdot 4C_4H_8O$ (1.98 Å)[10], $Cr_2(\eta^3\text{-}C_3H_5)_4$ (1.98 Å)[11], and the ultra-

short $Cr_2(DMP)_4$ (1.85 Å)[12,13]. However, no binuclear chromium(0) compound is known with a short chromium-chromium distance and an electronic configuration suggestive of quadruple bonding.

4.3 THEORETICAL METHODS

Our basis set for C and O begins with Dunning's standard double-ζ contraction[14] of Huzinaga's primitive sets[15] and is designated (9s5p/4s2p). The double-ζ plus polarization (DZP) basis set used here adds one set of pure spherical harmonic *d* functions with orbital exponents α_d(C) = 0.75 and α_d(O) = 0.85 to the DZ basis set. For Cr, our loosely contracted DZP basis set, the Wachters' primitive set,[16] is used, but augmented by two sets of *p* functions and one set of *d* functions, contracted following Hood, Pitzer and Schaefer [17] and designated (14s11p6d/10s8p3d). For $Cr_2(CO)_8$ there are 338 contracted Gaussian functions in the present DZP basis set.

Electron correlation effects were included employing DFT methods, which are acknowledged to be a practical and effective computational tool, especially for organometallic compounds.[18] Among density functional procedures, the most reliable approximation is often thought to be the hybrid Hartree-Fock (HF)/DFT method, B3LYP, which uses the combination of the three-parameter Becke exchange functional with the Lee-Yang-Parr correlation functional.[19,20] However, another DFT method, which combines Becke's 1988 exchange functional with Perdew's 1986 nonlocal correlation functional method (BP86), has proven perhaps even more effective[21] for organotransition metal systems and is also used in this research.[22,23]

We fully optimized the geometries of all structures with the DZP B3LYP and DZP BP86 methods. At the same levels we also computed the vibrational frequencies by evaluating analytically the second derivatives of the energy with respect to the nuclear coordinates. The corresponding infrared intensities are evaluated analytically as well. All of the computations were carried out with the Gaussian 94 program,[24] in which the fine grid (75 302) is the default for evaluating integrals numerically, and the tight (10^{-8} hartree) designation is the default for the self-consistent field (SCF) convergence.

In the search for minima using all currently implemented DFT methods, low magnitude imaginary vibrational frequencies are suspect because of significant limitations in the numerical integration procedures used in the DFT computations. Thus, for an imaginary vibrational frequency with a magnitude less than 100 cm^{-1}, there is an energy minimum identical to or very close to the structure of the stationary point in question. Therefore, we generally do not follow such low imaginary vibrational frequencies. In the present case the B3LYP and BP86 methods agree with each other fairly well for predicting the structural characteristics of $Cr_2(CO)_8$. Slight discrepancies in the appearance of possibly artifactual imaginary harmonic vibrational frequency remains, however.

4.4 RESULTS AND DISCUSSION

4.4.1 GEOMETRIC STRUCTURES

Five isomers of $Cr_2(CO)_8$ stoichiometry, bridged and unbridged, were found in this computational study (Table 1). The B3LYP and BP86 functionals agree in the relative energetic orders of these isomers.

The lowest-lying minimum for $Cr_2(CO)_8$ has an unsymmetrical dibridged $(OC)_3CrCr(CO)_5$ structure with C_s symmetry (Figure 1), which can be derived directly from the C_s structure [8] of unsaturated $Cr_2(CO)_9$. Thus removal of one terminal CO group from Cr(1) in $Cr_2(CO)_9$ leads to the lowest-lying structure of $Cr_2(CO)_8$. In this structure the chromium-chromium distance is 2.295 Å B3LYP or 2.276 Å BP86, respectively, which is shortened slightly by 0.02 Å B3LYP or 0.01 Å BP86 from the chromium-chromium distances computed for $Cr_2(CO)_9$. In going from $Cr_2(CO)_9$ to this $Cr_2(CO)_8$ structure, one of the three bridging CO groups, which is a symmetrical bridge in $Cr_2(CO)_9$, becomes a very unsymmetrical semibridging CO in $Cr_2(CO)_8$ with Cr–C distances of 1.855 Å B3LYP or 1.837 Å BP86 to Cr(1) and 2.527 Å B3LYP or 2.512 Å BP86 to Cr(2). The approximate coordination geometries of the chromium atoms (Figure 1) are square pyramidal for Cr(1) and octahedral for Cr(2) if the ~2.5 Å distance from the semibridging CO group to Cr(2) is counted as a Cr–C bond. The bond angle Cr(1)CO relaxes from 163.9° B3LYP or 162.4° BP86 in $Cr_2(CO)_9$ to 171.4° B3LYP or 172.8° BP86, respectively, in this structure of $Cr_2(CO)_8$. Consequently, the Cr(1)–C(1) distance decreases from 1.934 Å B3LYP or 1.940 Å BP86 in $Cr_2(CO)_9$ to 1.855 Å B3LYP or 1.837 Å BP86 in $Cr_2(CO)_8$. These results are both suggestive of a stronger interaction between Cr(1) and C(1) in $Cr_2(CO)_8$ relative to $Cr_2(CO)_9$. Meanwhile, the interaction between the Cr(2) and C(1) is weakened from $Cr_2(CO)_9$ to $Cr_2(CO)_8$, which leads to a longer Cr(2)–C(1) distance and a shorter Cr(2)–C(2) distance. Otherwise, the structures of this lowest energy isomer of $Cr_2(CO)_8$ and $Cr_2(CO)_9$ are very similar. Thus in both structures the two chromium atoms have square planar $Cr(CO)_2(\mu\text{-}CO)_2$ environments involving two bridging carbonyl groups and two terminal carbonyl groups. The B3LYP functional predicts all real vibrational frequencies. However, the BP86 functional computes a very small imaginary frequency (28 cm^{-1}).

The isomer of next lowest energy is a C_i symmetrical dibridged $(OC)_4CrCr(CO)_4$ structure lying about 8 kcal/mol above the global minimum (Figure 2). The chromium-chromium bond distance in this structure is significantly longer than that for the global minimum (2.514 Å B3LYP or 2.469 Å BP86). Notably, the two bridging carbonyls are coplanar with the two chromium atoms and bent to about 160°. Both B3LYP and BP86 functionals predict a very small imaginary frequency (36 cm^{-1} or 35 cm^{-1}, respectively), which may be due to numerical noise.

The third $Cr_2(CO)_8$ isomer also has a dibridged structure and lies energetically above the global minimum by 13.4 to 18.7 kcal/mol (Figure 3). Notably, this structure has a significantly longer chromium-chromium distance, namely 2.747 Å B3LYP or 2.712 Å BP86. For the two bridging COs the Cr–C–O angles are roughly linear and the Cr–O distance is significantly shorter (2.503 Å B3LYP or 2.466 Å BP86) than the other $Cr_2(CO)_8$ isomers. This suggests a direct interaction between the chromium and oxygen atoms of these two bridging CO groups in accord with these CO groups functioning as four-electron donors rather than the usual two-electron donors. In this case the chromium-chromium bond needs only to be a double bond rather than a quadruple bond to give both chromium atoms the favored 18-electron configuration. This conclusion is in accord with the significantly longer chromium-chromium distance in this isomer as compared with the other isomers (Table 1). Both the B3LYP and the BP86 functionals give consistent agreement for the vibrational frequency calculations leading to similar small imaginary frequencies (36 cm^{-1} or 35 cm^{-1}, respectively).

The energetically highest lying isomers found for $Cr_2(CO)_8$ are two non-bridged structures, namely the symmetrical D_{2d} isomer $(OC)_4CrCr(CO)_4$ and the unsymmetrical C_s isomer $(OC)_3CrCr(CO)_5$ (Figures 4 and 5). These isomers lie approximately 20 kcal/mol above

the global minimum and are predicted to be genuine minima by both the B3LYP and BP86 functionals. The D_{2d} structure possesses the shortest chromium-chromium distance (2.279 Å B3LYP and 2.217 Å BP86) among the five isomers of $Cr_2(CO)_8$. The unsymmetrical $(OC)_3CrCr(CO)_5$ structure of the C_s isomer is very similar to that of the unsymmetrical C_s isomer $(OC)_3MnMn(CO)_5$ of $Mn_2(CO)_8$, lying only ~2 kcal/mol above the D_{2d} more symmetrical global minimum of $Mn_2(CO)_8$[3,25]. The chromium-chromium distance is 2.327 Å B3LYP or 2.267 Å BP86, which is shorter by 0.074 Å than that for $(OC)_3MnMn(CO)_5$.

4.4.2 VIBRATIONAL FREQUENCIES

The first three low-lying structures can be considered as minima on the potential energy surface (PES) with the small observed imaginary harmonic vibrational frequencies being an artifact of the DFT method. An interesting contradiction again exists between the B3LYP and BP86 functionals for the global minimum structure of $Cr_2(CO)_8$ (Figure 1) as in the previous work on $Cr_2(CO)_9$[8]. Only the BP86 method predicts one small imaginary frequency 28 cm^{-1} (a") for the lowest energy structure, and it is predicted to be a genuine minimum with the B3LYP method. For other isomers, the two methods agree with each other very well.

The B3LYP and BP86 vibrational frequencies for the five isomers of $Cr_2(CO)_8$ are listed in Tables 2 through 6. As expected, the CO stretching frequencies have the highest infrared intensities and are expected to dominate the vibrational spectrum. Note also that, for molecules such as $Mn_2(CO)_{10}$, $Fe_2(CO)_9$, and $Co_2(CO)_8$, the BP86 method predicts vibrational frequencies more reliably than B3LYP. For $Mn_2(CO)_{10}$, for example, agreement between BP86 and experimental CO stretching frequencies is typically within 10 cm^{-1}.

4.4.3 THERMOCHEMISTRY

The energy of unsymmetrical dissociation of $Cr_2(CO)_8$ to $Cr(CO)_3$ and $Cr(CO)_5$ fragments is predicted to be 35 kcal/mol with the B3LYP functional or 44 kcal/mol with the BP86 functional. Similarly the energy of symmetrical dissociation of $Cr_2(CO)_8$ to two $Cr(CO)_4$ fragments is computed to be 34 kcal/mol (B3LYP) or 44 kcal/mol(BP86). This demonstrates that the interaction between the two chromium fragments for $Cr_2(CO)_8$ is similar to that previously found for $Cr_2(CO)_9$, but different from the much weaker interactions between the two mononuclear chromium carbonyl fragments found for $Cr_2(CO)_{10}$ and $Cr_2(CO)_{11}$. For comparison, the dissociation energy of $Cr_2(CO)_9$ to $Cr(CO)_4$ and $Cr(CO)_5$ fragments is predicted to be 32 kcal/mol with the B3LYP functional or 43 kcal/mol with the BP86 functional, while dissociation to $Cr(CO)_3$ and $Cr(CO)_6$ fragments is predicted to be 41 kcal/mol (B3LYP) or 30 kcal/mol (BP86). The dissociation energy of $Cr_2(CO)_9$ to $Cr_2(CO)_8$ and CO is calculated to be 37 kcal/mol with the B3LYP functional or 44 kcal/mol with the BP86 functional.

4.4.4 MOLECULAR ORBITALS

Electron density plots of the six valence molecular orbitals (MOs) of $Cr_2(CO)_8$ in C_s symmetry are shown in Figure 6. These range from the sixth highest occupied orbital (HOMO-5) to the highest occupied orbital (HOMO). The symmetry-adapted linear combinations of the *d* atomic orbitals provide the bonding and antibonding interactions between the metal atoms. The results suggest that HOMO-5, HOMO-4 and HOMO-3 are primarily the direct *d-d* bonding orbitals.

For instance, HOMO-5 appears to be a strong Cr-Cr σ bonding orbital. The orbitals with antibonding character appear to be HOMO-2, HOMO-1, and the HOMO.

Comparison plots have been made for the $Cr_2(CO)_9$ molecule, global minimum of C_s symmetry, and these are seen in Figure 7. Basically, the MOs of the $Cr_2(CO)_9$ are rather similar to those of $Cr_2(CO)_8$. The similarity of the MOs suggests that $Cr_2(CO)_8$ is a potentially stable molecule like $Cr_2(CO)_9$. It also explains the similarity of the dissociation energies to fragments from $Cr_2(CO)_8$ and $Cr_2(CO)_9$.

4.5 CONCLUDING REMARKS

Several of the structures predicted for $Cr_2(CO)_8$, including the global minimum, require chromium-chromium bonds of order four to give the two chromium atoms the 18-electron configuration. In general, the computed chromium-chromium distances for such structures fall in the range 2.2 to 2.3 Å. These distances are appreciably longer than the 1.85 Å chromium-chromium distances found experimentally in $Cr_2(DMP)_4$. The latter molecule, however, involves formally chromium (II) derivatives rather than the present chromium (0) in $Cr_2(CO)_8$. These significant metal-metal bond length differences may relate to the difference in formal metal oxidation state or to the very different types of ligands.

4.6 ACKNOWLEDGMENTS

We are grateful for the support of this work by NSF Grants CHE-0136186 and CHE-0209857.

4.7 LITERATURE REFERENCES

1. Kenny, J.; King, R. B.; Schaefer, H. F., *Inorg. Chem.*, **2001**, *40*, 900.
2. Xie, Y.; King, R. B.; Schaefer, H. F., *J. Am. Chem. Soc.*, **2000**, *122*, 8746.
3. Xie, Y.; Jang, J. H.; King, R. B.; Schaefer, H. F., *Inorg. Chem.*, **2003**, *42*, 5219.
4. Green, M. L. H., *J. Organomet. Chem.* **1995**, *500*, 127.
5. A useful monograph on metal-metal multiple bonds is Cotton, F. A.; Walton, R. A. Multiple Bonds Between Metal Atoms Clarendon Press: Oxford, 2th edition **1993**.
6. Richardson, N. A.; Xie, Y.; King, R. B.; Schaefer, H. F., *J. Phys. Chem. A*, **2001**, *105*, 11134.
7. Li, S.; Richardson, N. A.; Xie, Y.; King, R. B.; Schaefer, H. F., *Faraday Discuss.*, **2003**, *124*, 315.
8. Li, S.; Richardson, N. A.; King, R. B.; Schaefer, H. F., *J. Phys. Chem., A, **2003**, 107*, 10118.
9. Cotton, F. A.; DeBoer B. G.; LaPrade, M. D.; Pipal , J. R., Ucko, D. A., *J. Amer. Chem. Soc., **1970***, *92*, 2926.
10. Krausse, J.; Marx, G.; Schodl, G., *J. Organometal. Chem.*, ***1970***, *21*, 159.
11 Aoki, T.; Furusaki, A.; Tomiie, Y.; Ono, K.; Tanaka, K., *Bull. Chem. Soc. Jap.*, ***1969***, *42*, 545.
12. Cotton, F. A.; Koch, S.; Millar, M., *J. Am. Chem. Soc.*, **1977**, *99*, 7372.
13. Cotton, F. A.; Koch, S. A.; Millar, M., *Inorg. Chem.*, **1978**, *17*, 2087.
14. Dunning, T. H., *J. Chem. Phys.*, **1970**, *53*, 2823.
15. Huzinaga, S., *J. Chem. Phys.*, **1965**, *42*, 1293.
16. Wachters, A. J. H., *J. Chem. Phys.*, **1970**, *52*, 1033.

17. Hood, D. M.; Pitzer, R. M.; Schaefer, H. F., *J. Chem. Phys*., **1979**, *71*, 705.

18. Ziegler, T., *Can. J. Chem*., **1995**, *73*, 743.

19. Becke, A. D., *J. Chem. Phys.*, **1993**, *98*, 5648.

20. Lee, C., Yang, W.; Parr, R. G., *Phys. Rev. B*, **1988**, *37*, 785.

21. Jonas, V.; Thiel, W., *Organometal.*, **1998**, *17*, 353.

22. Becke, A. D., *Phys. Rev. A*, **1988**, *38*, 3098.

23. Perdew, J. P., *Phys. Rev. B*, **1986**, *33*, 8822; *34*, 7046.

24. Gaussian 94 (Revision B. 3), Frisch, M. J.; Trucks, G. W.; Schlegel, H. B.; Gill, P. M. W.; Johnson, B. G.; Robb, M. A.; Cheeseman, J. R.; Keith, T. A.; Petersson, G. A.; Montgomery, J. A.; Raghavachari, K.; Al-Laham, M. A.; Zakrzewski, V. G.; Ortiz, J. V.; Foresman, J. B.; Cioslowski, J.; Stefanov, B. B.; Nanayakkara, A.; Challacombe, M.; Peng, C. Y.; Ayala, P. Y.; Chen, W.; Wong, M. W.; Andres, J. L.; Replogle, E. S.; Gomperts, R.; Martin, R. L.; Fox, D. J.; Binkley, J. S.; Defrees, J. D.; Baker, J.; Stewart, J. P.; Head-Gordon, M.; Gonzalez, C.; Pople, J. A., Gaussian, Inc., Pittsburgh PA, **1995.**

25 Barckholtz, T. A.; Bursten, B. E., *J. Am. Chem. Soc*., **1998**, *120*, 1926.

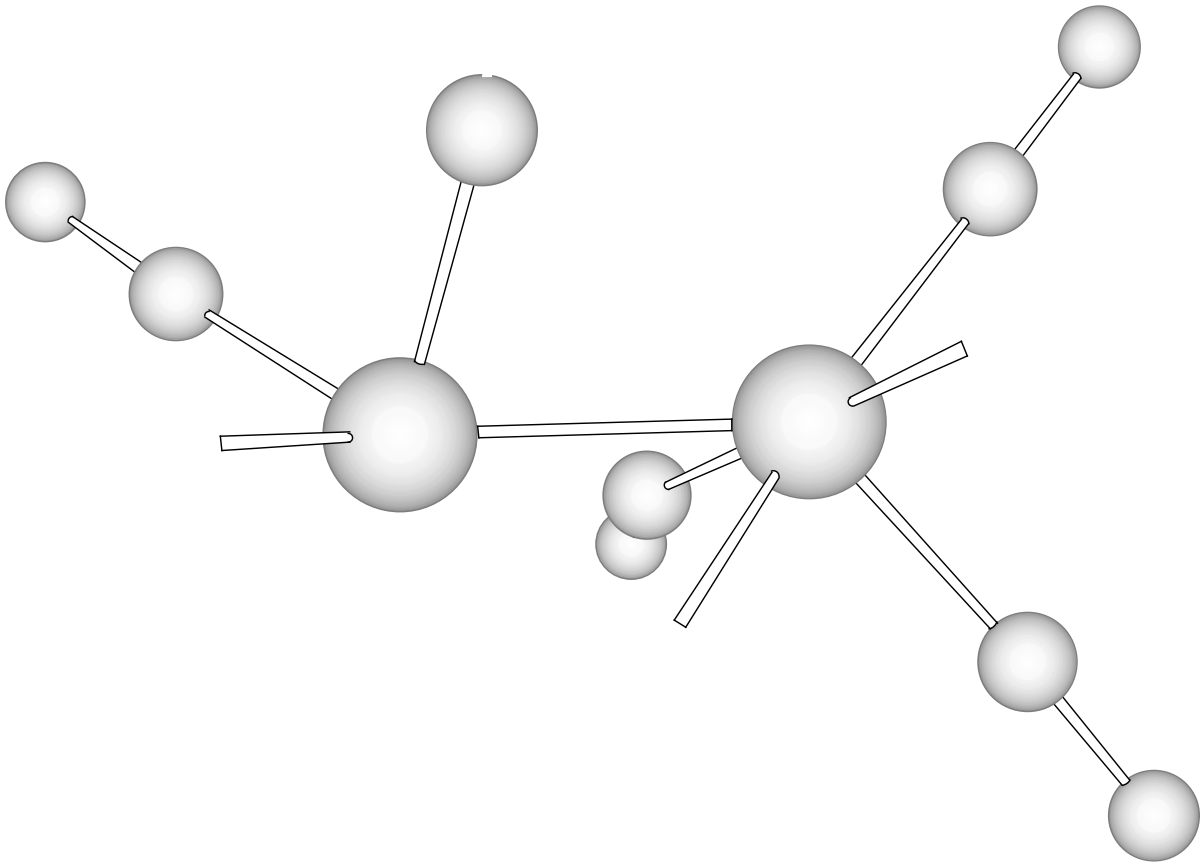

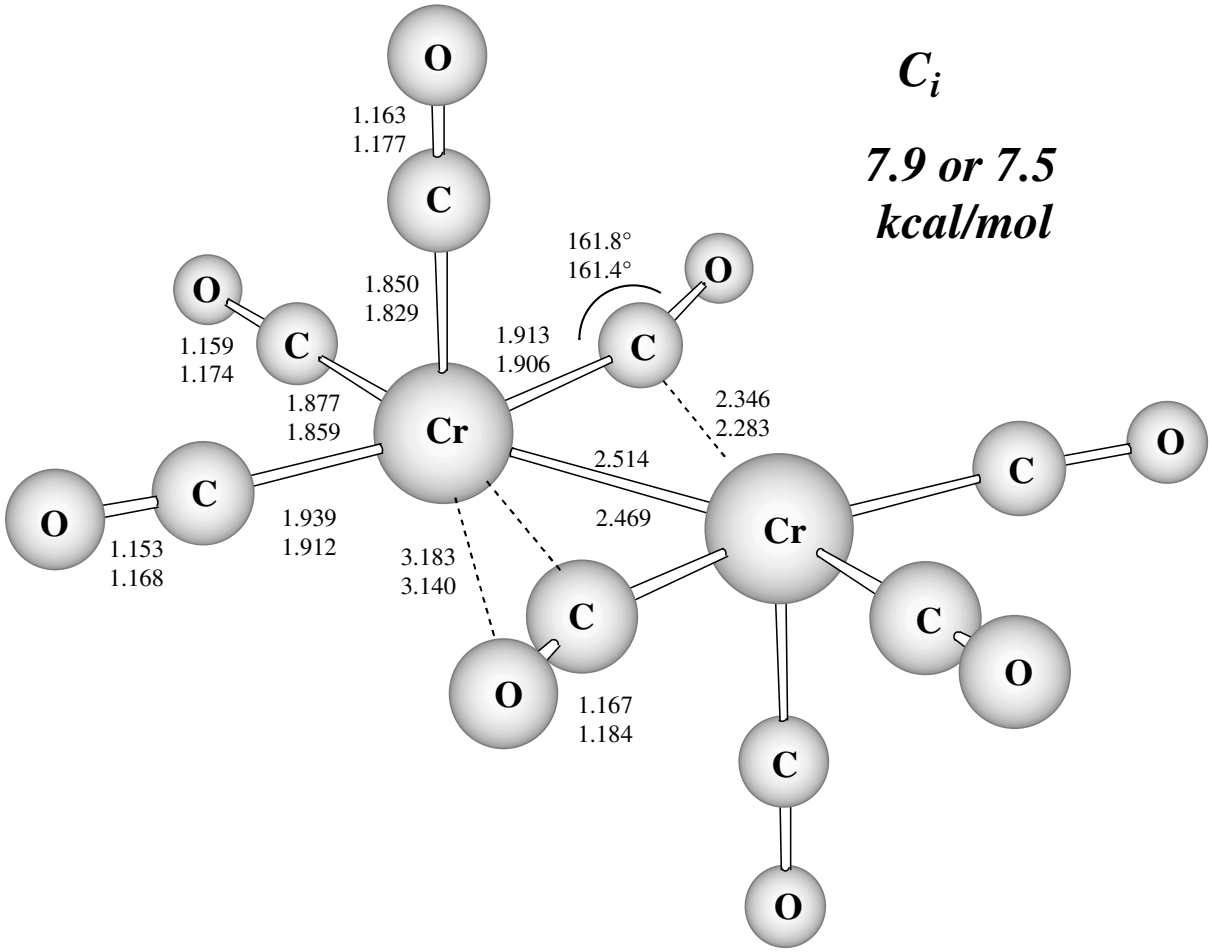

Figure 4.2 The symmetrically dibridged structure for singlet $Cr_2(CO)_8$ with C_i symmetry. This structure has one small imaginary harmonic vibrational frequency with both the B3LYP and BP86 methods. Distances are reported in angstroms.

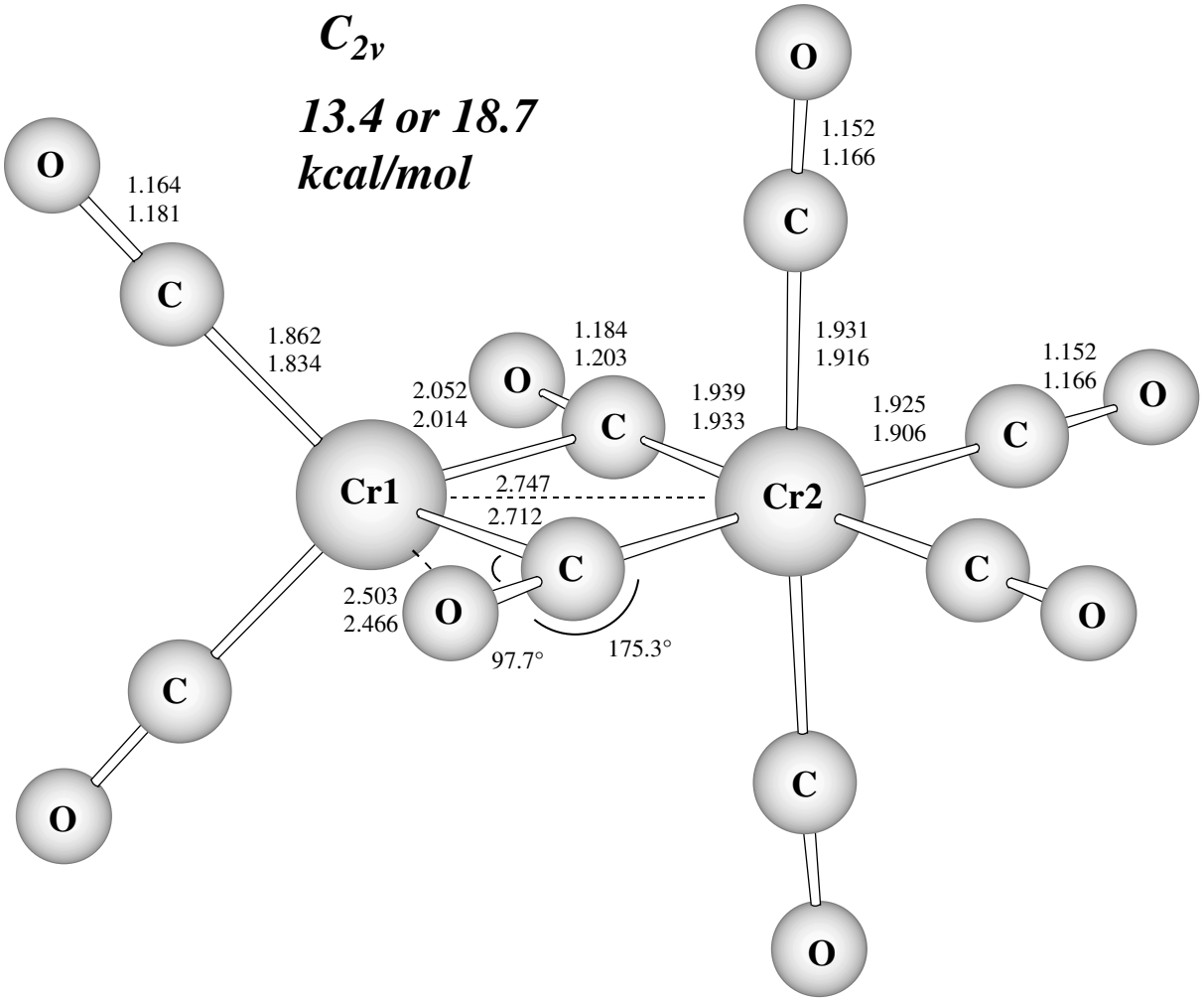

Figure 4.3 The asymmetrically dibridged structure for singlet $Cr_2(CO)_8$ with C_{2v} symmetry. This structure has one small imaginary harmonic vibrational frequency for B3LYP and BP86methods. Distances are reported in angstroms.

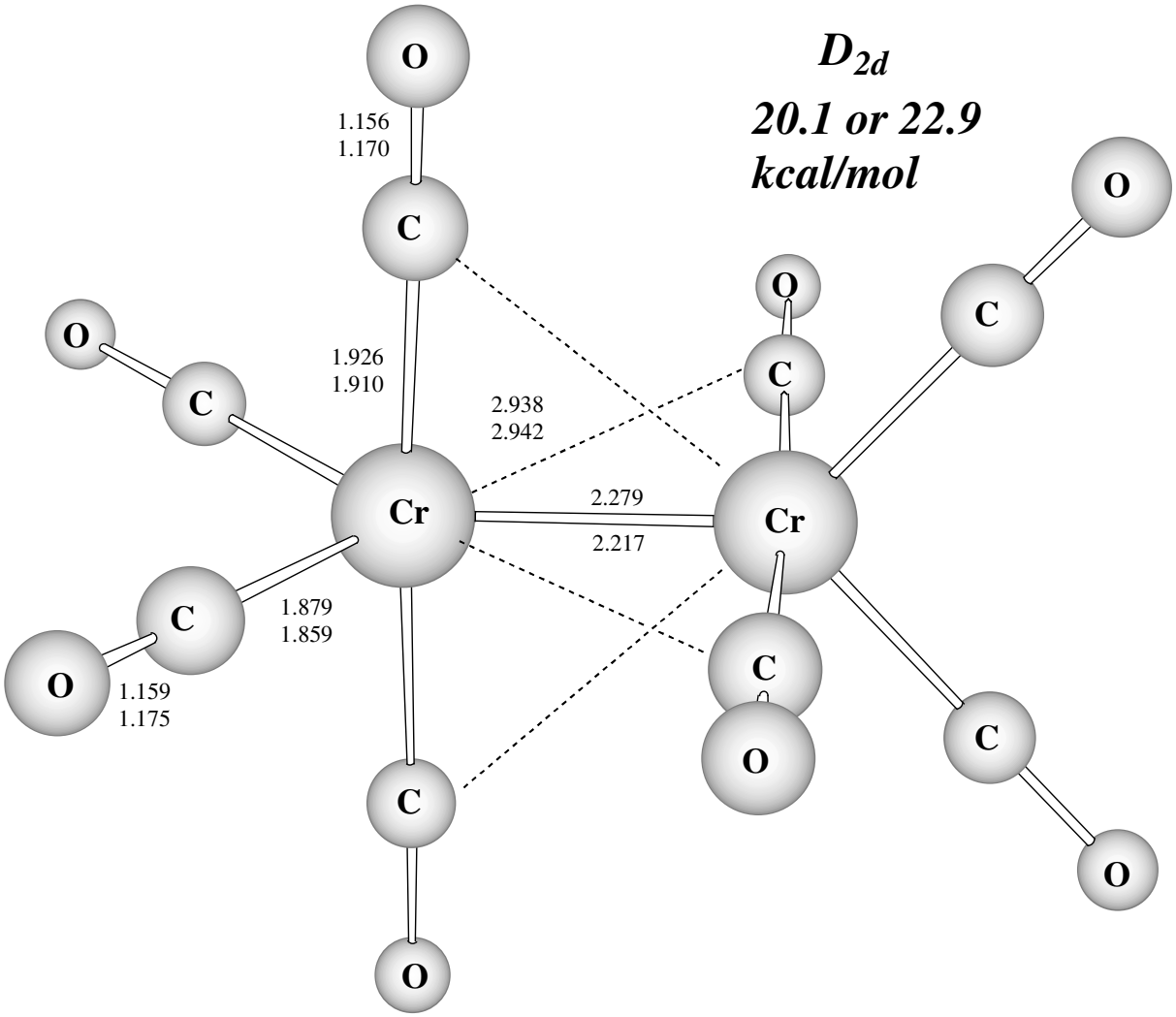

Figure 4.4 The symmetrically nonbridged minimum energy structure for singlet $Cr_2(CO)_8$ with D_{2d} symmetry. This structure has all real harmonic vibrational frequency for B3LYP and BP86 methods. Distances are reported in angstroms.

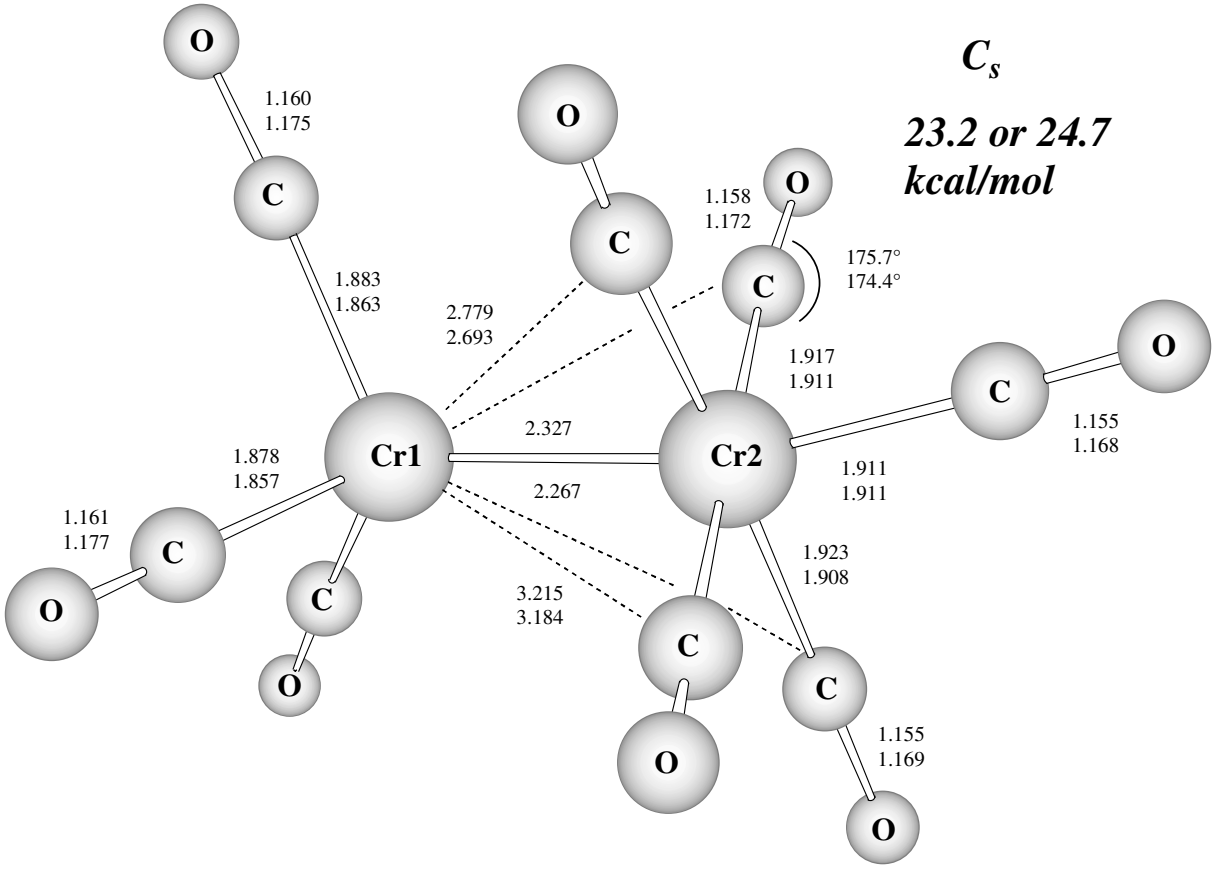

Figure 4.5 The asymmetrically nonbridged minimum energy structure for singlet $Cr_2(CO)_8$ with C_s symmetry. This structure has all real harmonic vibrational frequencies for B3LYP and BP86 methods. Distances are reported in angstroms.

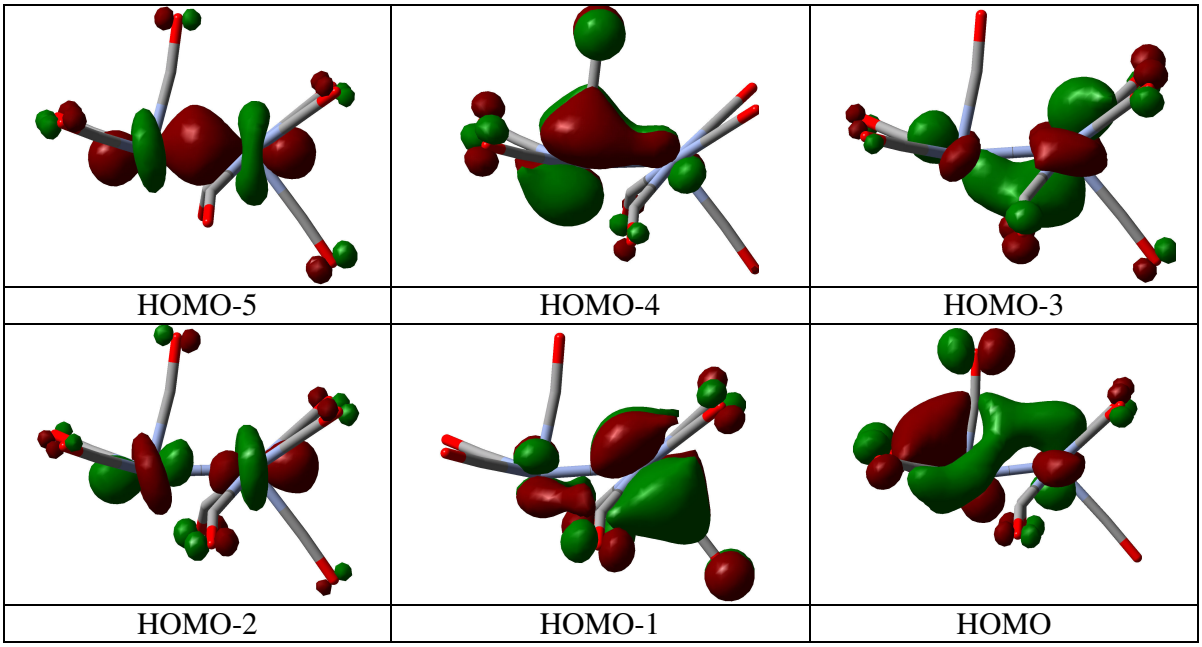

Figure 4.6 Valence molecular orbital plots for singlet $Cr_2(CO)_8$ in C_s symmetry, showing from the sixth highest occupied valence molecular orbital HOMO-5 to the HOMO.

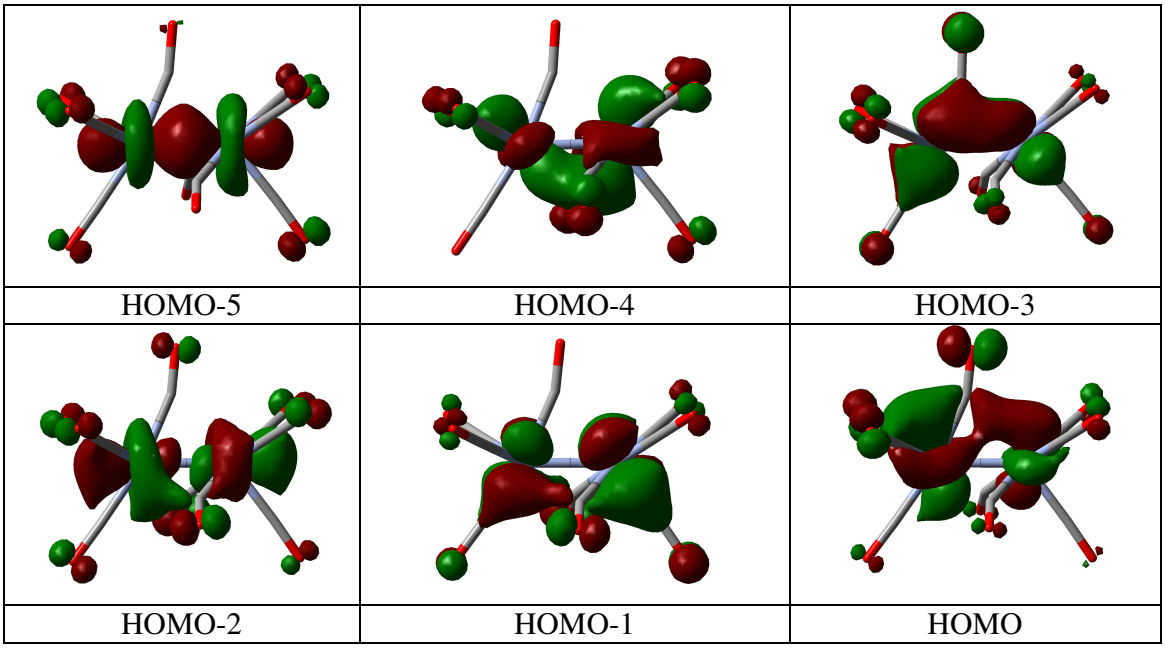

Figure 4.7 Valence molecular orbital plots for singlet $Cr_2(CO)_9$ in C_s symmetry, showing from the sixth highest occupied valence molecular orbital HOMO-5 to the HOMO.

Table 4.1 Relative energies of singlet $Cr_2(CO)_8$ and its dissociation limits $2Cr(CO)_4$ and $Cr(CO)_3 + Cr(CO)_5$.

SPECIES	SYM.	STATE	Cr-Cr BOND DISTANCE (Å)		IMAGINARY HARMONIC VIBRATIONAL FREQUENCIES		RELATIVE ENERGY (KCAL/MOL)	
			B3LYP	BP86	B3LYP	BP86	B3LYP	BP86
$Cr_2(CO)_8$	C_s	^1A	2.295	2.276	none	28i (a)	0.0	0.0
	C_i	^1A	2.514	2.469	36i (a_u)	35i (a_u)	7.9	7.5
	C_{2v}	$^1A_1$	2.747	2.712	53i (b_2)	65i (b_2)	13.4	18.7
	D_{2d}	$^1A_1$	2.279	2.217	none	none	20.1	22.9
	C_s	$^1A_1$	2.327	2.267	none	none	23.2	24.7
$2Cr(CO)_4$	C_{2v}	$^1A_1$			none	none	34.2	43.9
$Cr(CO)_3 + Cr(CO)_5$	C_{3v} & C_{4v}	$^1A_1$ & $^1A_1$			none	none	34.5	44.0

Table 4.2 The harmonic vibrational frequencies (cm^{-1}) and infrared intensities (km/mol, in parentheses) for the dibridged C_s structure, the global minimum of $Cr_2(CO)_8$.

B3LYP				BP86			
a		a		a		a	
48	(1)	30	(1)	47	(1)	28i	
77	(0)	47	(0)	76	(0)	44	(0)
85	(0)	54	(0)	83	(0)	48	(0)
90	(0)	66	(0)	88	(0)	63	(0)
93	(2)	81	(0)	91	(2)	77	(0)
107	(1)	106	(0)	105	(1)	104	(0)
142	(2)	124	(2)	139	(1)	129	(1)
157	(17)	270	(0)	171	(13)	262	(0)
242	(16)	362	(0)	253	(12)	368	(0)
341	(84)	376	(0)	345	(87)	381	(0)
373	(34)	414	(12)	380	(34)	422	(1)
401	(6)	421	(3)	406	(4)	430	(3)
427	(39)	431	(11)	443	(30)	434	(7)
438	(4)	477	(12)	454	(7)	472	(3)
457	(8)	494	(13)	470	(4)	494	(12)
485	(5)	526	(1)	485	(1)	509	(0)
506	(10)	591	(10)	509	(0)	590	(14)
549	(14)	640	(68)	538	(12)	630	(51)
583	(30)	1994	(642)	577	(28)	1903	(636)
614	(83)	2036	(1375)	613	(72)	1952	(944)
628	(113)	2075	(756)	632	(75)	1984	(676)
657	(22)			654	(18)		
1980	(215)			1900	(178)		
1996	(689)			1907	(540)		
2051	(1380)			1969	(991)		
2068	(2342)			1984	(2233)		
2138	(166)			2045	(167)		

Table 4.3 The harmonic vibrational frequencies (cm^{-1}) and their infrared intensities (km/mol, in parentheses) for the dibridged C_i structure of $Cr_2(CO)_8$. This structure is predicted (Table 4.1) to lie about 8 kcal/mol above the $Cr_2(CO)_8$ global minimum.

B3LYP				BP86			
a_g		a_u		a_g		a_u	
40	(0)	36i		38	(0)	35i	
79	(0)	34	(0)	78	(0)	35	(0)
83	(0)	59	(2)	82	(0)	55	(2)
87	(0)	68	(2)	86	(0)	66	(2)
114	(0)	86	(0)	114	(0)	85	(0)
127	(0)	94	(2)	126	(0)	93	(1)
172	(0)	103	(2)	174	(0)	102	(2)
192	(0)	171	(2)	211	(0)	173	(1)
364	(0)	350	(2)	370	(0)	347	(7)
375	(0)	362	(14)	378	(0)	367	(6)
388	(0)	375	(23)	404	(0)	395	(14)
420	(0)	405	(7)	426	(0)	412	(3)
440	(0)	440	(72)	454	(0)	458	(68)
445	(0)	456	(61)	463	(0)	462	(14)
476	(0)	468	(9)	481	(0)	482	(4)
520	(0)	515	(20)	508	(0)	511	(8)
573	(0)	572	(3)	561	(0)	559	(0)
595	(0)	577	(35)	600	(0)	577	(34)
629	(0)	622	(51)	623	(0)	612	(45)
674	(0)	663	(120)	672	(0)	661	(107)
1959	(0)	1987	(1340)	1870	(0)	1894	(905)
2015	(0)	2022	(1834)	1937	(0)	1945	(1534)
2053	(0)	2053	(2045)	1966	(0)	1969	(1488)
2133	(0)	2089	(2453)	2039	(0)	1996	(2498)

Table 4.4 The harmonic vibrational frequencies (cm^{-1}) and their infrared intensities (km/mol, in parentheses) for the dibridged C_{2v} structure of $Cr_2(CO)_8$. This structure is predicted (Table 4.1) to lie about 17 kcal/mol above the $Cr_2(CO)_8$ global minimum.

B3LYP				BP86			
a_1		a_2		a_1		a_2	
71	(0)	39	(0)	66	(0)	34	(0)
75	(0)	77	(0)	75	(0)	76	(0)
95	(0)	94	(0)	92	(0)	93	(0)
153	(5)	340	(0)	158	(6)	328	(0)
208	(0)	422	(0)	213	(0)	426	(0)
380	(1)	475	(0)	398	(0)	449	(0)
397	(1)	526	(0)	411	(2)	513	(0)
441	(81)			452	(43)		
458	(0)			474	(2)		
507	(4)			492	(0)		
595	(0)			595	(0)		
642	(26)			644	(67)		
687	(542)			691	(423)		
1880	(100)			1786	(105)		
2041	(1981)			1947	(1541)		
2092	(343)			2010	(308)		
2149	(476)			2065	(537)		
b_1		b_2		b_1		b_2	
42	(0)	53i		34	(1)	65i	
53	(0)	45	(0)	53	(0)	39	(0)
92	(1)	92	(0)	86	(1)	89	(0)
193	(0)	125	(1)	188	(0)	127	(0)
326	(3)	314	(4)	326	(4)	306	(5)
397	(1)	363	(1)	407	(0)	364	(1)
418	(5)	433	(33)	430	(3)	441	(19)
499	(1)	501	(18)	486	(0)	503	(1)
532	(3)	525	(2)	547	(0)	538	(9)
683	(147)	657	(111)	681	(128)	651	(91)
1881	(848)	1992	(979)	1783	(640)	1898	(854)
2089	(734)	2079	(1694)	2005	(650)	1998	(1425)

Table 4.5 The harmonic vibrational frequencies (cm^{-1}) and their infrared intensities (km/mol, in parentheses) for the non-bridged D_{2d} structure of $Cr_2(CO)_8$. This structure is predicted (Table 4.1) to lie about 22 kcal/mol above the $Cr_2(CO)_8$ global minimum.

	B3LYP			BP86	
a_1	59	(0)		49	(0)
	69	(0)		68	(0)
	193	(0)		214	(0)
	386	(0)		401	(0)
	429	(0)		433	(0)
	491	(0)		470	(0)
	626	(0)		621	(0)
	2043	(0)		1959	(0)
	2136	(0)		2046	(0)
a_2	79	(0)		79	(0)
	347	(0)		354	(0)
	532	(0)		521	(0)
b_1	33	(0)		30	(0)
	83	(0)		83	(0)
	376	(0)		378	(0)
	552	(0)		544	(0)
b_2	48	(5)		29	(9)
	86	(5)		82	(4)
	369	(119)		371	(135)
	394	(36)		401	(0)
	498	(21)		484	(22)
	542	(0)		534	(1)
	2040	(2958)		1957	(1985)
	2072	(714)		1991	(875)
e	22	(1)		22	(1)
	54	(0)		50	(0)
	81	(2)		74	(2)
	111	(0)		107	(0)
	343	(1)		345	(0)
	392	(4)		387	(2)
	427	(36)		439	(17)
	461	(14)		477	(4)
	582	(82)		583	(83)
	623	(4)		627	(2)
	2021	(11)		1933	(208)
	2045	(2735)		1962	(2080)

Table 4.6 The harmonic vibrational frequencies (cm^{-1}) and their infrared intensities (km/mol, in parentheses) for the non-bridged C_s structure of $Cr_2(CO)_8$. This structure is predicted (Table 4.1) to lie about 24 kcal/mol above the $Cr_2(CO)_8$ global minimum.

B3LYP				BP86			
a		a		a		a	
19	(1)	14	(0)	11	(0)	16	(0)
61	(1)	37	(0)	59	(1)	37	(0)
67	(0)	56	(0)	66	(0)	54	(0)
79	(0)	66	(0)	77	(0)	63	(0)
85	(0)	78	(0)	81	(0)	78	(0)
89	(1)	92	(1)	85	(1)	88	(1)
104	(1)	108	(0)	103	(0)	108	(0)
118	(0)	342	(0)	120	(0)	336	(2)
187	(18)	359	(0)	205	(13)	360	(0)
332	(3)	370	(0)	324	(0)	374	(0)
378	(24)	391	(1)	383	(0)	401	(1)
385	(4)	400	(0)	394	(5)	405	(0)
402	(0)	429	(33)	405	(3)	420	(18)
419	(18)	457	(14)	424	(7)	458	(1)
444	(37)	484	(1)	445	(13)	469	(3)
458	(3)	511	(2)	467	(5)	486	(4)
516	(2)	566	(29)	491	(2)	573	(28)
534	(2)	642	(80)	520	(2)	635	(65)
569	(21)	1999	(370)	560	(15)	1905	(469)
585	(21)	2042	(2046)	588	(37)	1959	(1487)
638	(77)	2067	(337)	630	(112)	1983	(304)
655	(181)			639	(113)		
2009	(226)			1918	(326)		
2042	(1366)			1957	(889)		
2055	(2023)			1971	(1689)		
2066	(1571)			1988	(1040)		
2138	(113)			2048	(202)		

CHAPTER 5

CHARACTERIZATION OF THE THREE LOWEST-LYING SINGLET ELECTRONIC STATES OF AlOH[1]

[1] Se Li, Kurt W. Sattelmeyer, Yukio Yamaguchi, Henry F. Schaefer III. 2003. Journal of chemical physics, 119: 12830–12841. Reprinted by permission of the American Institute of Physics.

5.1 ABSTRACT

Two linear ($^1\Sigma^+$ and $^1\Pi$) and three bent (1 $^1A'$, 2 $^1A'$, and 1 $^1A''$) lowest-lying electronic singlet states of AlOH have been systematically investigated employing *ab initio* self-consistent-field, configuration interaction with single and double excitations, coupled cluster with single and double excitations (CCSD), CCSD with perturbative triple excitations [CCSD(T)], and CCSD with iterative partial triple excitations (CCSDT-3 and CC3) quantum mechanical methods with basis sets up to augmented correlation consistent polarized valence quadruple zeta (aug-cc-pVQZ). The linear $^1\Sigma^+$ state is found to be a remarkably low-energy transition state between the two equivalent bent 1 $^1A'$ structures, while the linear $^1\Pi$ state is a second-order saddle point, which leads to the bent 2 $^1A'$ and 1 $^1A''$ states. The bent ground ($\tilde{X}$ $^1A'$) state of AlOH is predicted to have a bond angle of 157° at the aug-cc-pVQZ CC3 level of theory and is classified as a quasilinear molecule, confirming previous studies. Employing the equation-of-motion coupled cluster method, the first singlet excited state ($\tilde{A}$ $^1A'$) is predicted to have a bond angle of 110° and to lie 114 kcal/mol (39 900 cm^{-1}, 4.94 eV) above the ground state, whereas the second singlet excited state ($\tilde{B}$ $^1A''$) is predicted to have a bond angle of 116° and to be located 119 kcal/mol (41 700 cm^{-1}, 5.17 eV) above the ground state. These theoretical energy separations are in excellent agreement with the experimental values T_0 ($\tilde{A}$ $^1A'$) = 114.57 kcal/mol (40 073 cm^{-1}, 4.968 eV) and T_0 ($\tilde{B}$ $^1A''$) = 119.36 kcal/mol (41 747 cm^{-1}, 5.176 eV). The barriers to linearity for the two bent singlet excited states are determined to be 11.6 kcal/mol for the $\tilde{A}$ $^1A'$ state and 6.2 kcal/mol for the $\tilde{B}$ $^1A''$ state.

5.2 INTRODUCTION

The AlOH molecule is of astrophysical interest because of the relatively high cosmic abundance of aluminum. In fact, this species is predicted by Tsuji[1] to be present in oxygen-rich stellar atmospheres. A series of important experimental studies have been carried out for this molecule. In 1980 Hauge, Kauffman, and Margrave reported[2] infrared (IR) matrix-isolation studies of the interactions and reactions of group IIIA metal atoms with water. The divalent HAlOH molecular species was formed via the reaction of an aluminum atom and water at 15 K. The monovalent AlOH molecular species was readily formed by further photolysis of the divalent HAlOH species. In an argon matrix two stretching vibrational frequencies for AlOH were measured at 3790 (OH stretch) and 810.3 cm^{-1} (AlO stretch). In 1983 the same Rice group performed[3] matrix-isolation studies by electronic spectroscopy of group IIIA metal–water photochemistry. They reported an investigation of the electronic structures of the group IIIA metal atom hydration reaction intermediates and their subsequent photolysis products. They observed UV-visible electronic absorption spectra for Al and H_2O isolated in a Krypton matrix (Al:H_2O:Kr = 1:10:675). The band at 22 103 cm^{-1} denoted by "*G*" was assigned to the reaction product (HAlOH). After a 5 min photolysis with light of λ>3000 Å, the "*G*" band (attributed to HAlOH) was totally destroyed and two new bands ("*H*" and "*I*") were generated. The "*I*" band at 40 227 cm^{-1} (115.01 kcal/mol, 4.988 eV) was assigned to a transition ($\tilde{A}\ ^1\Pi \leftarrow \tilde{X}\ ^1\Sigma^+$) of the AlOH molecule, which was the major photolysis product found in the IR matrix studies.[2]

Pilgrim, Robbins, and Duncan published[4] a photoelectron spectroscopic investigation of the AlOH molecule in 1993. The Georgia spectroscopic group initially had some difficulty definitively assigning their spectra, with both the AlOH or the HAlO species being possible

candidates. Coupled cluster methods including single and double excitations with perturbative triple excitations [CCSD(T)] showed[5] that the ground state of AlOH has a bent structure (with an equilibrium bond angle of 163°) that is predicted to be 41 kcal/mol more stable than the linear HAlO isomer. The experimental AlO fundamental stretching frequency of 895 cm^{-1} agreed much better with the predicted value of 845 cm^{-1} for the bent AlOH molecule than with 1056 cm^{-1} for the linear HAlO species. More significant is that Pilgrim *et al.* also reported two unspecified excited singlet states at T_0 = 40 073 cm^{-1} (114.57 kcal/mol, 4.968 eV) and T_0 = 41 747 cm^{-1} (119.36 kcal/mol, 5.176 eV) in their paper. These two singlet excited states are separated by only 1674 cm^{-1} (4.79 kcal/mol). In our group's previous paper, only the lowest 1 $^1A''$ state (one of the possible excited states) was considered, and this was at the SCF level of theory,[4,5] with the symmetry restrictions in the theoretical method used at that time. Identifying these two excited states is one of the motivations of the current research.

In the same year (1993) as Duncan's work, Apponi, Barclay, and Ziurys measured[6] the pure rotational spectrum of the AlOH and AlOD molecules in their $\tilde{X}\,^1\Sigma^+$ (v = 0) ground electronic states in the laboratory using direct absorption millimeter/submillimeter spectroscopy. The species were produced by the reaction of aluminum vapor with H_2O_2 or D_2O_2. The rotational constants of these molecules were determined, as well as the quadruple hyperfine constant for AlOH. The rotational spectra were consistent with a quasilinear ground electronic state, as predicted by theory.[5]

Previous theoretical work mainly focused on the electronic ground state of the AlOH system. Zyubina, Zyubin, Gorbik, and Charkin reported[7] the first *ab initio* study of the ground state AlOH–HAlO system using self-consistent-field (SCF) and self-consistent electron pairs (SCEP) theory with a DZ + d basis set in 1985. Hirota, Tanimoto, and Tokiwa investigated[8] this

system using *ab initio* SCF, configuration interaction with single and double excitations (CISD), and Møller–Plesset third-order (MP3) methods with the 6-311G and (9*s*8*p*3*d*2 *f*/7*s*6*p*3*d*2 *f*/4*s*3*p*2*d*) basis sets. Hirota *et al.* concluded that the most stable geometry is a bent form with an AlOH angle of 163°. In 1993 our group reported[5] a TZ2P(*f*,*d*) coupled cluster single and double excitations (CCSD) with perturbative triple excitations [CCSD(T)] study on the AlOH–HAlO system, as mentioned above. The activation energy for hydrogen migration from AlOH to HAlO in the ground state surface was predicted to be 77 kcal/mol. In the following year we reported a qualitative analysis of the same system, utilizing the derivatives of the orbital energies.[9] Recently two additional theoretical studies have been reported[10,11] on the AlOH and HAlO molecules. However, these theoretical studies are limited to the electronic ground states.

In the present study the ground state (closed shell) of AlOH will be investigated using *ab initio* SCF, CISD, CCSD,[12,13] CCSD(T),[14,15] and CCSD with iterative partial triple excitations (CCSDT-3[16] and CC3[17]) levels of theory. The singlet excited states will be characterized employing equation-of-motion (EOM) coupled cluster (CC) techniques,[18,19] which in certain cases are equivalent to the SAC-CI method[20] and the coupled cluster linear response theory (CCLRT).[21,22,23] The EOM-CC method does not suffer from the orbital instability problem because the excited state energies are determined as higher roots of the reference CC wave functions of the same spin and spatial symmetry. Therefore, the aforementioned excited states have been characterized with the EOM-CCSD, EOM-CCSDT-3, and EOM-CC3 methods.

5.3 ELECTRONIC STRUCTURE CONSIDERATIONS

In the previous theoretical studies,[5,7,8,9,10,11] the ground state of the linear AlOH molecule,

$$[\text{core}](5\sigma)^2(6\sigma)^2(2\pi)^4(7\sigma)^2, \quad \tilde{X}\,^1\Sigma^+ \qquad (1)$$

was found to be an inversion transition state, although Walsh's rules[24] predict a linear equilibrium structure. On the other hand, the HAlO molecule was found to have a linear equilibrium structure that is consistent with Walsh's rules. In Eq. (1), [core] denotes the six lowest-lying core orbitals (Al:1*s*-, 2*s*-, 2*p*-like and O:1*s*-like). An analysis of the SCF molecular orbitals (MOs) indicates that the 5σ and 6σ MOs describe the σ(OH) + σ(AlO) and σ(OH)–σ(AlO) bondings. The 2π MO is assigned to the weak AlO π bonding, while the 7σ MO is related to the lone-pair orbital localized on the Al atom. The $\tilde{X}\,^1\Sigma^+$ state of AlOH possesses an imaginary degenerate bending frequency [for example, $\omega_2(\pi) = 118i$ cm^{-1} at the cc-pVTZ SCF level of theory], which implies a bent equilibrium structure. Thus, the electron configuration for the true ground state of AlOH may be described as

$$[\text{core}](6a')^2(7a')^2(8a')^2(2a'')^2(9a')^2, \quad \tilde{X}\,^1A'. \quad (2)$$

The $6a'$ and $7a'$ MOs are associated with the OH and AlO σ bonding, while the $8a'$ and $2a''$ MOs are related to the weak AlO π bonding. The $9a'$ MO is assigned to the lone-pair orbital localized on the Al atom. A detailed qualitative analysis based on the orbital energy derivatives for the ground state AlOH molecule may be seen in our previous paper.[9]

The electron configuration of the linear structure for the first singlet excited state may be written as

$$[\text{core}](5\sigma)^2(6\sigma)^2(2\pi)^4(7\sigma)(3\pi), \quad \tilde{A}\,^1\Pi, \qquad (3)$$

where the 3π MO consists of an Al $3p$ orbital with weak π antibonding character. The 7σ and 3π orbitals of the $\tilde{A}\ ^1\Pi$ state are depicted in Figs. 1 and 2, respectively. The $\tilde{A}\ ^1\Pi$ state presents two distinct imaginary vibrational frequencies along the AlOH bending coordinate [for example, at the cc-pVTZ SCF level of theory, $\omega_2(\pi^+) = 647i$ cm^{-1} and $\omega_2(\pi^-) = 416i$ cm^{-1}]. Therefore, the $\tilde{A}\ ^1\Pi$ state of AlOH is subject to a Renner–Teller interaction,[25,26,27,28,29,30,31,32,33,34] and it is classified as a type D Renner molecule, as discussed by Lee, Fox, Schaefer, and Pitzer[31] for linear triatomic molecules. The imaginary bending frequency with the larger magnitude [$\omega_2(\pi^+)$] leads to the $\tilde{A}\ ^1A'$ state in a bent configuration, whereas the [$\omega_2(\pi^-)$] mode leads to the $\tilde{B}^1A''$ state when the molecule is bent. As a result, the $\tilde{A}\ ^1A'$ state is qualitatively expected to have a smaller bond angle than the $\tilde{B}^1A''$ state. Overall, the first singlet excited state has the following electron configuration:

$$[\text{core}](6a')^2(7a')^2(8a')^2(2a'')^2(9a')(10a'), \quad \tilde{A}\,^1A', \quad (4)$$

which is a single electron excitation in the molecular plane with respect to the ground state. The $10a'$ MO mainly consists of an Al ($3p$) orbital with weak antibonding π (in plane) character. The second singlet excited state is represented by

$$[\text{core}](6a')^2(7a')^2(8a')^2(2a'')^2(9a')(3a''), \quad \tilde{B}\,^1A'', \quad (5)$$

which is a single electron excitation to the plane perpendicular to the molecular plane. The $3a''$ MO is an Al ($3p$) orbital with weak antibonding π (out of plane) character. The electronegativity[35] of the O atom (3.5) is considerably larger than that of the Al atom (1.5). Therefore, the contribution of the O $2p$ orbital is greater for the bonding $\pi(2a'')$ orbital, while the contribution of the Al $3p$ orbital is dominant for the antibonding $\pi(3a'')$ orbital. The $9a'$ and $3a''$ orbitals of the $\tilde{B}^1A''$ state have features very similar to the 7σ and 3π orbitals of the $\tilde{A}\ ^1\Pi$ state shown in Figs. 1 and 2.

Since three open-shell singlet excited states are involved in the present study, it is essential to analyze the molecular orbital (MO) Hessian of the reference self-consistent-field (SCF) wave functions. The MO Hessian matrix is constructed from second derivatives of the SCF energy with respect to all independent MO rotations.[36,37,38] The signs and magnitudes of eigenvalues of the MO Hessian matrix provide useful information about the instability of the SCF wave function. For the linear ($\tilde{X}\ ^1\Sigma^+$) and bent ($\tilde{X}\ ^1A'$) AlOH, the eigenvalues of the MO Hessians are all positive, as expected. Thus, the ground state SCF wave functions are *stable* for the linear and bent geometrical configurations.

There is one negative eigenvalue (for example, $\lambda_1 = -0.119$ hartree at the cc-pVTZ SCF level of theory) and one zero eigenvalue of the MO Hessian for the linear $\tilde{A}\ ^1\Pi$ state. The zero eigenvalue is associated with a $3\pi_x$–$3\pi_y$ MO rotation, where the $3\pi_x$ and $3\pi_y$ orbitals are the π orbitals on the *xz* and *yz* plane (the *z* axis is assigned to the molecular axis), respectively. Interchanging the $3\pi_x$ and $3\pi_y$ orbitals does not alter the SCF energy. The negative eigenvalue is related to the 7σ–3π MO rotation. Therefore, the linear $\tilde{A}\ ^1\Pi$ state SCF wave functions are *unstable* for the linear configuration. A de-excitation of an electron from the 3π to 7σ orbital leads to the lower-lying $\tilde{X}\ ^1\Sigma^+$ state. The bent $\tilde{B}\ ^1A''$ state has two negative eigenvalues of the MO Hessian (for example, $\lambda_1 = -0.117$ and $\lambda_2 = -0.0033$ hartree at the cc-pVTZ SCF level of theory). The bent $\tilde{B}\ ^1A''$ state SCF wave functions are again *unstable*. The negative eigenvalue with a larger magnitude corresponds to the $3a''$–$9a'$ rotation, which MO rotation connects the $\tilde{B}\ ^1A''$ and $\tilde{X}\ ^1A'$ states. On the other hand, the negative eigenvalue with a smaller magnitude is associated with the $3a''$–$10a'$ rotation. This MO rotation indicates a lower-lying $\tilde{A}\ ^1A'$ state at the $\tilde{B}\ ^1A''$ state equilibrium geometry. The analyses based on the MO Hessians of the five (two linear

and three bent) singlet states are consistent with the discussion based on the bending frequencies mentioned above.

5.4 THEORETICAL PROCEDURES

In the present research, four correlation-consistent polarized valence basis sets [cc-pVTZ, cc-pV(T + d)Z, cc-pVQZ, and cc-pV(Q + d)Z] and two augmented correlation-consistent polarized valence basis sets (aug-cc-pVTZ and aug-cc-pVQZ) were employed in order to optimize geometries and to determine physical properties. The cc-pVXZ [where XZ = TZ, (T + d)Z, QZ, and (Q + d)Z] and aug-cc-pVXZ (where XZ = TZ and QZ) basis sets were those developed by Dunning and co-workers.[39,40,41] The cc-pV(X + d)Z basis sets were formed by augmenting a high-exponent *d* function to the (2*d*) sets and by replacing the (3*d*) set by the (4*d*) set for the second row atoms.[41]

The zeroth-order descriptions of the $\tilde{X}\,^1\Sigma^+$, $\tilde{A}\,^1\Pi$, $\tilde{X}\,^1A'$, and $\tilde{B}\,^1A''$ states of AlOH were obtained using single configuration SCF (restricted Hartree–Fock) wave functions. Correlation effects were included using the CISD method for the four states mentioned above. The cc-pVQZ CISD wave function of the $\tilde{X}\,^1A'$ state displays a CI coefficient of $C_0 = 0.957$ for the reference state at the optimized geometry. The CCSD,[12,13] CCSD(T),[14,15] CCSDT-3,[16] and CC3[17] levels of theory were also used for the closed shell $\tilde{X}\,^1\Sigma^+$ and $\tilde{X}\,^1A'$ states. The largest t_1 and t_2 amplitudes for the cc-pVQZ CCSD(T) wave function describing the $\tilde{X}\,^1A'$ state are 0.021 and 0.083 at the optimized geometry. The $\tilde{A}\,^1\Pi$, $\tilde{A}\,^1A'$, and $\tilde{B}\,^1A''$ states of AlOH were investigated employing the equation-of-motion (EOM) CCSD, EOM-CCSDT-3, and EOM-CC3 techniques. EOM-CCSDT-3 avoids a calculation of the most demanding (of order N^8, N being the number of

basis functions) contributions of the triples equation that involve T_3 itself, while in EOM-CC3 all terms of overall second order in the perturbation are kept, assuming that T_1, T_2, and T_3 are zeroth-, first-, and second-order operators for the excited state, respectively.

Using the EOM-CC techniques,[18,19] the linear $\tilde{A}\ ^1\Pi$ state was determined as the first root of $\tilde{X}\ ^1\Sigma^+ \rightarrow \tilde{A}\ ^1\Pi$ (in C_{2v} symmetry $\tilde{X}\ ^1A_1 \rightarrow\ ^1B_1$ or $\tilde{X}\ ^1A_1 \rightarrow\ ^1B_2$) excitation. The $^1A'$ and $^1A''$ components of the $\tilde{A}\ ^1\Pi$ state were determined as the first roots of $\tilde{X}\ ^1A' \rightarrow \tilde{A}\ ^1A'$ and $\tilde{X}\ ^1A' \rightarrow \tilde{B}\ ^1A''$ excitations relative to the closed shell CCSD, CCSDT-3, and CC3 reference wave functions. All correlated procedures were performed freezing the six core (Al:1*s*-, 2*s*-, 2*p*-like and O:1*s*-like) SCF molecular orbitals.

The SCF and CISD structures of the two linear ($\tilde{X}\ ^1\Sigma^+$ and $\tilde{A}\ ^1\Pi$) and two bent ($\tilde{X}\ ^1A'$ and $\tilde{B}\ ^1A''$) structures, and the CCSD and CCSD(T) structures of the two closed shell ($\tilde{X}\ ^1\Sigma^+$ and $\tilde{X}\ ^1A'$) structures were optimized using analytic derivative methods.[42,43,44] Harmonic vibrational frequencies at the SCF level were evaluated analytically, whereas at the CISD, CCSD, and CCSD(T) levels of theory they were obtained by finite differences of analytic gradients. For the two closed shell systems the CCSDT-3 and CC3 structures and harmonic vibrational frequencies were determined by numerical differentiation of total energies. For the three open-shell species the EOM-CC stationary points and harmonic vibrational frequencies were also determined by numerical differentiation of total energies. Computations were carried out with PSI-2[45] and a local version of the ACES II[46] program on IBM RS/6000 workstations and on our PC clusters.

5.5 RESULTS AND DISCUSSION

In Figs. 3,4,5,6,7 the representative optimized structures of the five lowest-lying singlet states of AlOH are depicted. In Tables I,II,III,IV,V the total energies, dipole moments, harmonic vibrational frequencies, infrared (IR) intensities, and zero-point vibrational energies (ZPVEs) of the five stationary points are presented. The dipole moments were determined with respect to the center of mass. The relative energies for the five singlet states are shown in Tables VI and VII.

5.5.1 GEOMETRIES

5.5.1.1 INEAR $\tilde{X}^1\Sigma^+$ STATE

The representative optimized geometries for the linear $\tilde{X}^1\Sigma^+$ state at four levels of theory with the three largest basis sets are presented in Fig. 3. Given a basis set, a more complete inclusion of correlation effects elongates both the AlO and OH distances, as is usually the case.[47,48,49,50,51] The augmentation of a basis set by diffuse functions slightly lengthens the two bond lengths, while the addition of an extra tight *d* function on the Al atom considerably shortens the AlO bond distance. At the aug-cc-pVQZ CC3 level of theory, the linear stationary point geometry is predicted to be a bit shorter, r_e(AlO) = 1.6829 Å and r_e(OH) = 0.9497 Å. The equilibrium bond length for the diatomic AlO ($X\ ^2\Sigma^+$) is experimentally determined to be r_e(AlO) = 1.6179 Å.[52] The experimentally estimated geometries of the diatomic OH, OH^+, and OH^- are r_e(OH) = 0.9706 Å, $r_e(OH^+)$ = 1.0289 Å, and $r_e(OH^-)$ = 0.970 Å.[52] Therefore, the AlO distance of AlOH is predicted to be longer than in AlO ($X\ ^2\Sigma^+$), while the OH distance in AlOH is seen to be shorter than in OH, OH^+, and OH^-. This feature implies that some electron density moves from Al to O.

5.5.1.2 LINEAR $\tilde{A}\ ^1\Pi$ STATE

The AlO and OH bond distances of the linear $\tilde{A}\ ^1\Pi$ state are predicted to be shorter than those for the linear ground state, as shown in Fig. 4. An augmentation of the basis set by diffuse functions generally decreases the AlO bond length and increases the OH bond distance. An addition of the extra *d* function on the Al atom again shortens the AlO bond distance. At the aug-cc-pVQZ EOM-CC3 level of theory, the linear stationary point geometry is r_e(AlO) = 1.6511 Å and r_e(OH) = 0.9475 Å.

5.5.1.3 BENT $\tilde{X}\ ^1A'$ STATE

The true ground state of AlOH favors a bent geometrical configuration. The representative optimized geometries for the bent $\tilde{X}\ ^1A'$ state at four levels of theory with the three largest basis sets are presented in Fig. 5. The AlO and OH bond distances are longer for the bent structure relative to the linear configuration. The bond angle appears to be quite sensitive to the level of correlation effects and basis set size. The AlO bond length generally increases with more advanced treatments of correlation effects, while the bond angle decreases. The predicted geometry at the aug-cc-pVQZ CC3 level of theory is r_e (AlO) = 1.6908 Å, r_e (OH) = 0.9512 Å, and θ_e (AlOH) = 156.8°. The AlO distance of $\tilde{X}\ ^1A'$ AlOH is still longer than that of $X\ ^2\Sigma^+$ AlO. The new bond angle is 5.8° smaller than our previously predicted value of 162.6° at the TZ2P(f,d) CCSD(T) level of theory.[5] However, our present CCSD(T) prediction with the aug-cc-pVQZ basis set is 156.9°, very close to the CC3 result. Apponi *et al.* determined[6] the r_0 bond lengths from the millimeter-wave AlOH/AlOD rotational constants to be r_0(AlO) = 1.682 Å and r_0(OH) = 0.878 Å. There is reasonable agreement between the experimental and theoretical values for

the AlO bond length. However, the experimental OH bond length must be too short and is significantly shorter than the theoretically predicted value. Apponi argued that this discrepancy can be primarily attributed to the zero-point vibrational energy (ZPVE) of the molecule in the ground vibrational state and large-amplitude bending vibrations.[6] When the theoretical bent structure is projected onto a linear molecular axis, the OH bond length is shortened to be 0.874 Å at the aug-cc-pVQZ CC3 level of theory, which is indeed consistent with the experimental deduction.

5.5.1.4 FIRST SINGLET EXCITED STATE ($\tilde{A}\ ^1A'$)

The optimized geometries for the $\tilde{A}\ ^1A'$ state at the three EOM-CC levels of theory are depicted in Fig. 6. An increase of basis set size shortens the AlO and OH bond distances, while it increases the bond angle. At the aug-cc-pVQZ EOM-CC3 level of theory, the optimized geometry is r_e(AlO) = 1.7583 Å, r_e(OH) = 0.9638 Å, and θ_e(AlOH) = 109.8°. The two bond lengths of the $\tilde{A}\ ^1A'$ state are considerably longer than those of the $\tilde{X}\ ^1\Sigma^+$, $\tilde{A}\ ^1\Pi$, and $\tilde{X}\ ^1A'$ states. The bond angle of the $\tilde{A}\ ^1A'$ state is significantly smaller than that of the $\tilde{X}\ ^1A'$ state. Since the second row atom in a molecule prefers a single bond to a multiple bond,[53,54] it is reasonable for the linear $\tilde{A}\ ^1\Pi$ excited state of AlOH to release the tension due to enforced multiple bond character and relax to bent configurations. On the other hand, Grev and Schaefer argued (see citation 18 in Ref. 4) that the excited state should be more bent than the ground state because of the repulsion of the excited 3*p* electrons toward the oxygen atom lone pairs.

5.5.1.5 SECOND SINGLET EXCITED STATE ($\tilde{B}\ ^1A''$)

The AlO and OH bond distances for the $\tilde{B}^1A''$ state are again longer than those for the $\tilde{X}^1\Sigma^+$, $\tilde{A}\ ^1\Pi$, and $\tilde{X}^1A'$ states, as shown in Fig. 7. The bent $\tilde{B}^1A''$ state of AlOH has a larger bond angle by several degrees compared to that of the $\tilde{A}\ ^1A'$ state. However, the bond angle is still significantly smaller than that of the bent ground $\tilde{X}^1A'$ state. At the aug-cc-pVQZ EOM-CC3 level of theory, the equilibrium structure is predicted to be r_e(AlO)=1.7523 Å, r_e(OH) =0.9641 Å, and θ_e(AlOH)=116.1°. These predicted smaller bond angles for the two excited singlet states compared to the bond angle of the ground state are consistent with discussions presented in Sec. II, above.

5.5.2 DIPOLE MOMENTS

The dipole moment of the linear ground $\tilde{X}^1\Sigma^+$ state is predicted to be about 1.0 Debye. Improved treatments of correlation effects and extension of the basis set generally decrease the magnitude of the dipole moment. Although the Al atom has a smaller electronegativity than the O and H atoms, the direction of the dipole moment is nevertheless $^-$AlOH$^+$. This feature is analogous to the dipole moments of the BF and CO molecules; the polarity of the two molecules are experimentally found to be $^-$BF$^+$ and $^-$CO$^+$.[52] The dipole moment of the linear $\tilde{A}\ ^1\Pi$ state is very sensitive to the augmentation of the basis set by diffuse functions, probably due to the enforced multiple bond character. The bent $\tilde{X}^1A'$ state has a slightly larger dipole moment than the linear $\tilde{X}^1\Sigma^+$ state. The bent $\tilde{B}^1A''$ state has a similar dipole moment as the bent ground $\tilde{X}$

$^1A'$ state. The dipole moment of the $\tilde{B}\,^1A''$ state is less sensitive to the basis set relative to that of the $\tilde{A}\,^1\Pi$ state.

5.5.3 VIBRATIONAL FREQUENCIES

The linear $\tilde{X}\,^1\Sigma^+$ state possesses a degenerate imaginary bending frequency at all levels of theory (in Table I). Therefore, this linear structure is an inversion transition state that connects the two equivalent bent equilibrium structures. The AlO harmonic stretching frequency (ω_3) for the diatomic $X\,^2\Sigma^+$ AlO is experimentally determined to be 979.2 cm^{-1}.[52] The corresponding theoretical AlO stretching frequency of 840 cm^{-1} for the $\tilde{X}\,^1\Sigma^+$ AlOH species at the aug-cc-pVQZ CC3 level of theory is significantly lower, reflecting the longer AlO bond length.

The two stretching frequencies (ω_1 and ω_3) are higher for the $\tilde{A}\,^1\Pi$ state than those for the $\tilde{X}\,^1\Sigma^+$ state owing to the shortened bond distances. The linear $\tilde{A}\,^1\Pi$ state presents two distinct imaginary bending frequencies at the SCF level of theory. The magnitudes of the imaginary frequencies are considerably larger than that of the linear ground state ($\tilde{X}\,^1\Sigma^+$). Therefore, the two bent equilibrium singlet excited states are expected to have smaller equilibrium bond angles and larger energy barriers to linearity.

For the bent ground state ($\tilde{X}\,^1A'$) in Table III, the three *real* harmonic vibrational frequencies are predicted to be ω_1 (OH stretch) = 3993 cm^{-1}, ω_2 (bend) = 173 cm^{-1}, and ω_3 (AlO stretch) = 831 cm^{-1} at the aug-cc-pVQZ CC3 level of theory. The AlO stretching frequency in AlOH is still lower than that of the diatomic AlO ($X\,^2\Sigma^+$). The predicted AlO stretching frequency (831 cm^{-1}) is closer to the experimental value of 810.3 cm^{-1} observed in a matrix isolated IR spectra[2] than the value of 895 cm^{-1} measured from photoelectron spectroscopic

experiments in the gas phase.[4] The experimentally determined OH stretching fundamental frequency[2] of 3790 cm^{-1} is reasonably close to our predicted harmonic value of 3993 cm^{-1}.

The theoretical OH (ω_1) stretching frequency (3820 cm^{-1} at the cc-pVQZ EOM-CC3 level) of the $\tilde{A}\ ^1A'$ state is considerably lower than the corresponding mode of the ground state ($\tilde{X}\ ^1A'$) owing to the longer OH bond distance and significantly higher than the experimental value of 3258.4 cm^{-1}.[4] The other two experimental frequencies of $\tilde{A}\ ^1A'$ AlOH were determined to be 654.2 (bend, ω_2) and 825.2 cm^{-1} (AlO stretch, ω_3) in the gas phase.[4] The theoretically predicted frequencies of 853 and 640 cm^{-1} at the cc-pVQZ EOM-CC3 level of theory agree quite well with the experimental values. According to our vibrational analysis, however, there is a strong mixing between the bending and AlO stretching vibrations, especially for the AlOH species. Therefore, it may be more appropriate to assign the 853 cm^{-1} vibration to an [AlO stretch + bend] mode and the 640 cm^{-1} vibration to an [AlO stretch–bend] mode. The interaction between bending and AlO stretching modes becomes much weaker for the AlOD molecule.

The OH stretching frequency (ω_1) of the $\tilde{B}^1A''$ state is also notably lower than that for the $\tilde{X}^1A'$ state, but it is close to the $\tilde{A}\ ^1A'$ state. This feature is more evident for the correlated level than the SCF level of theory. The two experimental frequencies of $\tilde{B}^1A''$ were determined to be 764.3 (AlO stretch, ω_1) and 588.2 cm^{-1} (bend, ω_2) in a gas phase.[4] Theoretically predicted frequencies of 769 and 592 cm^{-1} at the cc-pVQZ EOM-CC3 level of theory agree quite well with the experimental values. Again, it may be more appropriate to assign the 769 cm^{-1} vibration to an [AlO stretch + bend] mode and the 592 cm^{-1} vibration to an [AlO stretch–bend] mode.

5.5.4 ENERGETICS

At all levels of theory the bent $^1A'$ state is predicted to be the electronically lowest-lying isomer of AlOH, as shown in Tables VI and VII. The linear $^1\Sigma^+$ state isomer is an inversion transition state and lies less than 0.04 kcal/mol above the bent equilibrium ground state ($\tilde{X}\ ^1A'$). Therefore, the ground state of AlOH may be designated as a quasilinear molecule, confirming previous theoretical[5] and experimental[6] studies. The linear $\tilde{A}\ ^1\Pi$ structure is a second-order saddle point that splits into two bent equilibrium structures. Using the aug-cc-pVQZ basis set, the $\tilde{A}\ ^1\Pi$ state is predicted to lie 123.7 (EOM-CCSD), 123.4 (EOM-CCSDT-3), and 123.3 kcal/mol (EOM-CC3) above the bent ground state.

The bent first excited singlet state ($\tilde{A}\ ^1A'$) is located 114.2 (EOM-CCSD), 113.1 (EOM-CCSDT-3), and 112.9 kcal/mol (EOM-CC3) above the ground $\tilde{X}\ ^1A'$ state with the aug-cc-pVQZ basis set. The mean value of the $\tilde{A}\ ^1A' \leftarrow \tilde{X}\ ^1A'$ energy separations from 18 EOM-CC wave functions is evaluated to be T_e = 113.6 kcal/mol (39 730 cm^{-1}, 4.925 eV) and T_0 = 114.0 kcal/mol (39 890 cm^{-1}, 4.945 eV), which is in excellent agreement with the experimental values of T_0 = 115.01 kcal/mol (40 227 cm^{-1}, 4.988 eV) by Hauge *et al.*[3] and T_0 = 114.57 kcal/mol (40 073 cm^{-1}, 4.968 eV) by Pilgrim *et al.*[4]

The bent second singlet excited state ($\tilde{B}\ ^1A''$) is predicted to lie 119.0 (EOM-CCSD), 118.1 (EOM-CCSDT-3), and 117.9 kcal/mol (EOM-CC3) above the ground $\tilde{X}\ ^1A'$ state using the aug-cc-pVQZ basis set. The mean value of the $\tilde{B}\ ^1A'' \leftarrow \tilde{X}\ ^1A'$ excitation energies from 18 EOM-CC wave functions is determined to be T_e = 119.0 kcal/mol (41 620 cm^{-1}, 5.160 eV) and T_0 = 119.2 kcal/mol (41 710 cm^{-1}, 5.171 eV), which is in excellent agreement with the experimental value of T_0 = 119.36 kcal/mol (41 747 cm^{-1}, 5.176 eV) by Pilgrim *et al.*[4] The difference between

the two excitation energies is 5.21 kcal/mol (1820 cm^{-1}), which is reasonably consistent with the experimental energy separation of 4.79 kcal/mol (1674 cm^{-1}).[4] The EOM-CCSD, EOM-CCSDT-3, and EOM-CC3 techniques predict consistent excitation energies within 1.2 kcal/mol for the two singlet excited states. The barriers to linearity were determined to be 11.6 kcal/mol for the $\tilde{A}\ ^1A'$ state and 6.2 kcal/mol for the $\tilde{B}\ ^1A''$ state. These larger barriers to linearity are in accord with the arguments presented in Secs. II and IV C.

For an appropriate description of an open-shell singlet state, *two* Slater determinants are required. Therefore, the EOM techniques with high quality CC wave functions are very powerful for the investigation of single excitation open-shell singlet states relative to the reference closed-shell state, which may be described by *one* Slater determinant. The ground state (closed shell) of AlOH is well described by single reference wave functions. Furthermore, the two excited singlet states are adequately represented by single excitations relative to the ground state, hence excellent excitation energies for the AlOH system are provided by the EOM-CC methods in this study.

5.6 CONCLUDING REMARKS

The two linear ($\tilde{X}\ ^1\Sigma^+$ and $\tilde{A}\ ^1\Pi$) and three bent ($\tilde{X}\ ^1A'$, $\tilde{A}\ ^1A'$, and $\tilde{B}\ ^1A''$) lowest-lying singlet electronic states of AlOH have been investigated using *ab initio* quantum mechanical techniques. The ground state of AlOH has been confirmed to have a bent structure with a large bond angle of 157°. The AlO and OH bond distances of the two excited states ($\tilde{A}\ ^1A'$ and $\tilde{B}\ ^1A''$) are elongated relative to the ground state. The bond angles of the first excited state ($\tilde{A}\ ^1A'$) of 110° and the second excited state ($\tilde{B}\ ^1A''$) of 116° are significantly smaller compared to the bond angle of the

ground state. The excitation energies for the two excited states are predicted to be T_0 = 114.0 kcal/mol (39 890 cm^{-1}, 4.945 eV) for the $\tilde{A}\ ^1A'$ state and T_0 = 119.2 kcal/mol (41 710 cm^{-1}, 5.171 eV) for the $\tilde{B}^1A''$ state. The three EOM-CC (EOM-CCSD, EOM-CCSDT-3, and EOM-CC3) methods predicted the two single excitation energies with chemical accuracy of within 1 kcal/mol. The barriers to linearity for the two bent singlet excited states are determined to be 11.6 kcal/mol for the $\tilde{A}\ ^1A'$ state and 6.2 kcal/mol for the $\tilde{B}^1A''$ state, respectively.

5.7 ACKNOWLEDGMENTS

The authors would like to thank Professor Nicholas C. Handy for his very helpful discussion. This research was supported by the National Science Foundation, Grant No. CHE-0136186.

5.8 LITERATURE REFERENCES

1. T. Tsuji, Astron. Astrophys. **23**, 411 (1973).
2. R. H. Hauge, J. W. Kauffman, and J. L. Margrave, J. Am. Chem. Soc. **102**, 6005 (1980).
3. M. A. Douglas, R. H. Hauge, and J. L. Margrave, J. Chem. Soc., Faraday Trans. 1 **79**, 1533 (1983).
4. J. S. Pilgrim, D. L. Robbins, and M. A. Duncan, Chem. Phys. Lett. **202**, 203 (1993).
5. G. Vacek, B. J. DeLeeuw, and H. F. Schaefer, J. Chem. Phys. **98**, 8704 (1993).
6. A. J. Apponi, W. L. Barclay, and L. M. Ziurys, Astrophys. J. **414**, L129 (1993).
7. T. S. Zyubina, A. S. Zyubin, A. A. Gorbik, and O. P. Charkin, Zh. Neorg. Khim. **30**, 2739 (1985).

8. F. Hirota, M. Tanimoto, and H. Tokiwa, Chem. Phys. Lett. **208**, 115 (1993).

9. Y. Yamaguchi, B. J. DeLeeuw, G. Vacek, C. A. Richards, and H. F. Schaefer, J. Chem. Phys. **101**, 3006 (1994).

10. M. T. Swihart and L. Catoire, Combust. Flame **121**, 210 (2000).

11. C. J. Cobos, J. Mol. Struct. **581**, 17 (2002).

12. G. D. Purvis and R. J. Bartlett, J. Chem. Phys. **76**, 1910 (1982).

13. M. Rittby and R. J. Bartlett, J. Phys. Chem. **92**, 3033 (1988).

14. K. Raghavachari, G. W. Trucks, J. A. Pople, and M. Head-Gordon, Chem. Phys. Lett. **157**, 479 (1989).

15. G. E. Scuseria, Chem. Phys. Lett. **176**, 27 (1991).

16. J. Noga, R. J. Bartlett, and M. Urban, Chem. Phys. Lett. **134**, 126 (1987).

17. H. Koch, O. Christiansen, P. Jørgensen, A. M. S. deMeras, and T. Helgaker, J. Chem. Phys. **106**, 1808 (1997).

18. D. C. Comeau and R. J. Bartlett, Chem. Phys. Lett. **207**, 414 (1993).

19. J. F. Stanton and R. J. Bartlett, J. Chem. Phys. **98**, 7029 (1993).

20. H. Nakatsuji, Chem. Phys. Lett. **39**, 562 (1978).

21. H. J. Monkhorst, Int. J. Quantum Chem. **S11**, 421 (1977).

22. H. Koch and P. Jørgensen, J. Chem. Phys. **93**, 3333 (1990).

23. H. Koch, H. J. A. Jensen, P. Jørgensen, and T. Helgaker, J. Chem. Phys. **93**, 3345 (1990).

24. A. D. Walsh, J. Chem. Soc. (AUG), 2288 (1953).

25. G. Herzberg and E. Teller, Z. Phys. Chem. Abt. B **21**, 410 (1933).

26. R. Renner, Z. Phys. **92**, 172 (1934).

27. J. T. Hougen, J. Chem. Phys. **36**, 1874 (1961).

28. G. Herzberg, *Molecular Spectra and Molecular Structure III. Electronic Spectra and Electronic Structure of Polyatomic Molecules* (Van Nostrand, Princeton, NJ, 1966).

29. Ch. Jungen and A. J. Merer, in *Molecular Spectroscopy: Modern Research*, edited by K. N. Rao (Academic, New York, 1976), Vol. 2, pp. 127–164.

30. J. M. Brown and F. Jørgensen, Adv. Chem. Phys. **52**, 117 (1983).

31. T. J. Lee, D. J. Fox, H. F. Schaefer, and R. M. Pitzer, J. Chem. Phys. **81**, 356 (1984).

32. P. R. Bunker and P. Jensen, *Molecular Symmetry and Spectroscopy*, 2nd ed. (NRC Research, Ottawa, 1998).

33. P. Jensen, G. Osmann, and P. R. Bunker, in *Computational Molecular Spectroscopy*, edited by P. Jensen and P. R. Bunker (Wiley, Chichester, 2000), pp. 485–515.

34. J. M. Brown, in *Computational Molecular Spectroscopy*, edited by P. Jensen and P. R. Bunker (Wiley, Chichester, 2000), pp. 517–537.

35. L. Pauling, *The Nature of the Chemical Bond*, 3rd ed. (Cornell University Press, Ithaca, NY, 1960).

36. Y. Yamaguchi, I. L. Alberts, J. D. Goddard, and H. F. Schaefer, Chem. Phys. **147**, 309 (1990), and references therein.

37. N. A. Burton, Y. Yamaguchi, I. L. Alberts, and H. F. Schaefer, J. Chem. Phys. **95**, 7466 (1991).

38. T. D. Crawford, J. F. Stanton, W. D. Allen, and H. F. Schaefer, J. Chem. Phys. **107**, 10626 (1997).

39. T. H. Dunning, J. Chem. Phys. **90**, 1007 (1989).

40. D. E. Woon and T. H. Dunning, J. Chem. Phys. **98**, 1358 (1993).

41. T. H. Dunning, K. A. Peterson, and A. K. Wilson, J. Chem. Phys. **114**, 9244 (2001).

42. P. Pulay, Mol. Phys. **17**, 197 (1969).

43. P. Pulay, in *Modern Theoretical Chemistry*, edited by H. F. Schaefer (Plenum, New York, 1977), Vol. 4, pp. 153–185.

44. Y. Yamaguchi, Y. Osamura, J. D. Goddard, and H. F. Schaefer, *A New Dimension to Quantum Chemistry: Analytic Derivative Methods in Ab Initio Molecular Electronic Structure Theory* (Oxford University Press, New York, 1994).

45. PSI 2.0.8; C. L. Janssen, E. T. Seidl, G. E. Scuseria et al., PSITECH, Inc., Watkinsville, GA 30677, 1994.

46. ACES II: J. F. Stanton, J. Gauss, W. J. Lauderdale, J. D. Watts, and R. J. Bartlett. The package also contains modified versions of the MOLECULE Gaussian integral program of J. Almlöf and P. R. Taylor, the ABACUS integral derivative program written by T. U. Helgaker, H. J. Aa. Jensen, P. Jørgensen, and P. R. Taylor, and the PROPS property evaluation integral code of P. R. Taylor.

47. Y. Yamaguchi and H. F. Schaefer, J. Chem. Phys. **73**, 2310 (1980).

48. B. H. Besler, G. E. Scuseria, A. C. Scheiner, and H. F. Schaefer, J. Chem. Phys. **89**, 360 (1988).

49. J. R. Thomas, B. J. DeLeeuw, G. Vacek, and H. F. Schaefer, J. Chem. Phys. **98**, 1336 (1993).

50. J. R. Thomas, B. J. DeLeeuw, G. Vacek, T. D. Crawford, Y. Yamaguchi, and H. F. Schaefer, J. Chem. Phys. **99**, 403 (1993).

51. B. Galabov, Y. Yamaguchi, R. B. Remington, and H. F. Schaefer, J. Phys. Chem. A **106**, 819 (2002).

52. K. P. Huber and G. Herzberg, *Molecular Spectra and Molecular Structure. IV. Constants of Diatomic Molecules* (Van Nostrand Reinhold, New York, 1979).

53. W. Kutzelnigg, Angew. Chem., Int. Ed. Engl. **22**, 272 (1984).

54. W. Kutzelnigg, J. Mol. Struct. **169**, 403 (1988).

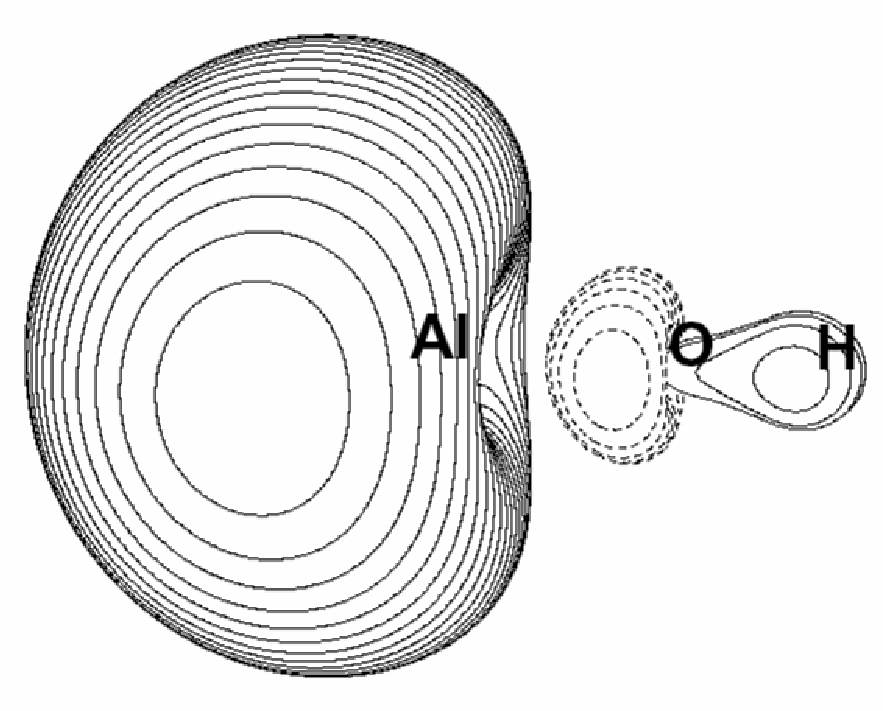

Figure 5.1 The 7σ molecular orbital for the $\tilde{A}\ ^1\Pi$ state of AlOH from the cc-pVTZ SCF method.

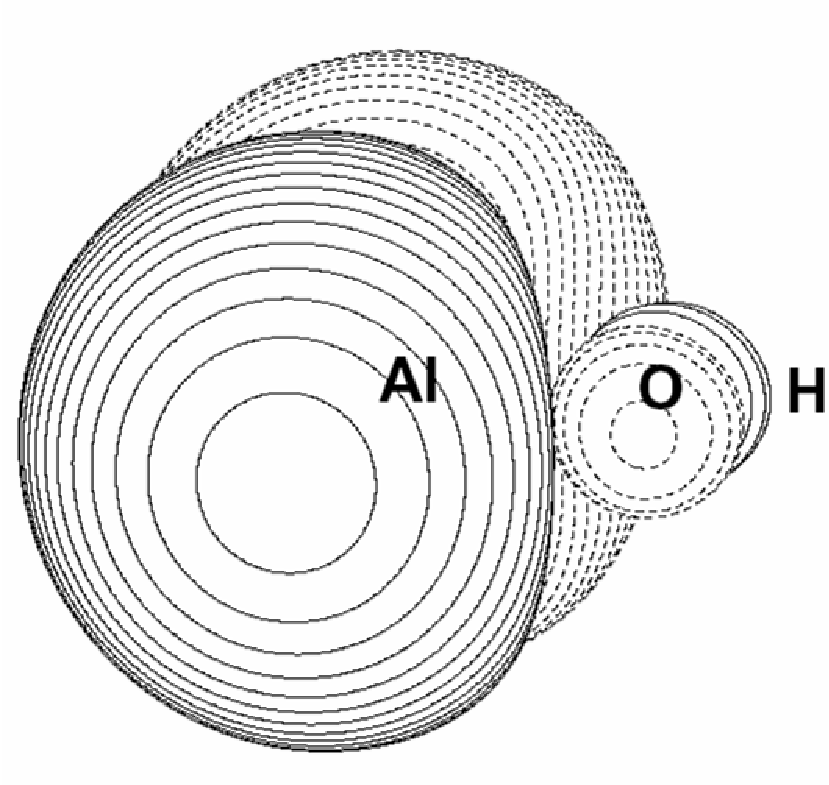

Figure 5.2 The 3π molecular orbital for the $\tilde{A}\ ^1\Pi$ state of AlOH from the cc-pVTZ SCF method.

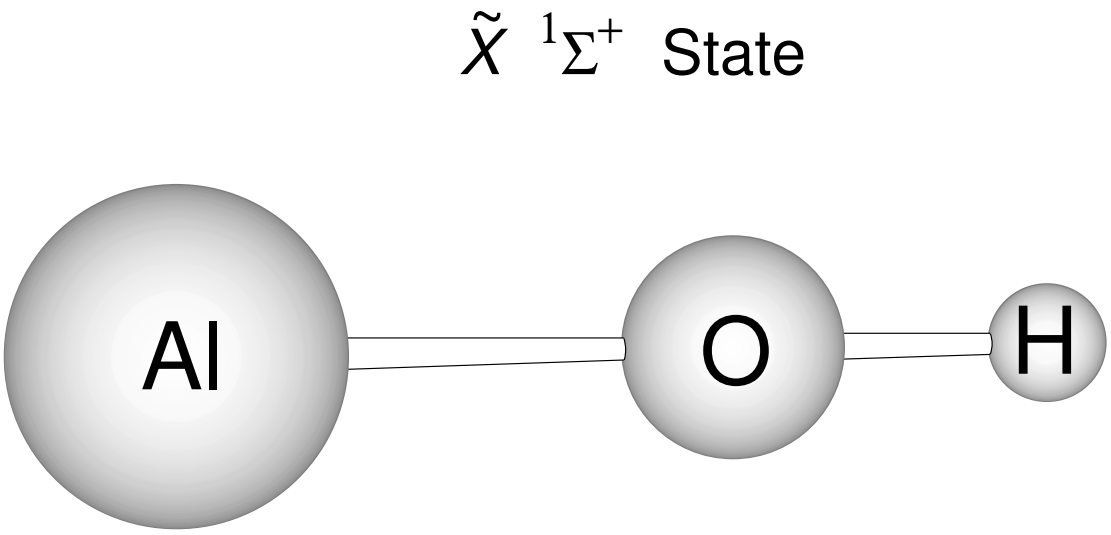

cc-pVQZ CCSD	1.6753	0.9455
cc-pV(Q+d)Z CCSD	1.6717	0.9455
aug-cc-pVQZ CCSD	1.6768	0.9460
cc-pVQZ CCSD(T)	1.6793	0.9486
cc-pV(Q+d)Z CCSD(T)	1.6756	0.9485
aug-cc-pVQZ CCSD(T)	1.6813	0.9492
cc-pVQZ CCSDT-3	1.6798	0.9484
cc-pV(Q+d)Z CCSDT-3	1.6761	0.9484
aug-cc-pVQZ CCSDT-3	1.6818	0.9491
cc-pVQZ CC3	1.6808	0.9490
cc-pV(Q+d)Z CC3	1.6771	0.9489
aug-cc-pVQZ CC3	1.6829	0.9497

Figure 5.3 Predicted geometries of the linear $\tilde{X}\,^1\Sigma^+$ stationary point state of the AlOH molecule at four levels of theory with the three largest basis sets. Bond lengths are in Å.

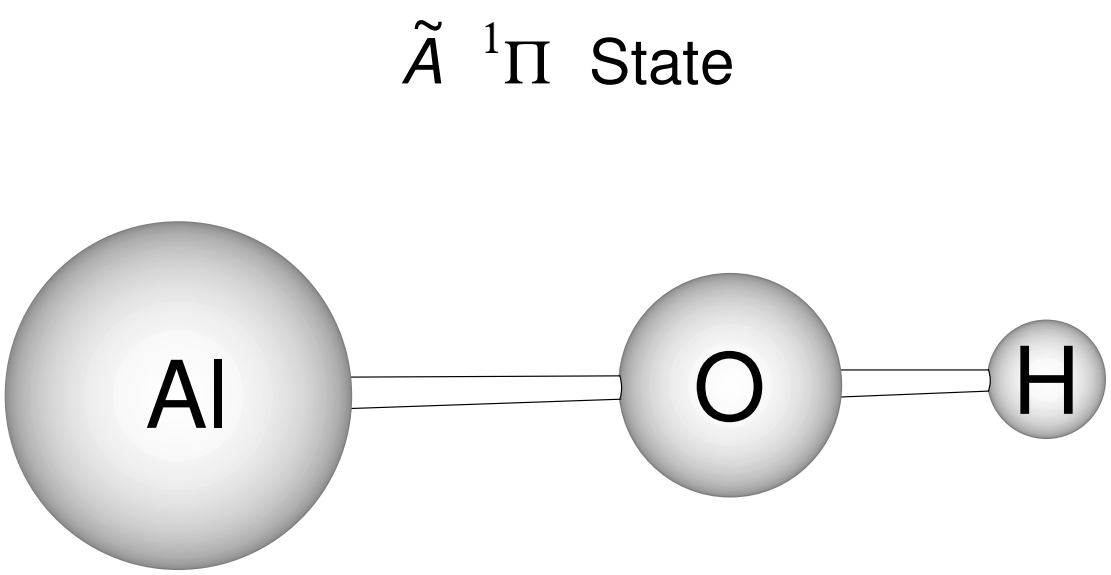

cc-pVQZ EOM-CCSD	1.6460	0.9434
cc-pV(Q+d)Z EOM-CCSD	1.6421	0.9434
aug-cc-pVQZ EOM-CCSD	1.6442	0.9442
cc-pVQZ EOM-CCSDT-3	1.6510	0.9461
cc-pV(Q+d)Z EOM-CCSDT-3	1.6472	0.9461
aug-cc-pVQZ EOM-CCSDT-3	1.6497	0.9470
cc-pVQZ EOM-CC3	1.6524	0.9466
cc-pV(Q+d)Z EOM-CC3	1.6486	0.9466
aug-cc-pVQZ EOM-CC3	1.6511	0.9475

Figure 5.4 Predicted geometries of the linear $\tilde{A}\ ^1\Pi$ state of the AlOH molecule at three levels of theory with the three largest basis sets. Bond lengths are in Å.

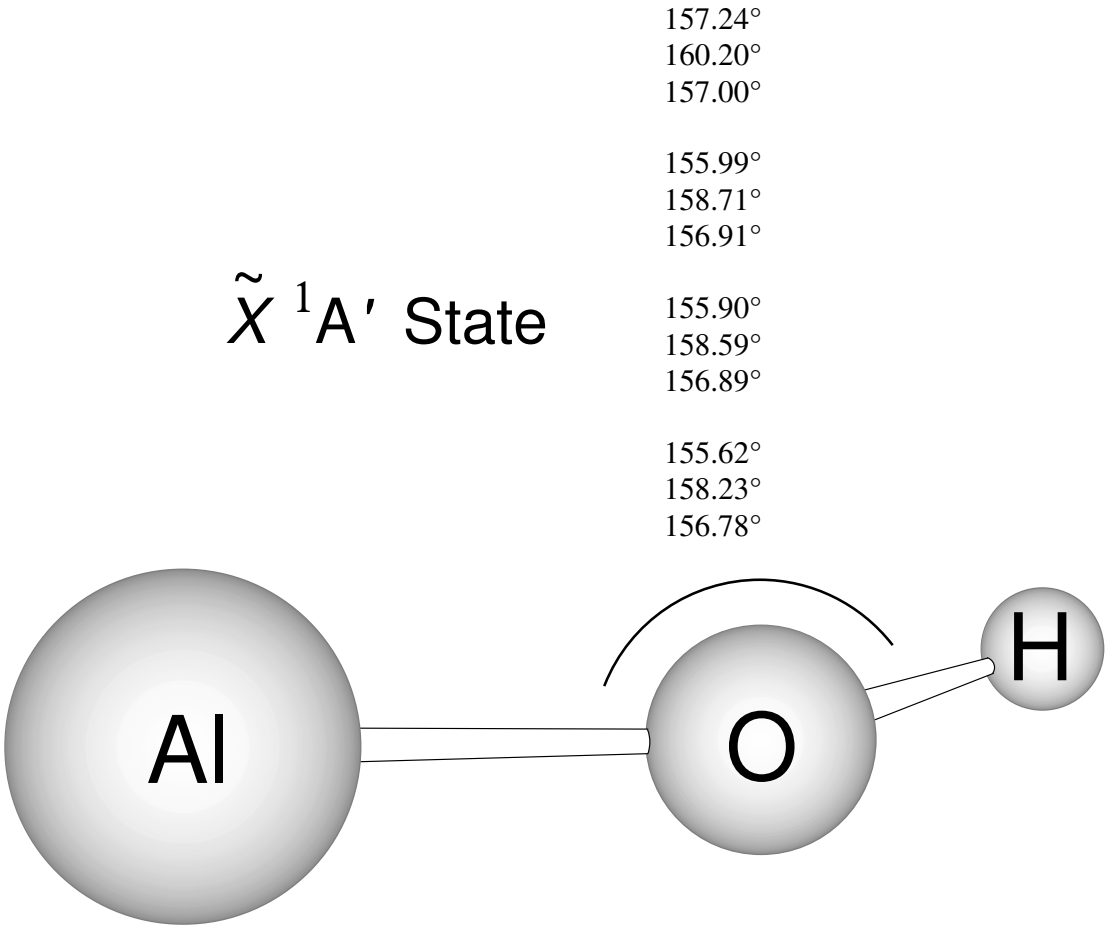

cc-pVQZ CCSD	1.6829	0.9469
cc-pV(Q+d)Z CCSD	1.6775	0.9465
aug-cc-pVQZ CCSD	1.6846	0.9474
cc-pVQZ CCSD(T)	1.6876	0.9501
cc-pV(Q+d)Z CCSD(T)	1.6822	0.9497
aug-cc-pVQZ CCSD(T)	1.6890	0.9507
cc-pVQZ CCSDT-3	1.6881	0.9500
cc-pV(Q+d)Z CCSDT-3	1.6828	0.9496
aug-cc-pVQZ CCSDT-3	1.6896	0.9506
cc-pVQZ CC3	1.6893	0.9505
cc-pV(Q+d)Z CC3	1.6840	0.9502
aug-cc-pVQZ CC3	1.6908	0.9512

Figure 5.5 Predicted geometries of the bent ground state ($\tilde{X}\,^1A'$) of the AlOH molecule at four levels of theory with the three largest basis sets. Bond lengths are in Å.

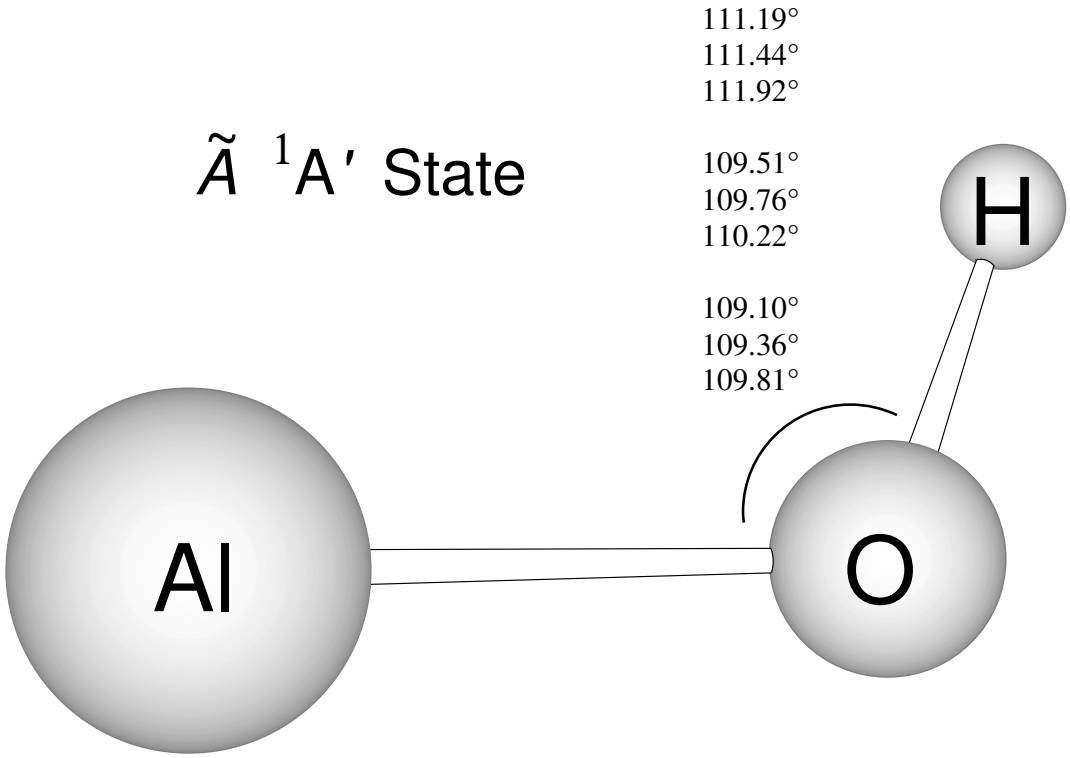

cc-pVQZ EOM-CCSD	1.7414	0.9581
cc-pV(Q+d)Z EOM-CCSD	1.7369	0.9580
aug-cc-pVQZ EOM-CCSD	1.7387	0.9584
cc-pVQZ EOM-CCSDT-3	1.7571	0.9623
cc-pV(Q+d)Z EOM-CCSDT-3	1.7525	0.9622
aug-cc-pVQZ EOM-CCSDT-3	1.7545	0.9628
cc-pVQZ EOM-CC3	1.7609	0.9633
cc-pV(Q+d)Z EOM-CC3	1.7562	0.9631
aug-cc-pVQZ EOM-CC3	1.7583	0.9638

Figure 5.6 Predicted geometries of the first singlet excited state ($\tilde{A}\ ^1A'$) of the AlOH molecule at three levels of theory with the three largest basis sets. Bond lengths are in Å.

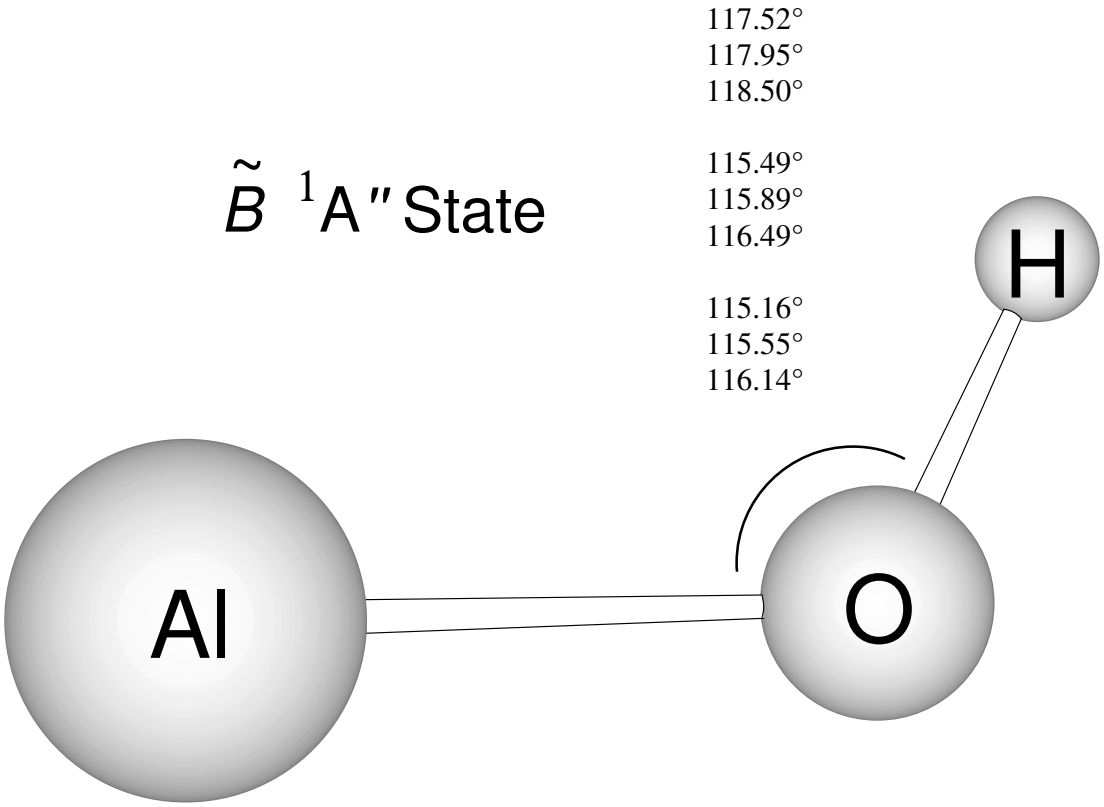

cc-pVQZ EOM-CCSD	1.7375	0.9585
cc-pV(Q+d)Z EOM-CCSD	1.7324	0.9582
aug-cc-pVQZ EOM-CCSD	1.7328	0.9586
cc-pVQZ EOM-CCSDT-3	1.7539	0.9629
cc-pV(Q+d)Z EOM-CCSDT-3	1.7486	0.9627
aug-cc-pVQZ EOM-CCSDT-3	1.7490	0.9632
cc-pVQZ EOM-CC3	1.7571	0.9638
cc-pV(Q+d)Z EOM-CC3	1.7517	0.9636
aug-cc-pVQZ EOM-CC3	1.7523	0.9641

Figure 5.7 Predicted geometries of the second singlet excited state ($\tilde{B}\ ^1A''$) of the AlOH molecule at three levels of theory with the three largest basis sets. Bond lengths are in Å.

Table 5.1 Theoretical predictions of the total energy (in hartree), dipole moment (in Debye), harmonic vibrational frequencies (in cm^{-1}), and zero-point vibrational energy (ZPVE in kcal mol^{-1}) for the linear $\tilde{X}\,^1\Sigma^+$ state of the AlOH molecule.

LEVEL OF THEORY	ENERGY	μ	$\omega_1(\sigma)$	$\omega_2(\pi)$	$\omega_3(\sigma)$	ZPVE
cc-pVTZ SCF	–317.446 322	1.311	4312	118i	882	7.43
cc-pV(T + d)Z SCF	–317.448 739	1.374	4314	91i	889	7.44
aug-cc-pVTZ SCF	–317.449 141	1.195	4310	45i	877	7.42
cc-pVQZ SCF	–317.456 997	1.271	4315	76i	891	7.44
cc-pV(Q + d)Z SCF	–317.458 088	1.296	4316	42i	892	7.44
aug-cc-pVQZ SCF	–317.457 443	1.235	4315	97i	887	7.44
cc-pVTZ CISD	–317.736 585	1.162	4135	120i	866	7.15
cc-pV(T + d)Z CISD	–317.738 965	1.221	4137	95i	873	7.16
aug-cc-pVTZ CISD	–317.744 909	0.965	4122	66i	852	7.11
cc-pVQZ CISD	–317.766 221	...	4144	68i	873	7.17
cc-pV(Q + d)Z CISD	–317.767 335	...	4144	68i	874	7.17
aug-cc-pVQZ CISD	–317.769 049	...	4139	96i	865	7.15
cc-pVTZ CCSD	–317.759 910	1.113	4072	146i	858	7.05
cc-pV(T + d)Z CCSD	–317.762 285	1.172	4074	127i	865	7.06
aug-cc-pVTZ CCSD	–317.768 901	0.889	4056	110i	842	7.00
cc-pVQZ CCSD	–317.790 902	1.019	4079	110i	864	7.07
cc-pV(Q + d)Z CCSD	–317.792 015	1.043	4080	91i	865	7.07
aug-cc-pVQZ CCSD	–317.793 948	...	4073	129i	856	7.05
cc-pVTZ CCSD(T)	–317.770 940	1.126	4028	149i	851	6.97
cc-pV(T + d)Z CCSD(T)	–317.773 281	1.183	4031	131i	857	6.99
aug-cc-pVTZ CCSD(T)	–317.781 061	0.867	4006	108i	832	6.92
cc-pVQZ CCSD(T)	–317.803 572	1.011	4030	112i	855	6.98
cc-pV(Q + d)Z CCSD(T)	–317.804 672	1.033	4031	94i	856	6.99
aug-cc-pVQZ CCSD(T)	–317.807 018	...	4022	126i	845	6.96
cc-pVTZ CCSDT-3	–317.770 640	...	4029	149i	848	6.97
cc-pV(T + d)Z CCSDT-3	–317.772 972	...	4032	131i	855	6.99
aug-cc-pVTZ CCSDT-3	–317.780 779	...	4007	108i	830	6.91
cc-pVQZ CCSDT-3	–317.803 263	...	4031	112i	853	6.98
cc-pV(Q + d)Z CCSDT-3	–317.804 360	...	4032	95i	854	6.99
aug-cc-pVQZ CCSDT-3	–317.806 738	...	4023	...	843	6.96
cc-pVTZ CC-3	–317.771 828	...	4022	149i	846	6.96
cc-pV(T + d)Z CC-3	–317.774 149	...	4024	132i	852	6.97
aug-cc-pVTZ CC-3	–317.782 104	...	3998	109i	827	6.90
cc-pVQZ CC-3	–317.804 566	...	4022	114i	850	6.97
cc-pV(Q + d)Z CC-3	–317.805 659	...	4023	97i	852	6.97
aug-cc-pVQZ CC-3	–317.808 084	...	4014	127i		

Table 5.2 Theoretical predictions of the total energy (in hartree), dipole moment (in Debye), harmonic vibrational frequencies (in cm^{-1}), and zero-point vibrational energy (ZPVE in kcal mol^{-1}) for the linear $\tilde{A}\ ^1\Pi$ state of the AlOH molecule.

LEVEL OF THEORY	ENERGY	μ	ω_1 (σ)	ω_2 (π^+)	ω_2 (π^-)	ω_3 (σ)	ZPVE
cc-pVTZ SCF	–317.259 913	0.669	4354	647i	416i	963	7.60
cc-pV(T + d)Z SCF	–317.262 634	0.728	4355	633i	391i	970	7.61
aug-cc-pVTZ SCF	–317.271 225	1.499	4329	497i	304i	985	7.60
cc-pVQZ SCF	–317.277 003	1.045	4344	558i	335i	990	7.62
cc-pV(Q + d)Z SCF	–317.278 300	1.085	4344	...	321i	990	7.63
aug-cc-pVQZ SCF	–317.280 543	1.526	4333	...	309i	996	7.62
cc-pVTZ CISD	–317.537 543	0.689	4186	...	501i	936	7.32
cc-pV(T + d)Z CISD	–317.540 152	0.743	4188	...	477i	942	7.33
aug-cc-pVTZ CISD	–317.551 256	1.216	4162	...	430i	939	7.29
cc-pVQZ CISD	–317.572 043	...	4185	...	429i	955	7.35
cc-pV(Q + d)Z CISD	–317.573 310	...	4186	...	417i	956	7.35
aug-cc-pVQZ CISD	–317.576 484	...	4177	...	...	953	7.33
cc-pVTZ EOM-CCSD	–317.556 663	...	4114	761i	589i	916	7.19
cc-pV(T + d)Z EOM-CCSD	–317.559 147	...	4116	744i	563i	923	7.20
aug-cc-pVTZ EOM-CCSD	–317.571 049	...	4089	674i	517i	919	7.16
cc-pVQZ EOM-CCSD	–317.592 216	...	4114	684i	510i	936	7.22
cc-pV(Q + d)Z EOM-CCSD	–317.593 410	...	4115	675i	499i	937	7.22
aug-cc-pVQZ EOM-CCSD	–317.596 966	...	4105	661i	497i	934	7.20
cc-pVTZ EOM-CCSDT-3	–317.567 993	...	4076	776i	612i	903	7.11
cc-pV(T + d)Z EOM-CCSDT-3	–317.570 422	...	4078	758i	586i	910	7.13
aug-cc-pVTZ EOM-CCSDT-3	–317.583 291	...	4046	690i	540i	904	7.08
cc-pVQZ EOM-CCSDT-3	–317.605 027	...	4072	698i	533i	922	7.14
cc-pV(Q + d)Z EOM-CCSDT-3	–317.606 199	...	4072	689i	522i	923	7.14
aug-cc-pVQZ EOM-CCSDT-3	–317.610 116	...	4061	677i	521i	919	7.12
cc-pVTZ EOM-CC3	–317.569 396	...	4068	781i	680i	899	7.10
cc-pV(T + d)Z EOM-CC3	–317.571 807	...	4070	762i	590i	906	7.11
aug-cc-pVTZ EOM-CC3	–317.584 768	...	4037	693i	544i	900	7.06
cc-pVQZ EOM-CC3	–317.606 504	...	4063	703i	539i	918	7.12
cc-pV(Q + d)Z EOM-CC3	–317.606 669	...	4064	695i	527i	919	7.12
aug-cc-pVQZ EOM-CC3	–317.611 609	...	4052	680i	524i	915	7.10

Table 5.3.1 Theoretical predictions of the total energy (in hartree), dipole moment (in Debye), harmonic vibrational frequencies (in cm^{-1}), infrared intensities (in parentheses in km mol^{-1}), and zero-point vibrational energy (ZPVE in kcal mol^{-1}) for the bent $\tilde{X}\,^1A'$ state of the AlOH molecule.

LEVEL OF THEORY	ENERGY	μ	$\omega_1(A')$	$\omega_2(A')$	$\omega_3(A')$	ZPVE
cc-pVTZ SCF	–317.446 376	1.337	4294(130.5)	173(182.7)	874(157.1)	7.64
cc-pV(T + d)Z SCF	–317.448 757	1.382	4303(139.4)	130(191.3)	885(160.4)	7.60
aug-cc-pVTZ SCF	–317.449 142	1.201	4307(137.6)	64(196.2)	876(184.7)	7.50
cc-pVQZ SCF	–317.457 006	1.281	4307(137.7)	108(191.9)	888(171.4)	7.58
cc-pV(Q + d)Z SCF	–317.458 089	1.298	4313(142.6)	59(196.2)	891(176.2)	7.52
aug-cc-pVQZ SCF	–317.457 462	1.251	4303(134.0)	136(186.4)	882(174.9)	7.61
cc-pVTZ CISD	–317.736 666	1.228	4111(96.3)	180(164.7)	855(132.6)	7.36
cc-pV(T + d)Z CISD	–317.738 996	1.254	4128(102.1)	111(170.1)	867(136.5)	7.30
aug-cc-pVTZ CISD	–317.744 916	1.000	4115(95.5)	94(179.9)	849(164.4)	7.23
cc-pVQZ CISD	–317.766 229	...	4136(-)	97(-)	869(-)	7.29
cc-pV(Q + d)Z CISD	–317.767 335	...	4143(-)	40(-)	873(-)	7.23
aug-cc-pVQZ CISD	–317.769 067	...	4128(-)	132(-)	861(-)	7.32
cc-pVTZ CCSD	–317.760 087	1.212	4036(86.6)	222(154.6)	842(120.5)	7.29
cc-pV(T + d)Z CCSD	–317.762 384	1.232	4046(91.8)	188(162.9)	853(123.3)	7.27
aug-cc-pVTZ CCSD	–317.768 950	0.992	4035(84.3)	155(165.1)	834(150.6)	7.18
cc-pVQZ CCSD	–317.790 954	1.092	4059(92.5)	160(167.4)	855(139.9)	7.25
cc-pV(Q + d)Z CCSD	–317.792 041	...	4065(-)	134(-)	859(-)	7.23
aug-cc-pVQZ CCSD	–317.794 016	...	4053(-)	175(-)	847(-)	7.26
cc-pVTZ CCSD(T)	–317.771 147	1.226	3990(79.8)	228(148.9)	833(109.8)	7.22
cc-pV(T + d)Z CCSD(T)	–317.773 403	1.243	4000(84.3)	195(157.0)	844(112.4)	7.20

Table 5.3.2 Theoretical predictions of the total energy (in hartree), dipole moment (in Debye), harmonic vibrational frequencies (in cm^{-1}), infrared intensities (in parentheses in km mol^{-1}), and zero-point vibrational energy (ZPVE in kcal mol^{-1}) for the bent $\tilde{X}\,^1A'$ state of the AlOH molecule. (Continued)

AUG-CC-PVTZ CCSD(T)	–317.781 109	0.976	3986 (75.3)	152 (161.1)	824 (143.0)	7.09
cc-pVQZ CCSD(T)	–317.803 632	1.092	4009 (83.8)	165 (161.9)	845 (129.8)	7.18
cc-pV(Q + d)Z CCSD(T)	–317.804 705	...	4014(-)	140(-)	849(-)	7.15
aug-cc-pVQZ CCSD(T)	–317.807 085	...	4002(-)	172(-)	837(-)	7.16
cc-pVTZ CCSDT-3	–317.770 844	...	3991(-)	228(-)	831(-)	7.22
cc-pV(T + d)Z CCSDT-3	–317.773 092	...	4001(-)	195(-)	842(-)	7.20
aug-cc-pVTZ CCSDT-3	–317.780 827	...	3987(-)	153(-)	822(-)	7.09
cc-pVQZ CCSDT-3	–317.803 324	...	4010(-)	167(-)	843(-)	7.18
cc-pV(Q + d)Z CCSDT-3	–317.804 395	...	4015(-)	142(-)	847(-)	7.15
aug-cc-pVQZ CCSDT-3	–317.806 806	...	4003(-)	172(-)	835(-)	7.16
cc-pVTZ CC3	–317.772 036	...	3983(-)	229(-)	829(-)	7.21
cc-pV(T + d)Z CC3	–317.774 273	...	3993(-)	196(-)	839(-)	7.19
aug-cc-pVTZ CC3	–317.782 153	...	3978(-)	154(-)	818(-)	7.08
cc-pVQZ CC3	–317.804 631	...	4001(-)	169(-)	841(-)	7.16
cc-pV(Q + d)Z CC3	–317.805 696	...	4006(-)	144(-)	844(-)	7.14
aug-cc-pVQZ CC3	–317.808 153	...	3993(-)	173(-)	831(-)	7.14
Expt. (Ref. 2)			3790(-)		810.3	
Expt. (Ref. 4)					895	

Table 5.4 Theoretical predictions of the total energy (in hartree), harmonic vibrational frequencies (in cm^{-1}), and zero-point vibrational energy (ZPVE in kcal mol^{-1}) for the bent $\tilde{A}\ ^1A'$ state of the AlOH molecule.

LEVEL OF THEORY	ENERGY	ω_1 (A')	ω_2 (A')	ω_3 (A')	ZPVE
cc-pVTZ EOM-CCSD	–317.577 509	3877	888	661	7.76
cc-pV(T + d)Z EOM-CCSD	–317.578 918	3881	884	668	7.77
aug-cc-pVTZ EOM-CCSD	–317.587 564	3866	857	667	7.71
cc-pVQZ EOM-CCSD	–317.608 606	3895	861	689	7.78
cc-pV(Q + d)Z EOM-CCSD	–317.609 354	3897	859	690	7.79
aug-cc-pVQZ EOM-CCSD	–317.612 042	3892	851	685	7.76
cc-pVTZ EOM-CCSDT-3	–317.590 363	3821	882	615	7.60
cc-pV(T + d)Z EOM-CCSDT-3	–317.591 640	3826	878	624	7.62
aug-cc-pVTZ EOM-CCSDT-3	–317.601 121	3807	850	622	7.55
cc-pVQZ EOM-CCSDT-3	–317.622 823	3835	855	650	7.63
cc-pV(Q + d)Z EOM-CCSDT-3	–317.623 524	3837	852	653	7.64
aug-cc-pVQZ EOM-CCSDT-3	–317.626 515	...	...	...	...
cc-pVTZ EOM-CC3	–317.592 108	3806	880	603	7.56
cc-pV(T + d)Z EOM-CC3	–317.593 350	3812	876	613	7.58
aug-cc-pVTZ EOM-CC3	–317.602 931	3791	848	614	7.51
cc-pVQZ EOM-CC3	–317.624 603	3820	853	640	7.60
cc-pV(Q + d)Z EOM-CC3	–317.625 291	3822	850	643	7.60
aug-cc-pVQZ EOM-CC3	–317.628 311	...	...	...	...
Expt. (Ref. 4)		3258.4	825.2	654.2	

Table 5.5.1 Theoretical predictions of the total energy (in hartree), dipole moment (in Debye), harmonic vibrational frequencies (in cm^{-1}), infrared intensities (in parentheses in km mol^{-1}), and zero-point vibrational energy (ZPVE in kcal mol^{-1}) for the bent $\tilde{B}\,^1A''$ state of the AlOH molecule.

LEVEL OF THEORY	ENERGY	μ	ω_1 (A')	ω_2 (A')	ω_3 (A')	ZPVE
cc-pVTZ SCF	–317.263 461	1.121	4230 (174.3)	887 (29.3)	558 (149.1)	8.11
cc-pV(T + d)Z SCF	–317.265 599	1.106	4238 (183.0)	897 (33.7)	533 (153.0)	8.10
aug-cc-pVTZ SCF	–317.272 796	0.961	4236 (226.9)	919 (54.9)	454 (189.5)	8.02
cc-pVQZ SCF	–317.278 910	0.971	4244 (208.6)	923 (44.8)	477 (166.9)	8.07
cc-pV(Q + d)Z SCF	–317.279 994	0.975	4248 (214.5)	926 (46.8)	462 (167.5)	8.06
aug-cc-pVQZ SCF	–317.281 961	1.000	4248(-)	936(-)	439(-)	8.04
cc-pVTZ CISD	–317.545 048	1.136	3992 (129.5)	816 (3.4)	620 (95.5)	7.76
cc-pV(T + d)Z CISD	–317.546 781	1.118	4000 (133.5)	822 (3.3)	607 (103.1)	7.76
aug-cc-pVTZ CISD	–317.556 432	0.945	3992 (135.7)	826 (8.5)	582 (152.8)	7.72
cc-pVQZ CISD	–317.576 889	...	4022(-)	842(-)	574(-)	7.77
cc-pV(Q + d)Z CISD	–317.577 832	...	4025(-)	845(-)	564(-)	7.77
cc-pVTZ EOM-CCSD	–317.568 157	...	3867(-)	790(-)	610(-)	7.53
cc-pV(T + d)Z EOM-CCSD	–317.569 571	...	3875(-)	787(-)	612(-)	7.54
aug-cc-pVTZ EOM-CCSD	–317.579 636	...	3866(-)	782(-)	608(-)	7.51
cc-pVQZ EOM-CCSD	–317.600 292	...	3897(-)	790(-)	613(-)	7.58
cc-pV(Q + d)Z EOM-CCSD	–317.601 084	...	3901(-)	791(-)	609(-)	7.58

Table 5.5.2 Theoretical predictions of the total energy (in hartree), dipole moment (in Debye), harmonic vibrational frequencies (in cm^{-1}), infrared intensities (in parentheses in km mol^{-1}), and zero-point vibrational energy (ZPVE in kcal mol^{-1}) for the bent $\tilde{B}\,^1A''$ state of the AlOH molecule. (Continued)

AUG-CC-PVQZ EOM-CCSD	–317.604 346	...	3897(-)	791(-)	607(-)	7.57
cc-pVTZ EOM-CCSDT-3	–317.580 922	...	3807(-)	784(-)	573(-)	7.38
cc-pV(T + d)Z EOM-CCSDT-3	–317.582 201	...	3815(-)	779(-)	579(-)	7.40
aug-cc-pVTZ EOM-CCSDT-3	–317.593 035	...	3804(-)	768(-)	583(-)	7.37
cc-pVQZ EOM-CCSDT-3	–317.614 346	...	3833(-)	773(-)	597(-)	7.44
cc-pV(Q + d)Z EOM-CCSDT-3	–317.615 088	...	3836(-)	772(-)	596(-)	7.44
aug-cc-pVQZ EOM-CCSDT-3	–317.618 627	...	...	...	...	...
cc-pVTZ EOM-CC3	–317.582 551	...	3793(-)	781(-)	564(-)	7.35
cc-pV(T + d)Z EOM-CC3	–317.583 802	...	3801(-)	777(-)	572(-)	7.36
aug-cc-pVTZ EOM-CC3	–317.594 727	...	3790(-)	766(-)	577(-)	7.34
cc-pVQZ EOM-CC3	–317.616 019	...	3820(-)	769(-)	592(-)	7.41
cc-pV(Q + d)Z EOM-CC3	–317.616 750	...	3823(-)	769(-)	592(-)	7.41
aug-cc-pVQZ EOM-CC3	–317.620 312	...	...	...	...	...
Expt. (Ref. 4)				764.3	588.2	

Table 5.6 Excitation energies, T_e values in kcal mol^{-1} (T_0 values in parentheses) for the four singlet states relative to the $\tilde{X}\,^1A'$ state of the AlOH.

LEVEL OF THEORY	$\tilde{X}\,^1\Sigma^+$	$\tilde{A}\,^1\Pi$	$\tilde{A}\,^1A'$	$\tilde{B}\,^1A''$
cc-pVTZ SCF	0.03	117.01		114.78(115.25)
cc-pV(T + d)Z SCF	0.01	116.79		114.93(115.43)
aug-cc-pVTZ SCF	0.00_1	111.64		110.66(111.18)
cc-pVQZ SCF	0.01	112.95		111.76(112.25)
cc-pV(Q + d)Z SCF	0.00_1	112.82		111.76(112.30)
aug-cc-pVQZ SCF	0.01	111.02		110.13(110.56)
cc-pVTZ CISD	0.05	124.95		120.24(120.64)
cc-pV(T + d)Z CISD	0.02	124.78		120.62(121.08)
aug-cc-pVTZ CISD	0.00_4	121.52		118.28(118.77)
cc-pVQZ CISD	0.01	121.85		118.81(119.29)
cc-pV(Q + d)Z CISD	0.00	121.75		120.00(120.45)
aug-cc-pVQZ CISD	0.01	120.85		-
cc-pVTZ EOM-CCSD		127.65	114.57(115.04)	120.44(120.68)
cc-pV(T + d)Z EOM-CCSD		127.53	115.13(115.63)	120.99(121.26)
aug-cc-pVTZ EOM-CCSD		124.18	113.82(114.35)	118.80(119.13)
cc-pVQZ EOM-CCSD		124.71	114.43(114.96)	119.64(119.97)
cc-pV(Q + d)Z EOM-CCSD		124.64	114.64(115.20)	119.83(120.18)
aug-cc-pVQZ EOM-CCSD		123.65	114.19(114.69)	119.02(119.33)
cc-pVTZ CCSD	0.11			
cc-pV(T + d)Z CCSD	0.06			
aug-cc-pVTZ CCSD	0.03			
cc-pVQZ CCSD	0.03			
cc-pV(Q + d)Z CCSD	0.02			
aug-cc-pVQZ CCSD	0.04			
cc-pVTZ CCSD(T)	0.13			
cc-pV(T + d)Z CCSD(T)	0.08			
aug-cc-pVTZ CCSD(T)	0.03			
cc-pVQZ CCSD(T)	0.04			
cc-pV(Q + d) CCSD(T)	0.02			
aug-cc-pVQZ CCSD(T)	0.04			
Expt. T_0 value, Ref. 3 (1983)			(115.01)	
Expt. T_0 value, Ref. 4 (1983)			(114.57)	(119.36)

Table 5.7 Excitation energies, T_e values in kcal mol^{-1} (T_0 values in parentheses) for the four singlet states relative to the $\bar{X}\,^1A'$ state of the AlOH.

LEVEL OF THEORY	$\bar{X}\,^1\Sigma^+$	$\tilde{A}\,^1\Pi$	$\tilde{A}\,^1A'$	$\bar{B}\,^1A''$
cc-pVTZ EOM-CCSDT-3		127.29	113.25(113.63)	119.18(119.34)
cc-pV(T + d)Z EOM-CCSDT-3		127.18	113.86(114.28)	119.79(119.99)
aug-cc-pVTZ EOM-CCSDT-3		123.96	112.77(113.23)	117.84(118.12)
cc-pVQZ EOM-CCSDT-3		124.43	113.27(113.72)	118.59(118.85)
cc-pV(Q + d)Z EOM-CCSDT-3		124.37	113.50(113.99)	118.79(119.08)
aug-cc-pVQZ EOM-CCSDT-3		123.42	113.13(113.58[a])	118.08(118.34[a])
cc-pVTZ CCSDT-3	0.13			
cc-pV(T + d)Z CCSDT-3	0.08			
aug-cc-pVTZ CCSDT-3	0.03			
cc-pVQZ CCSDT-3	0.04			
cc-pV(Q + d)Z CCSDT-3	0.02			
aug-cc-pVQZ CCSDT-3	0.04			
cc-pVTZ EOM-CC3		127.16	112.91(113.26)	118.90(119.04)
cc-pV(T + d)Z EOM-CC3		127.05	113.53(113.92)	119.52(119.69)
aug-cc-pVTZ EOM-CC3		123.86	112.46(112.89)	117.61(117.87)
cc-pVQZ EOM-CC3		124.33	112.97(113.41)	118.36(118.61)
cc-pV(Q + d)Z EOM-CC3		124.89	113.21(113.67)	118.57(118.84)
aug-cc-pVQZ EOM-CC3		123.33	112.85(113.29[a])	117.87(118.12[a])
cc-pVTZ CC3	0.13			
cc-pV(T + d)Z CC3	0.08			
aug-cc-pVTZ CC3	0.03			
cc-pVQZ CC3	0.04			
cc-pV(Q + d)Z CC3	0.02			
aug-cc-pVQZ CC3	0.04			
Expt. T_0 value, Ref. 3 (1983)			(115.01)	
Expt. T_0 value, Ref. 4 (1993)			(114.57)	(119.36)

[a] cc-pVQZ EOM-CC zero-point vibrational energies were used.

CHAPTER 6

FUTURE WORK

I plan to apply the advanced quantum mechanical computational techniques to modern organometallic chemistry, particularly the excited states and photochemical reactions of dinuclear organometallic complexes containing metal-metal multiple bonds, one of the most rapidly developing new fields in modern chemistry.

More recently, the new technique of time-dependent density functional theory (TD-DFT) has been developed and applied to probe excited electronic states. This method may be used to explore the rich and diverse photochemistry of dinuclear organometallic complexes and to elucidate reaction mechanisms and products to be expected from accessible experimental data. TD-DFT overcomes the earlier limitation of traditional DFT, which has proven successful only for ground states. Experience in this area is just building up, but the preliminary results are very encouraging. TD-DFT is fast becoming one of the techniques of choice to obtain accurate and reliable predictions for excited-state properties. In the coming years, TD-DFT will be extended to many other areas, such as catalysis, clusters, materials, surface sciences and bioinorganic chemistry.